Master's thesis

NTNU
Norwegian University of Science and Technology
Faculty of Information Technology and Electrical Engineering
Department of Engineering Cybernetics

Mia Olea Vettestad

Response Amplitude Operator Estimation and Prediction of Heave Motions

Master's thesis in Engineering Cybernetics
Supervisor: Ole Morten Aamo
January 2020

NTNU
Norwegian University of Science and Technology

Mia Olea Vettestad

Response Amplitude Operator Estimation and Prediction of Heave Motions

Master's thesis in Engineering Cybernetics
Supervisor: Ole Morten Aamo
January 2020

Norwegian University of Science and Technology
Faculty of Information Technology and Electrical Engineering
Department of Engineering Cybernetics

NTNU
Norwegian University of
Science and Technology

Abstract

Offshore well drilling operations from floating rigs or drilling ships are associated with considerable challenges, especially related to weather conditions.

During offshore drilling, the rig is heave compensated by a system which keeps the drill string steady relative to the formation (Kvernland et al., 2018). However, whenever the drill string is set in slips for connections of new drill pipe sections, the drill string is attached to the rig and will move along with the heaving motion of the rig. This can cause a piston-like movement in the bottom of the well, which introduces an unacceptable risk of mud loss or kick due to significant downhole pressure oscillations (Landet et al., 2013).

Specifically, the heaving motion of the rig when the drill string is set in slips is an especially challenging factor in the North Sea where the majority of the subsea wells are drilled from floating rigs (Godhavn, 2010). In harsh weather, the heaving motion can have an amplitude of more than 3 meters and an associated period of 10-20 seconds, introducing downhole pressure variations in the order of 10-20 bars (Kvernland et al., 2019).

Today, the only remedy for this problem is to wait for wind and waves to subside, increasing the Non-Productive Time (NPT) and thereby costs. Therefore, Kvernland et al. (2019) at Heavelock AS developed a well-simulator which predicts the downhole pressure oscillations based on input variables such as drill pipe movement, drilling fluid properties, pump flow, weather forecasts and rig motion and characteristics, among others.

Specifically, the rig characteristics in the simulator are given as response amplitude operators (RAO), which describes the relation between ocean waves and rig motion. The RAO, which only depends on the rig type, is used to predict the heaving motion of the rig which is related to the downhole pressure oscillations.

The RAO is usually determined at the design stage by the manufacturer (Clauss et al., 1992). However, simulations indicates that a constant RAO only depending on the rig type can give inaccurate rig heave predictions. Moreover, software programs, such as WAMIT (Lee and Newman, 2006) and ShipX (Fathi), require information regarding the geometry of the rig as well as a valid license.

Thus, the objective of this MSc project is to develop a RAO estimation and rig heave prediction methodology based on data available on the rig for the purposed-developed simulator. A data-driven method for RAO estimation could potentially improve the simulator's ability to predict rig heave motions and thereby the ability to predict downhole pressure oscillations.

Therefore, an important part of this project was to determine which measurements that are available on the rig. Thus, this report presents the format of the data available on the rig in addition to weather forecasts services.

Moreover, two methods for RAO estimation and rig heave prediction based on real measurements are presented. One method is categorized as parametric as it models the heaving motion as a mass-spring-damper system, while the other is non-parametric. Both methods are tested with real wave spectra and model wave spectra as well as real heave amplitude measurements.

Additionally, if sea state parameters or wave spectra are unavailable, sea state parameters from weather forecasts can be utilized to predict the heaving motion of the rig. Thus, both methods are tested with model wave spectra based on sea state parameters from

weather forecasts services.

Furthermore, quantified calculations of the performance of the methods indicate that the non-parametric method overall performs better with real measurements than the parametric method. However, none of the proposed methods are tested with the simulator and thus it remains to conclude whether the proposed RAO estimation and rig heave prediction methodology improves downhole pressure predictions.

Sammendrag

Å bore etter olje fra flytende plattformer er ofte assosiert med store utfordringer, særlig relatert til vær- og vindforhold.

Under boreoperasjonen er boreplattformen hiv-kompensert ved hjelp av et system som holder borestrengen stødig i forhold til formasjonen (Kvernland et al., 2018). Dette kontrollsystemet må frakobles når borestrengen festes til riggen for tilkobling av nye borerør. Dermed følger borestrengen riggens bevegelser, noe som forårsaker en stempel-lignende bevegelse i bunnen av brønnen, noe som igjen introduserer en uakseptabel risiko for tap av borevæske og brønnspark (Landet et al., 2013).

Det er særlig riggens vertikale bevegelse, hiv, som skaper ekstra utfordringer i områder der majoriteten av brønnene bores fra flytende rigger, slik som i Nordsjøen (Godhavn, 2010). Under krevende værforhold, der hiv-bevegelsens amplitude kan komme opp i over 3 meter med en tilhørende periode på 10-20 sekunder, kan trykkvariasjonene i bunnen av brønnen komme opp i 10-20 bar (Kvernland et al., 2019).

Den eneste tilgjengelige løsningen på problemet er å vente til vær- og vindforhold avtar, noe som øker den ikke-produktive tiden (NPT) og dermed også kostnadene. Nettopp denne problemstillingen motiverte Kvernland et al. (2019) ved Heavelock AS til å utvikle en brønn-simulator som predikerer trykkvariasjonene i bunnen av brønnen basert på en rekke input-parametere slik som borerørets bevegelse, borevæskens egenskaper, pumperate, værmeldinger og riggens bevegelser og karakteristikk.

I simulatoren er riggens karakteristikk gitt som reponse amplitude operatorer (RAO), som beskriver forholdet mellom bølger og riggens bevegelser. RAOen, som kun er avhengig av riggtypen, blir direkte anvendt for å predikere riggens hiv-bevegelse, som igjen er tilknyttet trykkvariasjonene i bunnen av brønnen.

RAO blir vanligvis beregnet av rigg-produsentene under designfasen (Clauss et al., 1992), men simuleringer antyder at konstante, pre-definerte RAOer kun basert på riggtype kan gi upresise prediksjoner av riggens hiv-bevegelser. I tillegg krever software programmer som WAMIT (Lee and Newman, 2006) og ShipX (Fathi), informasjon om riggens geometri og ikke minst en gyldig lisens.

Formålet med denne masteroppgaven er derfor å utvikle en prosedyre for RAO estimering og hiv-prediksjon basert på tilgjengelig data fra riggen og værmeldingstjenester. En datadrevet metode for RAO estimering kan potensielt forbedre simulatorens evne til å predikere riggens hiv-bevegelse og dermed også trykkvariasjonene i bunnen av brønnen.

En viktig del av oppgaven var derfor å undersøke hvilke data som er tilgjengelig på riggen, samt formatet, i tillegg til hvilke værmeldingstjenester som gir prognoser på sjøtilstand.

Som et resultat ble to metoder for RAO estimering og hiv-prediksjon utviklet, én parametrisk metode som modellerer riggens hiv-bevegelse som et masse-fjær-demper system og én ikke-parametrisk metode. Begge metodene ble testet med ekte målinger i form av riggens hiv-amplitude, målt bølgespektrum og modellbølgespektrum basert på målt sjøtilstand. I tillegg ble metodene testet med modellbølgespektrum basert på meldt sjøtilstand fra værmeldingstjenester.

Tallfestede beregninger av ytelse indikerer at den ikke-parametriske metoden presterer bedre med ekte målinger enn det den parametriske metoden gjør. Ingen av metodene er rik-

tignok testet med simulatoren og det gjenstår dermed å konkludere om de foreslåtte metodene for RAO estimering og hiv-prediksjon faktisk forbedrer prediksjonen av trykkvariasjonene i bunnen av brønnen.

Preface

This thesis is the final project of the degree Master of Science at the Norwegian University of Science and Technology (NTNU) at the Department of Engineering Cybernetics. The project related to this thesis was completed during the Fall and Winter of 2019 and 2020 in collaboration with Heavelock AS.

The project was mainly executed with the programming platform MATLAB and provided wave and rig heave measurements.

I would like to use this opportunity to thank Professor Ole Morten Aamo at the Department of Engineering Cybernetics for being an enthusiastic and insightful supervisor. I am grateful for his commitment to this project and for always keeping his office door open whenever I experienced challenges.

Moreover, I would like to thank Martin Kvernland, Dmitri Gorski and Mateus Sant'Ana from Heavelock AS for always welcoming my questions and for providing helpful insight into the oil and gas industry.

Most importantly, I would like to give special thanks to Rune Bjørkli, Senior Engineer at Equinor ASA, for providing actual wave and rig heave measurements and for always finding time for my questions. The majority of the results from this thesis would not have been possible to obtain without his extremely valuable help.

Furthermore, I would like to thank Ole Johan Aarnes, Scientist at the Norwegian Meteorological Institute, for helping me with the weather forecast data server `thredds.met.no` and especially for being so patient when I needed help reading the forecast data.

Lastly, I would like to thank my helpful discussion partner Bendik Eger.

Mia Olea Vettestad
Trondheim, January 23, 2020

Table of Contents

Abstract i

Sammendrag iii

Preface v

Table of Contents ix

Abbreviations x

1 Introduction 1
1.1 Task Description 2

2 Background Theory 5
2.1 System Identification 5
2.1.1 The System Identification Loop 6
2.1.2 Models 7
2.1.3 Methods 10
2.2 Marine Craft Motion 12
2.2.1 Heave Equation of Motion 13
2.2.2 Response Amplitude Operator 14
2.3 Wave Spectrum Theory and Models 18
2.3.1 Sea State Parameters 18
2.3.2 The JONSWAP Spectrum 19
2.3.3 The Torsethaugen Spectrum 21

3 An Overview of Available Data 25
3.1 Weather Observations and Forecasts 25
3.1.1 StormGeo 25
3.1.2 The Norwegian Meteorological Institute 25
3.2 Actual Measurements From An Oil Rig 26

4 The Implementation of the Proposed RAO Estimation and Heave Prediction Methods **29**
4.1 A Parametric Method for RAO Estimation and Heave Prediction 29
4.1.1 Model Structure 30
4.1.2 Estimation Algorithm 30
4.1.3 Input and Output Generation 31
4.1.4 Heave Prediction from Generated Data 34
4.1.5 Heave Prediction Based on Measured Data 37
4.1.6 Validation of the Parametric Method 38
4.2 A Non-Parametric Method for RAO Estimation and Heave Prediction . . 38
4.2.1 Input and Output Generation 39
4.2.2 Mean RAO vs Previous RAO 39
4.2.3 Heave Prediction Based on Measured Data 40
4.3 RAO Estimation and Heave Prediction Based on Forecasts 40
4.3.1 Extracting Sea State Parameters 40
4.4 Statistical Analysis 42

5 RAO Estimation Based on Measured Data **43**
5.1 The Non-Parametric Method With Measured Wave Spectrum as Input . . 44
5.2 The Non-Parametric Method With Model Wave Spectrum as Input 50

6 Heave Prediction Based on Measured Data **57**
6.1 The Parametric Method 57
6.1.1 Measured Wave Spectrum as Input 58
6.1.2 Model Wave Spectrum as Input 61
6.2 The Non-Parametric Method 64
6.2.1 Measured Wave Spectrum as Input 64
6.2.2 Model Wave Spectrum as Input 70

7 RAO Estimation and Heave Prediction Based on Weather Forecasts **77**
7.1 The Parametric Method With Model Wave Spectrum Based on Weather Forecasts 78
7.2 The Non-Parametric Method With Model Wave Spectrum Based on Weather Forecasts 81
7.2.1 Average of 4 RAOs 82
7.2.2 Last RAO 86

8 Discussion and Conclusion **91**
8.1 Accessing Data 91
8.2 The Results 92
8.3 Conclusion 94

9 Further Work **95**
9.1 Simulations 95
9.2 Extended Heave Model 95

Bibliography **97**

Appendices **101**

A System Identification **103**

B Listings **105**

Abbreviations

AR	=	Autoregressive
ARX	=	Autoregressive Extra Input
BJ	=	Box-Jenkins
BHA	=	Bottom Hole Assembly
DOF	=	Degrees Of Freedom
ECMWF	=	European Centre for Medium-Range Weather Forecasts
ETFE	=	Empirical Transfer Function Estimate
FFT	=	Fast Fourier Transform
ITTC	=	International Towing Tank Conference
JONSWAP	=	Joint North Sea Wave Project
LTI	=	Linear Time-Invariant
MA	=	Moving Average
MRU	=	Motion Reference Unit
NPT	=	Non-Productive Time
NRMSE	=	Normalized Root-Mean-Square Error
OE	=	Output Error
PDF	=	Probability Density Function
PSD	=	Power Spectral Density
RAO	=	Response Amplitude Operator
RMS	=	Root-Mean-Square
SISO	=	Single-Input Singe-Output

Chapter 1

Introduction

Some aspects of this chapter, specifically the parts involving well drilling and Heavelock AS, are inspired by Vettestad (2019).

Offshore oil drilling from floating rigs or drilling ships introduces severe challenges, often related to weather conditions. Specifically, the major pressure fluctuations in the well when the drill pipe is set in slips, caused by the heaving motion of the floater, can introduce an unacceptable risk of mud loss or kick (Landet et al., 2013).

During offshore drilling, a heave compensation system keeps the drill string steady relative to the formation (Kvernland et al., 2018). Thus, the vertical motion of the oil rig due to sea waves will not affect the drill string or the downhole pressure. However, approximately every 28-30 meters the drill string is set in slips for connection of a new drill pipe section (Kvernland et al., 2019). During these connections the drill string is attached to the rig and will therefore move along with the heaving motion of the rig, causing a piston-like movement in the bottom of the well and introducing significant downhole pressure oscillations referred to as surge and swab effects.

The heaving motion is especially an extra challenging factor in the North Sea where the majority of subsea wells are drilled form floating rigs (Godhavn, 2010). In harsh weather, the heaving motion can have an amplitude of more than 3 meters and an associated period of 10-20 seconds, introducing downhole pressure variations in the order of 10-20 bars (Kvernland et al., 2019).

Kvernland et al. (2019) describe several proposed methods of reducing surge and swab effects, such as mechanical heave compensation of the drill floor. However, this requires a large capital investment as mechanical installations in this scale are very expensive.

Thus, the only remedy for downhole heave-induced pressure oscillations is to wait for wind and waves to subside, resulting in a more time-consuming and possibly more expensive drilling operation as high costs are related to Non-Productive Time (NPT).

The challenges related to heave-induced downhole pressure oscillations inspired Kvernland et al. (2019) at Heavelock AS to design a simulator which models dynamic interactions between the drilling fluid and the drill string in an accurate manner, which gives it ability to predict fast downhole changes.

The purposed-developed software utilizes input variables such as wave height from weather forecasts, drill pipe movements, drilling fluid properties, pump flow as well as well design, drill pipe, rig heave motion and characteristics and Bottom Hole Assembly (BHA) data to simulate heave-induced downhole pressure.

Specifically, the rig characteristics are given as response amplitude operators (RAO), which describes the relation between ocean waves and rig motion. The RAO, which in the simulator only depends on the rig type, is used to predict the heaving motion of the rig which is related to the downhole pressure oscillations.

The RAO is usually determined at the design stage, which allows the manufacturer to make appropriate modifications for safety purposes or to improve the performance (Clauss et al., 1992). However, simulations indicate that a constant RAO only depending on the rig type can give inaccurate rig heave predictions. Moreover, software programs, such as WAMIT (Lee and Newman, 2006) and ShipX (Fathi), which can be used to calculate the RAO require information regarding the geometry of the rig as well as a valid license. Additionally, WAMIT computations does not account for all physical effects, like mooring loads, forces on risers and empirical corrections based on model tests (Lee and Newman, 2006).

Nevertheless, Heavelock AS's simulator aims to determine a dynamic rig heave limit based on how much surge and swab the particular well can tolerate (Heavelock AS). Therefore, the simulator can give valuable insight into risks and well pressure margins during both well planning and at the operational phase.

The simulator has been validated with data from the North Sea provided by Equinor ASA, giving an accuracy of the simulated versus measured peak-to-peak surge and swab effects between 76.7% to 98.2%, depending on the test cases (Kvernland et al., 2019).

Furthermore, the accuracy of the simulator depends on the input data, thus the accuracy of the rig heave prediction, and thereby the RAO, are important. Therefore, the objective of this MSc project is to design a methodology for estimating the RAO based on data available from the rig, specifically wave and rig heave measurements. Further, the estimated RAO should be utilized when predicting future heaving motion of the rig in order to accurately predict the downhole pressure in the well.

1.1 Task Description

The objective of this project is to develop an algorithm for RAO estimation based on available data from the rig to predict the rig heave motion. As highlighted in Kvernland et al. (2019), information regarding the expected surge and swab effects in the near future is not available on the rig, neither is the exact magnitude in real time of those effects.

However, the well-simulator designed by Heavelock AS (Kvernland et al., 2019), intends to provide accurate information regarding surge and swab effects. The simulator utilizes a predefined RAO only depending on the rig type. However, simulations indicate that a constant RAO can give inaccurate rig heave predictions. Therefore, a data-driven RAO estimation method could potentially improve the simulator's ability to predict downhole pressure oscillations.

In order to design a RAO estimation methodology, estimation methods and system identification in general, as well as RAO estimation methods in particular has to be exam-

ined. Therefore, a brief introduction to system identification, including parameter estimation will be given in Chapter 2. Additionally, principles of marine craft motion, involving the heave motion and RAO will be presented as well as wave spectrum theory and models.

Furthermore, the estimation methodology depends on available data. As a result, the project involves investigating the availability of heave and ocean wave measurements from both the oil rigs as well as weather forecast services, which will be presented in Chapter 3.

Chapter 4 will describe how the proposed RAO estimation and heave prediction methods are implemented, while Chapter 5 to 7 present the performance of the proposed methods illustrated with three different experiments. Specifically, Chapter 5 will demonstrate the estimation of RAO based on real measurements. Further, Chapter 6 will present the performance of the heave prediction methodology with real measurements, while Chapter 7 will show how the proposed methods predict rig heave motion based on weather forecasts. Moreover, Chapter 8 will discuss these results and conclude the report.

Finally, suggestions regarding further improvements, applications and experiments will be presented in Chapter 9.

Chapter 2

Background Theory

This chapter will give a brief introduction to system identification and parameter estimation methods, mainly based on Ljung (1999). Additionally, marine craft motion, including response amplitude operator (RAO), and wave spectrum theory will be presented, mainly based on Fossen (2011) and Faltinsen (1990).

2.1 System Identification

Lennart Ljung, one of the pioneers in system identification and control theory, defines system identification as techniques for building mathematical models of dynamical systems based on observed data (Ljung, 1999). Based on three fundamental entities:

1. A data set
2. A set of candidate models
3. A rule by which the candidate models can be assessed using the data

system identification provides powerful techniques with a wide application area.

First of all, the input-output data, or the data set, should be maximally informative for the intended purpose, which means that the data set has to be selected with care. Furthermore, the single most important, and yet often the most difficult, aspect of system identification is to decide which collection of models will best fit the system to identify. Sometimes these models are chosen based on some a priori knowledge of the system, like basic physical laws or other well-established relationships. However, standard linear models without reference to the physical background may also be employed. The former is often referred to as grey box modeling while the latter is often referred to as black box modeling. Lastly, the identification method involves determining the best model in the set, guided by the data. The evaluation of model quality is typically based on how the models perform when they attempt to reproduce the measured data.

2.1.1 The System Identification Loop

The system identification procedure loop is illustrated in Figure 2.1. System identification starts with collecting information about the system, data, followed by selecting a model set. Finally, the ”best” model in the set is chosen as the mathematical representation of the system. However, it is likely that the model first obtained will not pass the model validation tests. Therefore, various steps of the procedure must be revised.

The model may be inadequate for a variety of reasons such as

- The numerical procedure failed to find the best model according to the validation criterion
- The validation criterion was not well chosen
- The model set itself was not appropriate, meaning that it did not contain any good enough descriptions of the system
- The data was not informative enough to provide guidance in selecting good models

Therefore, the major part of system identification consists of addressing the problems listed above in an iterative manner. In particular, deficient model sets are often the cause of unsatisfying system identification. Further, prior information about the system and the outcomes of previous attempts can lead the system identification process closer to a good enough description of the system for the intended purpose.

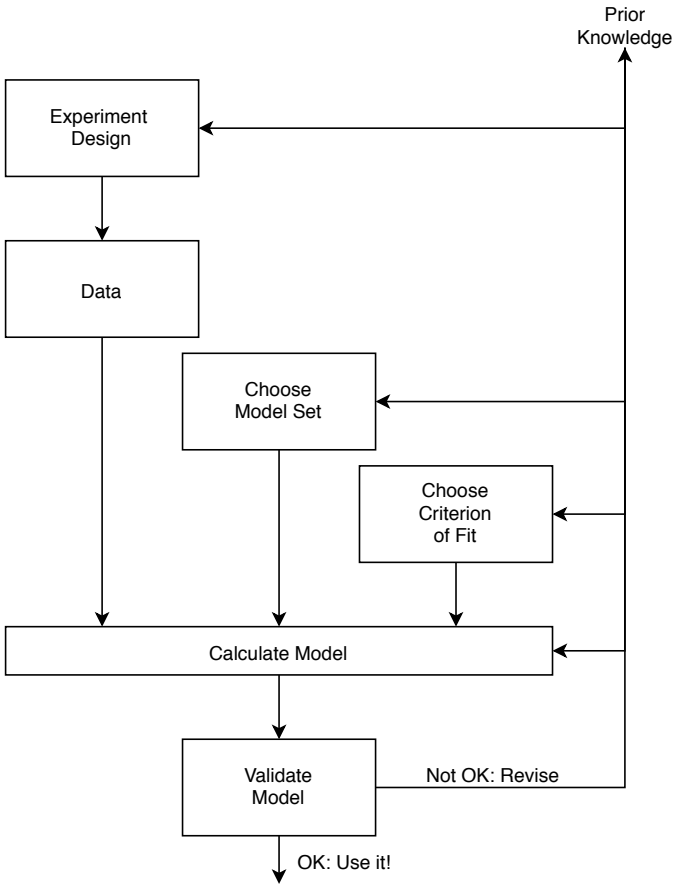

Figure 2.1: The system identification loop. First of all, collect data, then choose a model set before picking the "best" model within that set. If the validation criterion does not hold, repeat. Remake of Figure 1.10 in Ljung (1999).

2.1.2 Models

A model of a dynamical system is defined as a description of the system's properties. Mathematical or analytical models, which describe the relationship between the system variables in terms of mathematical expressions, are often effective models and are extensively used in all fields of engineering. However, a model can never be acknowledged as a true description of the system. Preferably, it can at best be considered as a good enough description of certain aspects which are of particular interest. Nevertheless, all models attempt to link observations together into some pattern.

Generally speaking, a model structure is a parametrized mapping from past inputs and outputs, Z^{t-1} to the space of the model outputs (Ljung, 1999), see Equation 2.1

$$\hat{y}(\theta|t) = g(\theta, Z^{t-1}) \tag{2.1}$$

Where θ is a vector containing the unknown parameters.

A first step when selecting a model is to determine a class of models within which the search for the most suitable model is to be conducted.

A linear time-invariant (LTI) model is presented in Equation 2.2, with $f_e(\cdot)$ being the probability density function (PDF) of the disturbance $e(t)$. Thus, a particular model corresponds to specifications of the three functions G, H and $f_e(\cdot)$. Typically, rational transfer functions and finite-dimensional state-space descriptions are used to specify G and H.

$$y(t) = G(q)u(t) + H(q)e(t) \tag{2.2}$$

Furthermore, Equation 2.2 can be rewritten as shown in Equation 2.3, depending on the parameter vector θ.

$$y(t) = G(q, \theta)u(t) + H(q, \theta)e(t) \tag{2.3}$$

Equation Error Structure

One of the most simple input-output relationships is obtained by describing it as a linear difference equation. The model in Equation 2.4 is often referred to as an equation error model or structure due to the white-noise term $e(t)$ entering as a direct error.

$$y(t) + a_1 y(t-1) + \cdots + a_{n_a} y(t-n_a) = b_1 u(t-1) + \cdots + b_{n_b} u(t-n_b) + e(t) \tag{2.4}$$

Where the parameters to be estimated can be represented as

$$\theta = [a_1 a_2 \cdots a_{n_a} b_1 \cdots b_{n_b}]^T \tag{2.5}$$

An by introducing

$$A(q) = 1 + a_1 q^{-1} + \cdots + a_{n_a} q^{-n_a} \tag{2.6}$$

and

$$B(q) = b_1 q^{-1} + \cdots + b_{n_b} q^{-n_b} \tag{2.7}$$

Eventually, equation 2.4 can be rewritten as Equation 2.3 with

$$G(q, \theta) = \frac{B(q)}{A(q)} \quad , \quad H(q, \theta) = \frac{1}{A(q)} \tag{2.8}$$

The model structure defined in Equation 2.4 will also be referred to as an ARX structure, where AR refers to the autoregressive part $A(q)y(t)$ and X to the extra input $B(q)u(t)$. Notice that q, the argument of $A(q)$ and a polynomial in q^{-1}, is used to be consistent with the definition of the z-transform and Fourier transform, see Equation 2.9.

$$G(z) = \sum_{k=1}^{\infty} g(k) z^{-k} \tag{2.9}$$

Where $G(z)$ is the z-transform of $g(k)_1^\infty$. Thus, the transfer function $G(q)$ from u to y, $y(t) = G(q)u(t)$, will be denoted as

$$G(q) = \sum_{k=1}^{\infty} g(k) q^{-k} \tag{2.10}$$

In order to be consistent with Equation 2.9.

General Models

Furthermore, the structure presented in Equation 2.3 can be expanded to a general family of model structures, consisting of the five polynomials A, B, C, D and F, resulting in Equation 2.11.

$$A(q)y(t) = \frac{B(q)}{F(q)}u(t) + \frac{C(q)}{D(q)}e(t) \tag{2.11}$$

Depending on which of the five polynomials in Equation 2.11 that are used, this general structure can result in 32 different model sets. Table 2.1 shows some of these model structures.

Polynomials Used in Equation 2.11	Name of Model Structure
B	FIR
AB	ARX
ABC	ARMAX
AC	ARMA
ABD	ARARX
$ABCD$	ARARMAX
BF	OE
$BFCD$	BJ

Table 2.1: Some common black-box SISO models as special cases of Equation 2.11. Based on Table 4.1 in Ljung (1999). MA refers to moving average, FIR to finite input response, OE to output error and BJ to Box-Jenkins.

Linear Regression

The white noise in Equation 2.4 is assumed to go through the denominator dynamics of the system, $A(q)$, before being added to the output, which from a physical point of view might seem odd. Nevertheless, the predictor of the equation error model set defines a linear regression, which makes the structure a prime choice in many applications.

Thus, the predictor $\hat{y}(t|\theta)$ for Equation 2.4, presented in Equation 2.12, is referred to as linear regression since the predictor is a scalar product between a known data vector, $\varphi(t)$ and the parameter vector θ, see Equation 2.14

$$\hat{y}(t|\theta) = B(q)u(t) + [1 - A(q)]y(t) \tag{2.12}$$

With φ is given as

$$\varphi(t) = [-y(t-1) \cdots - y(t-n_a)u(t-1) \cdots u(t-n_b)]^T \tag{2.13}$$

Then the predictor can be presented as

$$\hat{y}(t|\theta) = \theta^T \varphi(t) = \varphi(t)^T \theta \tag{2.14}$$

2.1.3 Methods

System identification methods can roughly be categorized as parametric or non-parametric.

Parametric Estimation Methods

Parametric methods are model-based, which means that a set of candidate models has been selected and parametrized as a model structure using the parameter vector θ. The problem of determining or estimating θ then decides the best model within the model set.

In mathematical notation, a parameter estimation method is a mapping from the data Z^N to the set $D_{\mathcal{M}}$.

$$Z^N \to \hat{\theta}_N \in D_{\mathcal{M}} \tag{2.15}$$

Where $D_{\mathcal{M}}$ is the set of values over which θ ranges in a model structure and the data is defined by $Z^N = \{u(0), y(0), \cdots, u(N), y(N)\}$.

For parametric estimation methods, the candidate models have to be evaluated in some sense, preferably according to their ability to describe the observed data. The essence of a model is its ability to predict the output based on past measurements. Hence, a reasonable evaluation of a model is to judge its performance in respect of prediction.

A 1-step-ahead predictor is defined in Equation 2.16 and is called a predictor model. Notice that the predictor does not depend on $f_e(\cdot)$, just G and H.

$$\hat{y}(\theta|t) = H^{-1}(q,\theta)G(q,\theta)u(t) + [1 - H^{-1}(q,\theta)]y(t) \tag{2.16}$$

The prediction error given by a certain model can thus be formulated as

$$\varepsilon(t, \theta_*) = y(t) - \hat{y}(t|\theta_*) \tag{2.17}$$

Therefore, a ”good” model will be a model which produces small prediction errors. Ljung (1999) introduces two approaches to qualify what small in this sense should mean. One option is to form a scalar-valued norm or criterion function that measures the size of ε, while the other is to demand that $\varepsilon(t, \hat{\theta}_N)$ is uncorrelated with a given data sequence.

One example of the former approach are prediction-error identification methods (PEM), which is a general term for the family of approaches which minimizes a norm of the form presented in Equation 2.18.

$$\hat{\theta}_N = \hat{\theta}_N(Z^N) = \underset{\theta \in D_{\mathcal{M}}}{\arg\min}\, V_N(\theta, Z^N) \tag{2.18}$$

Where the criterion function $V_N(\theta, Z^N)$ is a well-defined scalar function of the model parameter θ, for given data Z^N and defined as

$$V_N(\theta, Z^N) = \frac{1}{N}\sum_{t=1}^{N} \ell(\varepsilon_F(t, \theta)) \tag{2.19}$$

Where the norm $\ell(\cdot)$ is a scalar-valued, often positive, function and ε_F is the prediction error filtered through a stable linear filter $L(q)$, which acts like frequency weighting.

Hence, particular methods associated with specific names are obtained as special cases of 2.18, depending on the choice of $\ell(\cdot)$, $L(\cdot)$, the model structure and, in some cases, the choice of the method by which the minimization is realized.

The least-squares method is one example of a special case of the PEM presented in Equation 2.18. With a quadratic norm and linear parametrization, the least-squares criterion for linear regression forms a quadratic function in θ.

With $L(q) = 1$ and $\ell(\varepsilon) = \frac{1}{2}\varepsilon^2$, the least-squares criterion for linear regression then becomes

$$V_N(\theta, Z^N) = \frac{1}{N}\sum_{t=1}^{N} \frac{1}{2}[y(t) - \hat{y}]^2 = \frac{1}{N}\sum_{t=1}^{N} \frac{1}{2}[y(t) - \varphi(t)\theta]^2 \tag{2.20}$$

The least-squares estimate, $\hat{\theta}_N^{LS} = \arg\min V_N(\theta, Z^N)$, can be solved using QR factorization, see Appendix A.1.

Furthermore, as an alternative to norms or criterion functions which measure the size of ε, a certain finite-dimensional vector sequence $\{\zeta(t)\}$ derived from Z^{-1}, may be selected such that a certain transformation of $\varepsilon(t, \theta)$ is uncorrelated with this sequence. Thus, the θ value which satisfies Equation 2.21 would be the best estimate of $\hat{\theta}_N$ based on the observed data.

$$\frac{1}{N}\sum_{t=1}^{N} \zeta(t)\alpha(\varepsilon(t, \theta)) = 0 \tag{2.21}$$

Where $\alpha(\varepsilon)$ is the chosen transformation of ε, typically $\alpha(\varepsilon) = \varepsilon$.

Moreover, Equation 2.19 can be expressed in the frequency-domain, Equation 2.22, using Parseval's relationship, see Appendix A.2.

$$V_N(\theta, Z^N) = \frac{1}{N}\frac{1}{2}\sum_{k=1}^{N} |E_N(2\pi k/N, \theta)|^2 \tag{2.22}$$

Where E_N is the Fourier transform of $\varepsilon(t, \theta)$.

Non-Parametric Estimation Methods

Non-parametric methods on the other hand, relay on the fact that the system model behavior is represented in the measurements. Therefore, non-parametric methods require rich data sets and will in theory model an infinite amount of parameters. Non-parametric methods determine the impulse responses or transfer functions of a system directly, without first selecting a restricted set of possible models.

In the frequency-domain, Fourier analysis can be utilized to estimate the transfer function from the input to the output.

$$\hat{\hat{G}}(e^{i\omega}) = \frac{Y_N(\omega)}{U_N(\omega)} \tag{2.23}$$

Where $\hat{\hat{G}}(e^{i\omega})$ is referred to as the empirical transfer function estimate (ETFE) and $Y_N(\omega)$ and $U_N(\omega)$ are the discrete Fourier transforms of the output and the input, respectively. Evidently, Equation 2.23 holds for $U_N(\omega) \neq 0$. Further, no other assumptions have been imposed than linearity, thus this estimate is called empirical.

2.2 Marine Craft Motion

The term marine craft includes semi-submersible, floating rigs as well as ships, submarines, high-speed craft, torpedoes, remotely operated and autonomous underwater vehicles and other propelled and powered structures.

Marine crafts experience motion in 6 DOF, as illustrated in Figure 2.2. The rigid-body translatory motions in the horizontal and vertical plane are defined as surge (x), sway (y) and heave (z), respectively. Rotation about the x-axis is defined as roll, while rotation about the y-axis is defined as pitch and yaw is defined as rotation about the z-axis.

The basis equation for all 6 DOF models considered in Fossen (2011) are defined in Equation 2.24.

$$\mathbf{M}\dot{\boldsymbol{\nu}} + \mathbf{C}(\boldsymbol{\nu})\boldsymbol{\nu} + \mathbf{D}(\boldsymbol{\nu})\boldsymbol{\nu} + \mathbf{g}(\boldsymbol{\eta}) + \mathbf{g}_0 = \boldsymbol{\tau} + \boldsymbol{\tau}_{wind} + \boldsymbol{\tau}_{wave} \tag{2.24}$$

Where

$$\boldsymbol{\eta} = [x, y, z, \phi, \theta, \psi]^T \tag{2.25a}$$

$$\boldsymbol{\nu} = [u, v, w, p, q, r]^T \tag{2.25b}$$

$\boldsymbol{\eta}$ and $\boldsymbol{\nu}$ are vectors for generalized velocities and position/Euler angles, respectively. The model matrices $\mathbf{M}$, $\mathbf{C}$ and $\mathbf{D}$ represents inertia, Coriolis and damping, respectively. $\mathbf{g}(\boldsymbol{\eta})$ is a vector of generalized gravitation and buoyancy forces, while $\mathbf{g}_0$ stores static restoring forces and moments due to ballast systems and water tanks. The generalized forces in 6 DOF is stored in the vector $\boldsymbol{\tau}$.

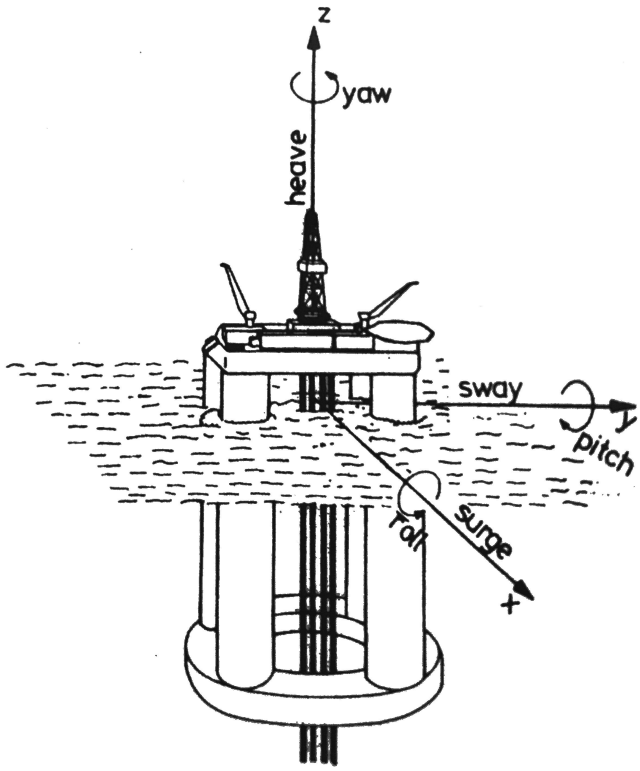

Figure 2.2: Rigid-body motions, illustrated on a deep concrete floater rig. Oscillatory translatory motions about the x-, y- and z-axis are referred to as surge, sway and heave, respectively. Oscillatory angular motions about the x-, y- and z-axis are defined as roll, pitch and yaw, respectively. Source: Faltinsen (1990), Figure 1.3.

2.2.1 Heave Equation of Motion

Equation 2.26 describes the undamped equation of motion in the mass-force domain for the heave motion in beam seas (Faltinsen, 1990) for a semi-submersible oil rig.

$$(M + A_{33})\frac{d^2\eta_3}{dt^2} + \rho g A_w \eta_3 = F_3(t) \tag{2.26}$$

Where A_w is the water plane area under the oil rig, η_3 is the heave displacement, M the mass and A_{33} the added mass which is defined by Salvesen et al. (1971), while F_3 is the hydrodynamic force in the z-direction. Lastly, g is the acceleration of gravity and ρ is the density of water.

The added mass and damping loads are steady-state hydrodynamic forces and moments due to forced harmonic rigid body motions (Faltinsen, 1990). The forced motion of the structure results in oscillating fluid pressures on the body. Forces and moments on the body can be found by integrating these fluid pressure forces over the body surface.

Equation 2.27 defines the force component due to harmonic motion mode, η_j in the x-, y- and z-direction for $k = 1, 2, 3$ and the moment components along the same axis for $k = 4, 5, 6$.

$$F_k = -A_{kj}\frac{d^2\eta_j}{dt^2} - B_{kj}\frac{d\eta_j}{dt} \tag{2.27}$$

Where A_{jk} is the added mass, B_{jk} is the damping coefficient and $j, k = 1, \cdots, 6$.

Specifically, the linear forced harmonic heave motion of a structure can be written as Equation 2.28. When the velocity potential is known, the pressure can be found by using a linearized Bernoulli's equation. The vertical force on the body can then be found by excluding the hydrostatic pressure and integrating the remaining pressure properly over the body. The linear part of this force is obtained by integrating the linearized pressure over the mean position of the body.

$$F_3 = -A_{33}\frac{d^2\eta_3}{dt^2} - B_{33}\frac{d\eta_3}{dt} \tag{2.28}$$

The added mass and damping coefficients depend on frequency and thereby the motion mode. Therefore, the added mass in heave for a body will not necessarily be the same as the added mass in sway.

2.2.2 Response Amplitude Operator

The major objective of this project is to estimate the RAO of an offshore oil rig to predict the heave motion.

The RAO of a marine craft describes how sea states affect the motion of the marine craft. Particularly, the vertical motion, heave, is of interest. Therefore, the RAO serves as a transfer function representing the relationship between the heave motion of the marine craft and the wave motion.

Specifically, the RAO is used to compute motion due to first- and second-order wave forces. The former describes wave-frequency motions observed as zero-mean oscillatory motions, while the latter are wave drift forces observed as nonzero slowly varying components.

The definition of RAO is based on the hypothesis that the relation between wave excitation and ship response is linear (Tannuri et al., 2003). This simplification is valid for small oscillations around the equilibrium position. However, nonlinear effects become relevant in critical situations where the ship response can reach high values. Moreover, the large number of mooring lines and risers increase the nonlinear viscous damping of the system.

Baghfalaki et al. (2012) present mathematical modeling of RAO and frequency-based analysis for coupled roll and yaw motions in regular waves. Generally, the RAO is represented in the frequency-domain with frequency-dependent excitation forces. Thus, frequency-dependent hydrodynamic coefficients are required to solve potential theory equations describing the RAO in the frequency-domain. The hydrodynamic coefficients and the wave force applied on the floating body is calculated based on the strip theory formulation by Salvesen et al. (1971).

The floating body, which is assumed to be rigid and slender, has six degrees of freedom (DOF) under the action of waves. Further, under the assumptions of linear and harmonic responses, lateral symmetry of the floating body, sinusoidal form of the indecent wave and by not considering the force component generated by the propeller, wind or current, the equation of motion in the frequency-domain representing linearly coupled conditions can be written as

$$\left[-\omega^2(M_{jk} + A_{jk}(\omega)) + i\omega B_{jk}(\omega) + C_{jk}\right] X_k(\omega)e^{i\omega t} = D_j F_j(\omega)e^{i\omega t} \tag{2.29}$$

for $j, k = 1, \cdots, 6$.

Here, M_{jk}, A_{jk}, B_{jk} and C_{jk} represent the mass, added mass, damping and restoring matrix coefficients, respectively. X_k is the displacement in the kth mode, while F_{jk} the wave force matrix and D_j is the wave amplitude of the jth mode of motion.

By rearranging Equation 2.29, the complex amplitude of the body in the jth mode in response to an incident wave of unit amplitude, frequency ω and direction θ, also known as the RAO, can be written as

$$Z_j(\omega, \theta) = \frac{X_k(\omega)}{D_j} = H_{jk}(\omega)^{-1} F_j(\omega) \tag{2.30}$$

Where

$$H_{jk} = -\omega^2(M_{jk} + A_{jk}(\omega)) + i\omega B_{jk}(\omega) + C_{jk} \tag{2.31}$$

From Equation 2.30, Baghfalaki et al. (2012) derive a decoupled 1-DOF Equation for the RAO, expressed in Equation 2.32.

$$Z_k(\omega, \theta) = \frac{F_k(\omega)}{-\omega^2(M_{kk} + A_{kk}(\omega)) + i\omega B_{kk}(\omega) + C_{kk}} \tag{2.32}$$

Furthermore, Fossen (2011) introduces two representations of the RAO; force RAO and motion RAO. For the former, the response will be generalized forces. In a linear system, however, it is possible to move the forces through a chain of integrators to obtain generalized position. The motion RAO can be used to translate wave amplitude to 1st-order wave-induced positions as illustrated in Figure 2.3.

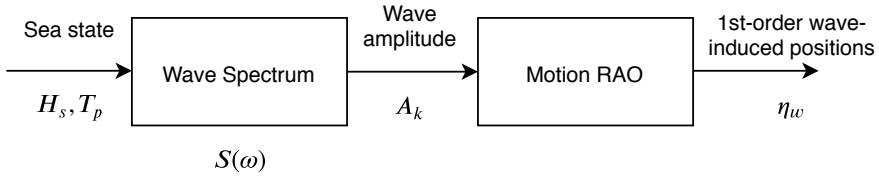

Figure 2.3: First-order wave-induced positions based on motion RAOs. The sea state parameters, significant wave height, H_s, and wave peak period, T_p, are the basis of a model wave spectrum, $S(\omega)$. The wave amplitude, A_k, is related to the wave spectrum by Equation 2.41 and together with the motion RAO, first-order wave-induced positions can be obtained. Remake of Figure 8.14 in Fossen (2011).

For motion RAOs, Fossen (2011) introduces the linear system in Equation 2.33.

$$[\mathbf{M}_{RB} + \mathbf{A}(\omega)]\ddot{\boldsymbol{\xi}} + \mathbf{B}(\omega)\dot{\boldsymbol{\xi}} + \mathbf{C}\boldsymbol{\xi} = \boldsymbol{\tau}_{wave1} \tag{2.33}$$

Where $\boldsymbol{\tau}_{wave1}$ are the 1st-order wave induced forces, $\mathbf{M}_{RB}$ is the rigid-body mass matrix, **A** the added mass matrix, **B** the damping matrix and **C** the spring stiffness matrix. The state vector, $\boldsymbol{\xi}$, represents perturbations with respect to a fixed equilibrium state.

Further, by assuming harmonic motions with $\bar{\boldsymbol{\xi}}$ as a vector of amplitudes, i.e.

$$\boldsymbol{\xi} = \bar{\boldsymbol{\xi}} \cos \omega t = \bar{\boldsymbol{\xi}} Re(e^{j\omega})$$

Then Equation 2.33, which is referred to as the seakeeping model by Fossen (2011), can be rewritten in the frequency domain as

$$-\omega^2[\mathbf{M}_{RB} + \mathbf{A}(\omega)]\bar{\boldsymbol{\xi}} - j\omega\mathbf{B}(\omega)\bar{\boldsymbol{\xi}} + \mathbf{C}\bar{\boldsymbol{\xi}} = \bar{\boldsymbol{\tau}}_{wave1} \tag{2.34}$$

Thus, the force-to-motion transfer function, Equation 2.35, is a low-pass filter representing the marine craft dynamics, which means that the first-order wave-induced position can be computed by low-pass filtering the generalized forces $\boldsymbol{\tau}_{wave1}$.

$$\mathbf{H}_v(j\omega) = \left[-\omega^2[\mathbf{M}_{RB} + \mathbf{A}(\omega)] - j\omega\mathbf{B}(\omega) + \mathbf{C}\right]^{-1} \tag{2.35}$$

Where the responses of Equation 2.34 can be written as

$$\bar{\boldsymbol{\xi}} = \mathbf{H}_v(j\omega)\bar{\boldsymbol{\tau}}_{wave1} \tag{2.36}$$

Moreover, the RAO can be obtained experimentally, either in full-scale or model-scale tests. However, wave-body interaction software are usually applied to perform the evaluation of RAOs (Tannuri et al., 2003). Nevertheless, such evaluations may introduce inaccuracies due to nonlinearities or loading conditions.

However, Fossen (2011) introduces several hydrodynamic programs based on potential theory which computes both force and motion RAOs. When the motion of the fluid can be approximated as two-dimensional, strip theory ((Salvesen et al., 1971) and (Faltinsen, 1990)), can be applied to estimate the hydrodynamic forces. In short, the principle of strip theory is to divide the underwater part of the ship into a number of strips. Hence, the 2D hydrodynamic coefficients for added mass can be computed for each strip and alternatively summed over the length of the body to obtain the three-dimensional coefficients.

Commonly used 2D programs which utilize strip theory are ShipX by MARINTEK, (Fathi), and Octopus Office by Armacon Inc. (Journée and Adegeest, 2003).

However, it is the 3D software program WAMIT, (Lee and Newman, 2006) which computes first- and second-order wave load transfer functions, among others, that has become the industry standard for the oil and gas industry. Specifically, the 3D panel code computes the linear wave forcing and motion characteristics of an offshore structure in the frequency domain (Ramachandran et al., 2013).

An alternative approach to the motion RAO in Figure 2.3 is to formulate the RAO as a state-space model where the wave spectrum is approximated by a linear filter. Additionally, the response of the motion RAOs and the linear marine craft dynamics in cascade can be modeled as constant tunable gains.

$$\mathbf{K} = \text{diag}\left\{K^{(1)}, K^{(2)}, K^{(3)}, K^{(4)}, K^{(5)}, K^{(6)}\right\}$$

Thus, the RAO model can be approximated as

$$\mathbf{H}_{rao}\mathbf{H}_v \approx \mathbf{K} \tag{2.37}$$

Where $\mathbf{H}_{rao}$ is the wave amplitude-to-force transfer function and $\mathbf{H}_v$ is the force-to-motion transfer function given by 2.35.

With Equation 2.37, the system can be illustrated as 2.4, where $\mathbf{H}_s(s)$ is the linear wave spectrum approximation, introduced in Section 4.1.3.

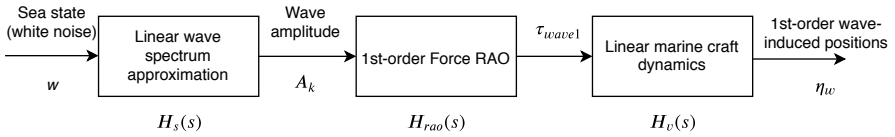

Figure 2.4: First-order wave-induced positions based on force RAOs. The linear approximation of the wave spectrum is obtained by Equation 4.6. The wave amplitude, A_k, is related to the wave spectrum by Equation 2.41 and together with the first-order force RAO and the linear marine craft dynamics, first-order wave-induced positions are obtained. Remake of Figure 8.15 in Fossen (2011).

Figure 2.5 shows the RAO for an actual oil rig for wave directions from $0°$ to $180°$ as a function of frequencies. The data is provided by Heavelock AS.

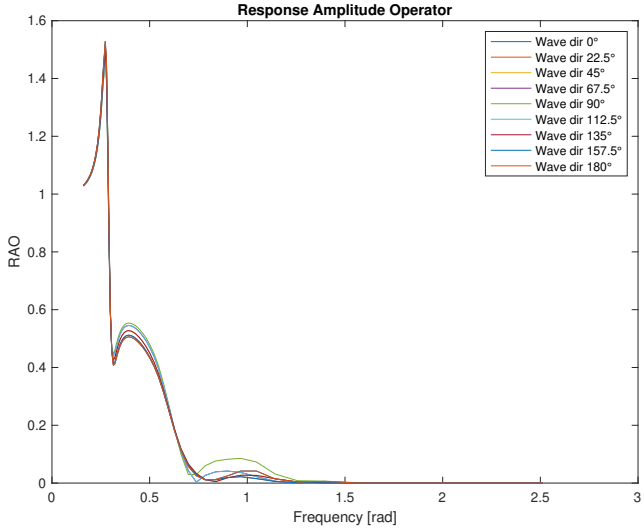

Figure 2.5: Response Amplitude Operator (RAO) for an actual oil rig as a function of frequencies for wave directions ranging from $0°$ to $180°$. Data provided by Heavelock AS.

Moreover, Clauss et al. (1992), Aarsnes et al. (2013), Molland (2008) and Tupper (2013) argue that the energy spectrum of the heave motion, S_h is related to the wave energy spectrum, S_w by the square of the RAO, see Equation 2.38.

$$S_h(\omega) = RAO(\omega)^2 S_w(\omega) \tag{2.38}$$

Thus, the RAO could be formulated as

$$RAO(\omega)^2 = \frac{S_h(\omega)}{S_w(\omega)} \tag{2.39}$$

2.3 Wave Spectrum Theory and Models

Statistical estimates of ocean waves can be obtained by simulating irregular waves using linear theory (Faltinsen, 1990). In the time domain, the wave elevation propagating along the positive x-axis can be represented as a sum of wave components, see Equation 2.40.

$$\zeta = \sum_{j=1}^{N} A_j \sin\left(\omega_j t - k_j x + \epsilon_j\right) \tag{2.40}$$

Where A_j is the wave amplitude, ω_j the circular frequency, k_j the wave number and ϵ_j the random phase angel.

Moreover, the wave amplitude is related to the frequency domain by the following equation

$$\frac{1}{2} A_j^2 = S(\omega_j)\Delta\omega \tag{2.41}$$

$S(\omega)$ being the wave spectrum and $\Delta\omega$ the constant difference between successive frequencies.

The wave spectrum can be estimated from measurements, assuming that the sea can be described as a stationary process. In practice, this means that the time frame is limited, from about $\frac{1}{2}$ hour up to 10 hours.

Furthermore, DNV (2010) defines the wave spectrum as the power spectral density (PSD) function of the vertical sea surface displacement.

The wave spectrum can either be represented as a function of frequencies, ω, and wave directions, θ, which is often referred to as a two-dimensional (2D) spectrum, or as a spectral density per frequency function, a one-dimensional (1D) spectrum.

2.3.1 Sea State Parameters

From the 1D wave spectrum, so-called integrated parameters, or sea state parameters can be obtained. These are often used to describe empirical wave spectra such as JONSWAP and Torsethaugen spectra.

The wave spectrum can be described by means of spectral moments, a series of characteristic numbers (Fossen, 2011), see Equation 2.42.

$$m_k := \int_0^\infty \omega^k S(\omega) d\omega \tag{2.42}$$

And for $k = 0$, Equation 2.42 can be simplified to Equation 2.43

$$m_0 = \int_0^\infty S(\omega) d\omega \tag{2.43}$$

Where the variance of the instantaneous wave elevation, which is Gaussian distributed with zero mean, is related to the first spectral moment by Equation 2.44.

$$\sigma^2 = m_0 \tag{2.44}$$

σ being the root-mean-square (RMS) value of the wave spectrum. This can be related to the definition of significant wave height, the mean of the one third highest waves by Equation 2.45.

$$H_s = 4\sigma = 4\sqrt{m_0} \tag{2.45}$$

Another important sea state parameter, the modal or peak frequency, ω_0, is derived by requiring that

$$\left(\frac{dS(\omega)}{d\omega} \right)_{\omega=\omega_0} = 0 \tag{2.46}$$

Hence, the peak frequency will be the frequency associated with the most energetic wave. Consequently, the modal period or wave peak period can be defined as

$$T_0 = T_p = \frac{2\pi}{\omega_0} \tag{2.47}$$

Lastly, the average wave period is defined as

$$T_1 = 2\pi \frac{m_0}{m_1} = 0.834 T_0 \tag{2.48}$$

2.3.2 The JONSWAP Spectrum

Parts of this section is based on the specialization project by Vettestad (2019).

From 1968 to 1969 Hasselmann et al. (1973) conducted a comprehensive measurement program in the North Sea between Iceland and Sylt, a German island, known as the Joint North Sea Wave Project (JONSWAP). In 1984 the 17th International Towing Tank Conference (ITTC) adopted the results from the measurement program as an ITTC standard.

The JONSWAP spectrum, which is a single-peaked, non-directional spectrum for wind seas, is presented as a function of integrated wave parameters, such as significant wave height, H_s, and average wave period, T_1. The spectral density function is defined by Fossen (2011) and Faltinsen (1990) as

$$S(\omega) = 155 \frac{H_s^2}{T_1^4} \omega^{-5} \exp\left(\frac{-944}{T_1^4} \omega^{-4} \right) \gamma^Y \tag{2.49}$$

, where Y is defined as

$$Y = \exp\left[-\left(\frac{0.191\omega T_1 - 1}{\sqrt{2}\sigma}\right)\right] \tag{2.50}$$

And σ, the spectral width parameter, is defined as

$$\sigma = \begin{cases} 0.07 & \omega \leq \frac{5.24}{T_1} \\ 0.09 & \omega > \frac{5.24}{T_1} \end{cases} \tag{2.51}$$

Hasselmann et al. (1973) suggest setting the non-dimensional peak shape parameter to the average value $\gamma = 3.3$. Increasing γ will result in a sharper peak in the spectrum.

However, Sørensen (2018) suggests representing Equation 2.49 as

$$S(\omega) = \alpha \frac{g^2}{\omega^5} \exp\left[-\frac{5}{4}\left(\frac{\omega_p}{\omega}\right)\right] \gamma^Y \tag{2.52}$$

Where g is the gravity constant and α is defined as

$$\alpha = 0.2 \frac{H_s^2 \omega_p^2}{g^2} \tag{2.53}$$

And Y from Equation 2.50 is rewritten as

$$Y = \exp\left[-\frac{1}{2}\left(\frac{\omega - \omega_p}{\sigma\omega}\right)^2\right] \tag{2.54}$$

Directly from Equation 2.47 and 2.48, we see that Equation 2.51 can be written as

$$\sigma = \begin{cases} 0.07 & \omega \leq \omega_0 \\ 0.09 & \omega > \omega_0 \end{cases} \tag{2.55}$$

Moreover, DNVGL (2018) emphasizes that the operational range for the JONSWAP spectrum is

$$3.6 < \frac{T_p}{\sqrt{H_s}} < 5 \tag{2.56}$$

and that the spectrum should be used with caution outside this interval. Additionally, $\gamma = 3.3$ is just an average value for experimental data, therefore DNVGL (2018) suggests that the peak shape parameter should be defined as

$$\gamma = \begin{cases} 5 & \frac{T_p}{\sqrt{H_s}} \leq 3.6 \\ \exp(5.75 - 1.15\frac{T_p}{\sqrt{H_s}}) & 3.6 < \frac{T_p}{\sqrt{H_s}} < 5 \\ 1 & \frac{T_p}{\sqrt{H_s}} \geq 5 \end{cases} \tag{2.57}$$

2.3.3 The Torsethaugen Spectrum

The Torsethaugen wave spectrum is a two-peaked spectrum and was originally developed by fitting two JONSWAP spectra to average measured spectra from the Norwegian Continental Shelf (Torsethaugen, 1993). The sea states were grouped with respect to wave peak period, T_p, and significant wave height, H_s.

For peak frequencies $\omega_0 > 0.6$rad/s two characteristic peaks in the spectrum appear, while $\omega_0 < 0.6$rad/s results in a single-peaked spectrum where swell dominates, i.e. low frequency waves (Fossen, 2011).

The Torsethaugen spectrum is defined by Equation 2.58 (Torsethaugen, 1993).

$$S(f_n) = \sum_{j=1}^{2} E_j S_{jn}(f_{jn}) \tag{2.58}$$

Where $j = 1$ is defined as the primary sea system and $j = 2$ as the secondary sea system. And E_1, E_2 is specified as Equation 2.59.

$$E_1 = \frac{1}{16} H_1^2 T_{p1} \quad , \quad E_2 = \frac{1}{16} H_2^2 T_{p2} \tag{2.59}$$

Additionally, S_{jn} is defined by Equation 2.60

$$S_{1n}(f_{1n}) = G_0 A_\gamma f_{1n}^{-4} e^{f_{1n}^{-4}} \gamma^{(exp-(1/2\sigma^2)(f_{1n}-1)^2)} \tag{2.60a}$$
$$S_{2n}(f_{2n}) = G_0 f_{2n}^{-4} e^{f_{2n}^{-4}} \tag{2.60b}$$

Where $G_0 = 3.26$, $A_\gamma = (1 + 1.1[ln\gamma]^{1.19})/\gamma$, $f_{1n} = f \cdot T_{p1}$, $f_{2n} = f \cdot T_{p2}$ and

$$\sigma = \begin{cases} 0.07 & f_n < 1 \\ 0.09 & f_n > 1 \end{cases} \tag{2.61}$$

For wind sea dominated cases, i.e. where the wave peak period is less than the spectral peak period for fully developed sea, $T_p < T_{pf}$, the resulting parameters are defined as

$$H_1 = H_{w1} = R_w H_s \quad , \quad R_w = (1 - a_{10}) e^{-(\epsilon_l / a_1)^2} + a_{10} \tag{2.62a}$$
$$T_{p1} = T_{pw1} = T_p \tag{2.62b}$$
$$\gamma_{w1} = k_g s_p^{6/7} \quad , \quad s_p = \frac{2\pi}{g} \frac{H_{w1}}{T_{pw1}^2} \tag{2.62c}$$
$$H_2 = H_{w2} = (1 - R_w^2)^{1/2} H_s \tag{2.62d}$$
$$T_{p2} = T_{pw2} = T_{pf} + b_1 \tag{2.62e}$$
$$\gamma_{w2} = 1 \tag{2.62f}$$

For swell sea dominated cases, i.e. where $T_p > T_{pf}$, the resulting parameters are

defined as

$$H_1 = H_{s1} = R_s H_s \quad , \quad R_s = (1 - a_{20})e^{-(\epsilon_u/a_2)^2} + a_{20} \tag{2.63a}$$

$$T_{p1} = T_{ps1} = T_p \tag{2.63b}$$

$$\gamma_{s1} = k_g s_f^{6/7}(1 + a_3\epsilon_u) \quad , \quad s_f = \frac{2\pi}{g}\frac{H_s}{T_{pf}^2} \tag{2.63c}$$

$$H_2 = H_{s2} = (1 - R_s^2)^{1/2} H_s \tag{2.63d}$$

$$T_{p2} = T_{ps2} = a_f H_{s2}^{1/3} \tag{2.63e}$$

$$\gamma_{s2} = 1 \tag{2.63f}$$

Where the empirical parameters are defined in Table 2.2 and the non-dimensional scales for the spectral peak period are defined as

$$\epsilon_l = \frac{T_{pf} - T_p}{T_{pf} - T_l} \tag{2.64}$$

For wind sea and

$$\epsilon_u = \frac{T_p - T_{pf}}{T_u - T_{pf}} \tag{2.65}$$

For swell sea.

Parameter	Value	Unit
a_f	6.6	$\text{sm}^{1/3}$
a_e	2.0	$\text{sm}^{1/3}$
a_u	25.0	s
a_1	0.5	[]
a_{10}	0.7	[]
a_2	0.3	[]
a_{20}	0.6	[]
a_3	6.0	[]
b_1	2.0	s
k_g	35.0	[]

Table 2.2: The empirical parameters for the Torsethaugen wave spectrum defined by Torsethaugen (1993).

Figure 2.6 shows the Torsethaugen spectrum compared with a JONSWAP spectrum with $\gamma = 1$, from DNVGL (2018), and a JONSWAP spectrum with $\gamma = 3.3$, for $H_s = 5$m and $T_p = 12$s, leading to a peak frequency of $\omega_0 = 0.52$rad/s, which is why the Torsethaugen wave spectrum is single-peaked.

Moreover, Figure 2.7 shows the two-peaked Torsethaugen spectrum compared with JONSWAP spectra with $\gamma = 5$, from DNVGL (2018), and $\gamma = 3.3$ for $H_s = 5$m and $T_p = 4$s and thereby a peak frequency of $\omega_0 = 1.57$rad/s.

These examples are inspired by Figure 8.10 in Fossen (2011). Notice that the latter example, Figure 2.7, does not necessarily reflect a real sea state.

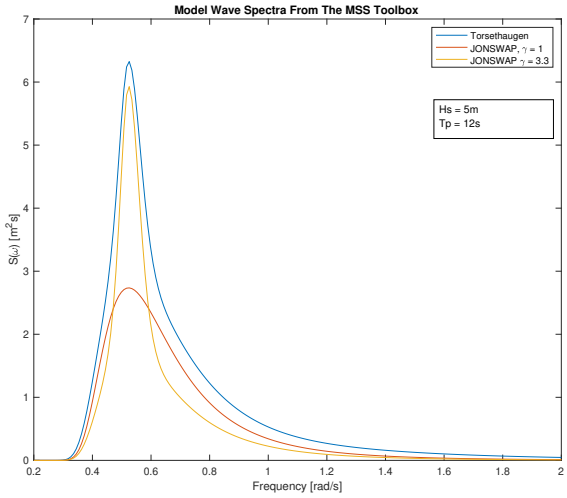

Figure 2.6: The Torsethaugen wave spectrum compared with a JONSWAP model with $\gamma = 1$ and $\gamma = 3.3$. The spectra are generated with the Marine Systems Simulator Toolbox by Fossen and Perez (2009). Here, the significant wave height is 5m, the wave peak period is 12s and peak frequent is 0.5236rad/s which is why the Torsethaugen is a single-peaked spectrum.

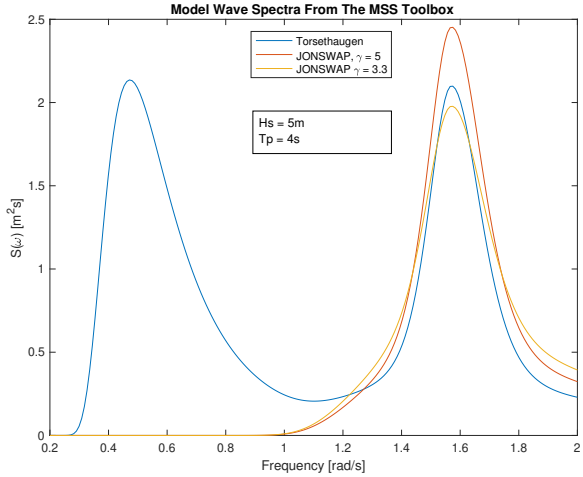

Figure 2.7: The Torsethaugen wave spectrum compared with a JONSWAP model with $\gamma = 5$ and $\gamma = 3.3$. The spectra are generated with the Marine Systems Simulator Toolbox by Fossen and Perez (2009). Here, the significant wave height is 5m, the wave peak period is 4s and peak frequent is 1.5708rad/s which is why the Torsethaugen is a two-peaked spectrum.

Chapter 3

An Overview of Available Data

One important aspect of this project was to investigate the available data format and its availability. The data format sets the outlines of the project and will give an indication of what it is possible to achieve. Additionally, the available data format will be an important factor when choosing the final estimation and prediction methodology.

This chapter will give an overview of the anticipated available data, both from the oil rig and from weather observation and forecast services. Taking into account the scope of this project, forecasts, observations or actual measurements of sea states and rig heave motion are of particular interest.

3.1 Weather Observations and Forecasts

Ideally, measurements of wave elevation and heave amplitude were available. However, sea state variables such as significant wave height and wave peak period can be used to calculate a model spectrum which together with heave amplitude measurements can give valuable information about the system. However, wave spectra will not provide information about the phasing between waves and rig heave motion.

3.1.1 StormGeo

One of the leading weather services for the oil and gas industry, StormGeo, offers offshore weather forecasts and motion forecasts of the rig. However, according to Roar Inge Hansen, Offshore Duty Forecaster at StormGeo, they do not have their own ocean wave measurements and referred to Equinor ASA for further details.

3.1.2 The Norwegian Meteorological Institute

The Norwegian Meteorological Institute offers multiple weather forecast and observation services. The online weather service, Yr, provides detailed weather forecasts and are

unique in the sense that they operate with a free data access policy (The Norwegian Meteorological Institute). Yr offers weather forecasts for about 1 million places in Norway and 10 million places worldwide, including oil platforms in the North Sea and the Norwegian Sea.

The data format available for download are either XML or GRIB. The latter option is well suited for chart plotters. However, neither give access to historical weather data and the XML files does not contain information about wave height or period.

Lastly, the Norwegian Meteorological Institute operates the data server `thredds.met.no` which contains ocean and ice models. Additionally, the data server provides free access to historical ocean wave forecasts. The Norwegian Meteorological Institute runs the wave model, MyWaveWam (Behrens, 2013), four times a day on a 4km grid covering Europe and the Arctic, resulting in four NetCDF weather forecast files each day. Additionally, the model is run twice daily with European Centre for Medium-Range Weather Forecasts (ECMWF) for rand values to provide weather forecasts 66 hours ahead.

The wave model solves the wave transport equation without any presumptions regarding the shape of the wave spectrum. As a result, the MyWaveWam model is more complex than idealized spectra based on empirical functions such as JONSWAP or Torsethaugen.

The integrated 1D wave spectrum is defined in Equation 3.1, where $F(f, \theta)$ is the 2D wave spectrum resulting from the wave transport equation.

$$E(f) = \int_0^{2\pi} F(f, \theta) d\theta \tag{3.1}$$

The parameters of interest from the forecast files are listed in Table 3.1. Implementation specific details are presented in Chapter 4.

Parameter	Unit	Description
Significant wave height	m	Calculated from the wave spectrum, see Equation 2.45
Wave peak period	s	Calculated from the wave spectrum, see Equation 2.47

Table 3.1: Sea state parameters from the Norwegian Meteorological Institute's data server `thredds.met.no`, which contains wave forecasts for Europe and the Arctic, among others.

3.2 Actual Measurements From An Oil Rig

Fortunately, Senior Engineer at Equinor ASA, Rune Bjørkli, provided access to actual wave radar measurements. The given data contains 1D wave spectrum and sea state parameters with a sampling rate of approximately 20 minutes.

The measurements are based on a wave radar of the MIROS SM-050 type, which uses a dual-footprint pulse Doppler method to measure waves (Miros Group, 2019). From a distance of 180 to 450 meters, depending on a installation height typically ranging from 25 to 80 meters, the wave radar observes the ocean surface in a semi-circle.

The parameters from the data set utilized in this project are presented in Table 3.2. The given wave spectrum represents the actual sea state and therefore no assumptions regarding the spectrum are made.

The measured spectrum and a model spectrum based on measured significant wave height and wave peak period are both used in the methods presented in Chapter 4.

Parameter	**Unit**	**Description**
Wave spectrum	m^2s	One-dimensional wave spectrum
Frequencies	Hz	Ranges from 0.03-0.3Hz with a resolution of 0.0078Hz
Significant wave height	m	Calculated from the wave spectrum, see Equation 2.45. Resolution of 0.1m and accuracy of $\pm 0.2m$ for $0 < Hs < 4$ and $\pm 5\%$ for $4 < Hs < 30$
Wave peak period	s	Calculated from the wave spectrum, see Equation 2.47. Resolution of 0.1s and an accuracy of $\pm 5\%$

Table 3.2: Wave parameters provided by Equinor based on measurements from a MIROS SM-050 wave and current radar. The sampling rate is 20 minutes and the data set provides data from 67 hours, which only 44 hours has associated heave amplitude measurements. Information regarding the resolution and accuracy of the parameters are specified in the wave radar datasheet (Miros Group, 2019).

Additionally, Senior Engineer Bjørkli gave access to associated heave amplitude measurements in meters with a sampling rate of 1 second. Since the wave peak period ranges in a rate of seconds, a lower sampling rate would not be able to capture the full impact ocean waves has on the vertical rig motion.

Table 3.3 shows the median, mean, maximum and minimum values of the given significant wave height and wave peak period in addition to the heave amplitude.

Parameter	**Median**	**Mean**	**Max**	**Min**
Significant Wave Height [m]	5.6796	5.6107	9.1471	2.8088
Wave Peak Period [s]	9.8462	11.1846	16.0000	7.5294
Heave Amplitude [m]	0.0000	0.0022	3.6700	-3.8800

Table 3.3: Statistical analysis of the sea state parameters and the heave amplitude from the data provided by Equinor ASA. Specifically, the median, mean, maximum and minimum values for the significant wave height, the wave peak period and the heave amplitude.

The given rig heave amplitude is illustrated in Figure 3.1. The heave amplitude is measured at approximately the center of the unit, thus representing a pure heave motion of the unit unaffected by other degrees of freedom. The measurements are obtained from a Motion Reference Unit (MRU), a common measuring device for marine applications which utilizes accelerometers and gyros.

Further details about the measurements have not been received.

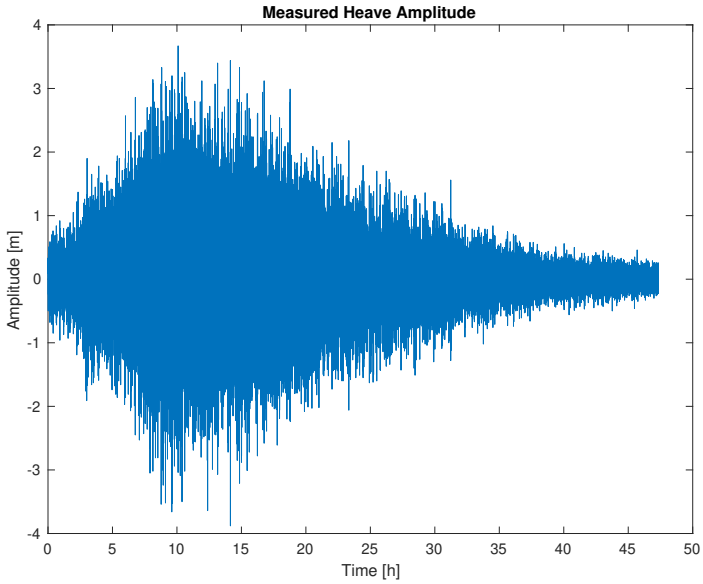

Figure 3.1: The rig heave amplitude from the given data set measured by a MRU and provided by Equinor ASA. The median, mean, maximum and minimum values of the rig heave is presented in Table 3.3.

Chapter 4

The Implementation of the Proposed RAO Estimation and Heave Prediction Methods

This chapter will present implementation specific details regarding the proposed RAO estimation and heave prediction methods. Specifically, two methods are introduced: a parametric method with an ARX model describing the heave motion dynamics and a non-parametric method based on Equation 2.39.

The two proposed methods are implemented with both measured wave spectrum and model wave spectrum based on the data set introduced in Section 3.2, as well as the measured heave amplitude.

Furthermore, the performance will be demonstrated in Chapter 5, 6 and 7.

4.1 A Parametric Method for RAO Estimation and Heave Prediction

As described in Section 2.1.3, system identification methods are classified as parametric when a priori assumptions are made regarding the structure of the dynamics. In other words, the system is expected to behave as a predefined model structure.

As introduced in Section 2.2.2, Fossen (2011) and Faltinsen (1990) represents the equation of motion in the vertical direction, heave, of a marine craft as a modified mass-spring-damper system. Moreover, the mathematical model of the RAO derived by Baghfalaki et al. (2012) also has the form of a mass-spring-damper system. However, simplifications need to be made in order to obtain a linear and decoupled system. Therefore, the heave motion is assumed to be decoupled from other degrees of freedom and will be simplified to a single-input single-output (SISO) system defined by Equation 4.1.

$$u = m\ddot{y} + d\dot{y} + ky \tag{4.1}$$

Where m is the mass, d the damping coefficient and k the spring constant. The equation is derived from Newton's second law.

The input to the system, u, is wave elevation and the output, y, is heave motion. However, the available data set does not include measurements of wave elevation, see Section 3.2. Therefore, the system has to be expressed in the frequency domain, resulting in an approximation of wave elevation generated by a model wave spectrum as described in Section 4.1.3.

The parametric method is implemented using the System Identification Toolbox in MATLAB (Ljung, 2014), based on Ljung (1999).

4.1.1 Model Structure

As described in Section 2.1, an important step in the system identification procedure is to decide the model structure. The mass-spring-damper system is expressed using an input-output relation often referred to as an equation error or ARX structure (Ljung, 1999), expressed as Equation 2.4. Eventually, Equation 2.4 can be rewritten as Equation 2.3 with

$$G(q,\theta) = \frac{B(q)}{A(q)} \quad , \quad H(q,\theta) = \frac{1}{A(q)} \tag{4.2}$$

For a SISO mass-spring-damper system, the order of the system matrices are $n_a = 2$, $n_b = 1$ and $n_h = 1$. Some experiments regarding the system order have been performed, however with little influence on the performance.

4.1.2 Estimation Algorithm

The model structure is implemented using the `arx` MATLAB function (MathWorks). The parametric method functions from the System Identification Toolbox in MATLAB, based on Ljung (1999), serve both as model structure and estimation algorithm.

Equation 4.1 can be rewritten as

$$y = \theta^T \varphi \tag{4.3}$$

Where θ holds the unknown parameters m, d and k, and φ is the known data vector.

The parameters, θ, are estimated using a least-squares method, see Section 2.1.3. The equation error model set predictor defines a linear regression, see Section 2.1.2, which makes this model structure particularly useful in describing basic linear and nonlinear systems
(Ljung, 1999).

The least-squares estimate is solved by QR factorization, see Appendix A.1, meaning that the ARX model parameters are estimated using Equation 4.4.

$$(J^T J)\theta = J^T y \tag{4.4}$$

Where J is the regressor matrix and y is the measured output. Thus, the parameter vector can be expressed as

$$\theta = (J^T J)^1 J^T y \tag{4.5}$$

4.1.3 Input and Output Generation

As described by Fossen (2011), the wave spectrum can be approximated by a second-order system with relative degree one, see Equation 4.6.

$$h(s) = \frac{K_w s}{s^2 + 2\lambda\omega_0 s + \omega_0^2} \tag{4.6}$$

Where the gain constant $K = 2\lambda\omega_0\sigma$, the dominating wave frequency ω_0 is defined by Equation 2.47 and σ, the wave intensity constant, is defined by Equation 4.7.

$$\sigma^2 = \max_{0<\omega<\infty} S(\omega) \tag{4.7}$$

The damping coefficient λ can be computed using a nonlinear least-squares curve fitting approach where the PSD function, Equation 4.8, fits the wave spectrum (Fossen and Perez, 2009).

$$P(\omega) = |h(j\omega)|^2 = \frac{4(\lambda\omega_0\sigma)^2\omega^2}{(\omega_0^2 - \omega^2)^2 + 4(\lambda\omega_0\omega)^2} \tag{4.8}$$

Ultimately, white noise is given as input to the transfer function $h(s)$ to generate wave elevation. This will serve as input to the mass-spring-damper model, see Figure 4.1. The transfer function in the Wave Generation block is an implementation of Equation 4.6 and inspired by the Marine Systems Simulator Toolbox by Fossen and Perez (2009).

The wave elevation will act as the applied force to the mass-spring-damper system, resulting in rig heave amplitude as output y for the Simulink system.

Now, the resulting input and output from Figure 4.1 will be represented in the time domain. However, as previously emphasized, the available data set does not contain wave elevation, only measured wave spectrum and sea state parameters. Therefore, the model needs to manage frequency domain input and output data. Thus, the final input and output data for the ARX model are the discrete Fourier transforms of the data generated in Simulink.

More precisely, the generated input based on measurements and the measured output are used to create an `iddata` object which is transformed to the frequency domain using discrete Fourier transform. However, this transformation has to be done carefully. Transforming the input and output data directly using the MATLAB function `fft` would give a two-sided spectrum with frequencies ranging from the negative half of the Nyquist frequency to the positive half of the Nyquist frequency.

However, the MATLAB `fft` function with an `iddata` object as input returns a frequency-domain `iddata` object with frequencies ranging from 0 to the Nyquist frequency. In order to preserve the signal power and noise level, the fast Fourier transforms (FFT) are normalized by dividing each transform by the square root of the length of the

original time-domain signal. This would be equivalent to taking the discrete Fourier transform of the time-domain input or output signal, y, and computing the one-sided spectrum from the first half of the FFT divided by the square root of the length of y:

$$\begin{aligned} Y &= \text{fft}(y) \\ N &= \text{length}(y) \\ P1 &= \frac{Y(1:N/2)}{\sqrt{N}} \end{aligned}$$

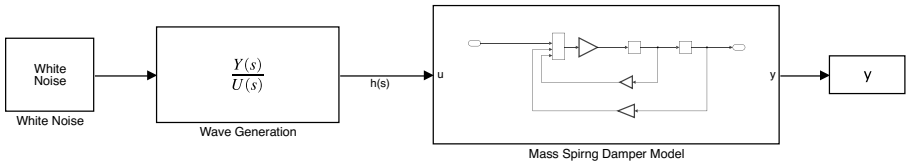

Figure 4.1: The Simulink model which generates data from a known mass-spring-damper system. The linear approximation of the wave amplitude, $h(s)$, expressed by Equation 4.6 is implemented in the Simulink block Wave Generation. Together with the Mass Spring Damper Model, Equation 4.1, the Simulink model generated heave amplitude, y.

Measured Wave Spectrum as Input

As described in Section 3.2, the given data set includes a 1D wave spectrum from a MIROS wave radar. Therefore, to minimize sources of error, the parametric method was tested with the measured wave spectrum. However, the input to the ARX model is still the linearly approximated wave response, $h(s)$ defined by Equation 4.6, but the spectrum which is approximated is the 1D wave spectrum from the given data set.

Model Wave Spectrum as Input

Furthermore, as a 1D wave spectrum from a wave radar might not always be accessible, the ARX model was tested with a model wave spectrum as well.

After trial and error, the Torsethaugen model spectrum was used in the final implementation with significant wave height and wave peak period from the given measurements. Specifically, the model wave spectrum was implemented with the Marine Systems Simulator Toolbox by Fossen and Perez (2009) and their `wavespec` function which implements the JONSWAP and Torsethaugen spectra as described in Section 2.3.2 and 2.3.3, respectively.

However, the model wave spectrum is evaluated for frequencies in radians per second, while the measured wave spectrum is in Hz. According to DNV (2010) a spectrum $S(\omega)$, given as a function of angular frequencies, is related to the spectrum $S(f)$, given as a function of frequencies in Hz, by Equation 4.9.

$$S(\omega) = \frac{S(f)}{2\pi} \tag{4.9}$$

Thus, the model wave spectrum in radians per second is multiplied by a factor of 2π.

One drawback when using a model wave spectrum instead of the measured wave spectrum is that the model spectra are single-peaked and does not fully capture the sea state for particularly low frequencies, see Figure 4.2. As a result, the model spectra are approximately zero for these low frequencies and Equation 2.39 does not hold. Therefore, when a model spectrum is used as the input spectrum, the frequency vector ranges from 0.0547Hz instead of 0.0312Hz. This range was found by trial and error.

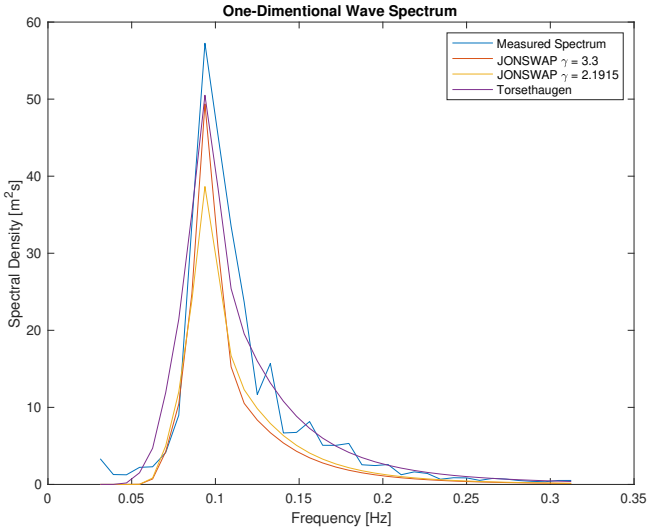

Figure 4.2: Measured wave spectrum compared with JONSWAP wave spectra with $\gamma = 3.3$ and $\gamma = 2.1915$, from Equation 2.57, and a one-peaked Torsethaugen spectrum. Notice the difference between the measured wave spectrum and the model wave spectra, specifically for low frequencies.

The area underneath the wave spectrum represents the total energy. Thus, the area underneath the model wave spectra should not differ much from the measured spectrum. Table 4.1 shows the total energy for the spectra illustrated in Figure 4.2. The model spectrum which most precisely captures the energy of the measured spectrum is the Torsethaugen spectrum.

Notice that this is an arbitrary example from the given data set, but the trend is that the Torsethaugen fits the measured spectrum better than the JONSWAP spectra.

Aarnes et al. (2019) validate 2D wave spectra obtained from ECMWF at the location of Gullfaks C. The 2D wave spectra has been compared against a Wavescan directional buoy and a Miros Doppler radar. Moreover, these spectra have been compared to model wave spectra, such as JONSWAP and Torsethaugen, both 2D and 1D, based on sea state parameters obtained from the 2D ECMWF spectra. Aarnes et al. (2019) conclude that the model, or idealized, spectra are only applicable in certain sea states which are typically less complex. Additionally, they found that the Torsethaugen wave spectrum is superior to JONSWAP in representing the observed 1D and 2D spectrum.

Spectrum	Area
Measured	299.8958
JONSWAP $\gamma = 3.3$	190.1251
JONSWAP $\gamma = 2.1915$	189.0640
Torsethaugen	302.8375

Table 4.1: The total energy of the measured and model wave spectra illustrated in Figure 4.2. The area underneath the wave spectrum represents the total energy. The Torsethaugen wave spectrum is the best fit to the measured wave spectrum.

Nevertheless, the input to the ARX model is still the linearly approximated wave response, $h(s)$ defined by Equation 4.6 with the model spectrum as the spectrum which is approximated.

4.1.4 Heave Prediction from Generated Data

In order to test the parametric method for RAO estimation and heave prediction, the ARX model was initially tested with an ideal case with generated wave and heave data from the Simulink system illustrated in Figure 4.1. By having full control of the system dynamics, i.e. the mass-spring-damper system, it is easier to identify implementation and fundamental errors. Thus, this case serves as a test for which the heave motion can be simplified to a SISO mass-spring-damper system.

The input data is generated based on arbitrary significant wave height and wave peak period values and these sea state parameters are used to generate a model wave spectrum.

After trial and error to obtain the desired dynamics, the parameter vector, θ, was set to

$$\theta = \begin{pmatrix} m \\ d \\ k \end{pmatrix} = \begin{pmatrix} 100 \\ 5 \\ 25 \end{pmatrix} \tag{4.10}$$

Validation

The model set for the ideal case was tested with three quarters of the measured input-output data while the remaining one quarter was used for validation. The measured output was compared with both simulated and predicted output from the identified model. The simulated model output is estimated based on measured input data and initial conditions. The predicted model output at some specified time in the future is based on measured input data and initial conditions in addition to measured output data (MathWorks, 2020d).

Specifically, the ideal case was tested using the MATLAB function `compare`, further explained in Section 4.1.6.

Figure 4.3 shows the magnitude and phase of the measured output compared with the magnitude and phase of the simulated model output. Figures 4.4, 4.5 and 4.6 shows the magnitude and phase of the measured output compared with the magnitude and phase of the predicted model output 1-step-ahead, 2-steps-ahead and 10-steps-ahead, respectively. The prediction time unit is seconds.

Increasing the prediction horizon results in a poorer estimate. As Ljung (1999) points out: *A model can never be accepted as a final and true description of the system.* Therefore, there will always be some prediction error which will accumulate over the increased prediction horizon.

Nevertheless, the ARX model works well with the generated input and output data, which makes it easier to debug the model tested with actual measurements.

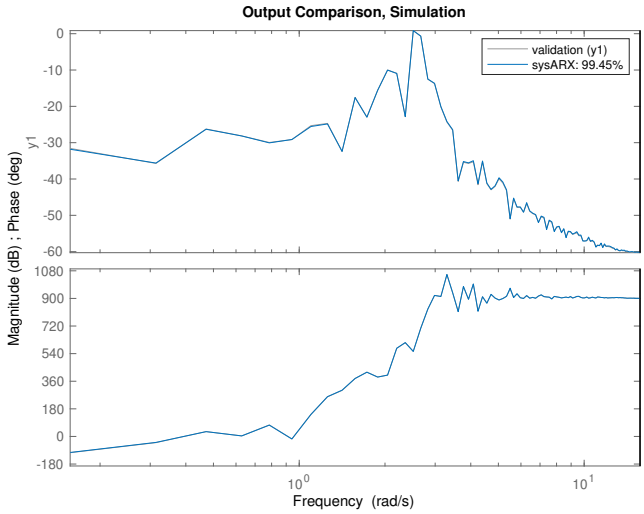

Figure 4.3: The simulated output response, sysARX, compared with the measured output response, validation. The plot is generated with the MATLAB `compare` function and the percentage in the upper right corner is the NRMSE fitness value where 100% is perfect fit.

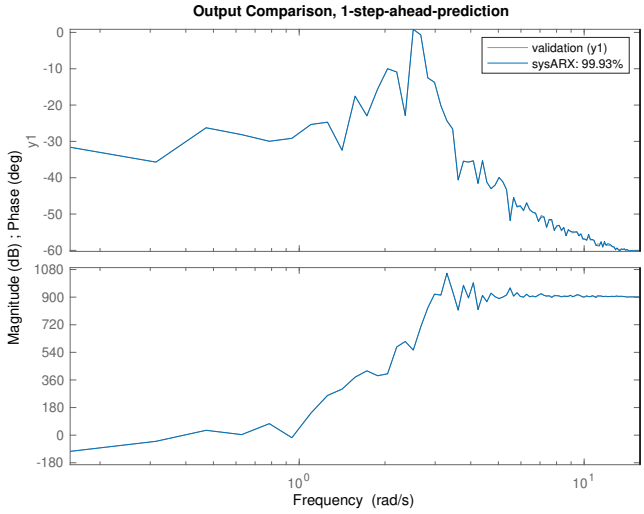

Figure 4.4: The 1-step-ahead predicted output response, sysARX, compared with the measured output response, validation. The plot is generated with the MATLAB `compare` function and the percentage in the upper right corner is the NRMSE fitness value where 100% is perfect fit.

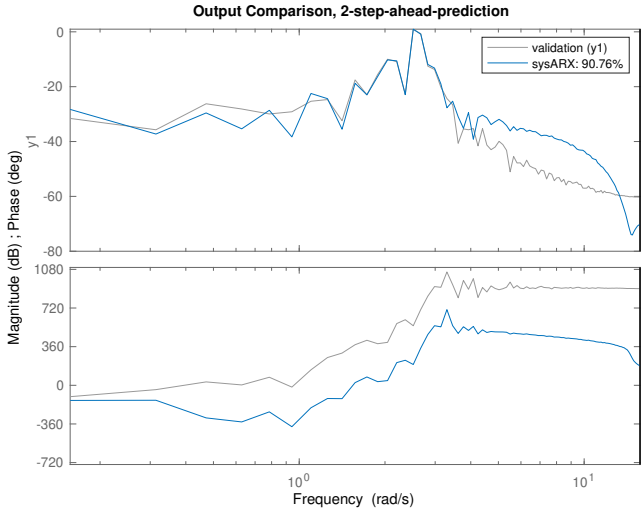

Figure 4.5: The 2-step-ahead predicted output response, sysARX, compared with the measured output response, validation. The plot is generated with the MATLAB `compare` function and the percentage in the upper right corner is the NRMSE fitness value where 100% is perfect fit.

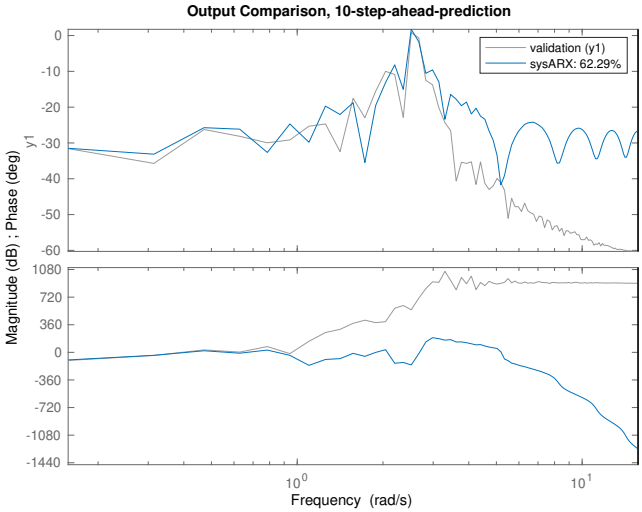

Figure 4.6: The 10-steps-ahead predicted output response, sysARX, compared with the measured output response, validation. The plot is generated with the MATLAB `compare` function and the percentage in the upper right corner is the NRMSE fitness value where 100% is perfect fit.

4.1.5 Heave Prediction Based on Measured Data

After the parametric method was tested with generated input and output data to design an ideal case, see Section 4.1.4, the ARX method was tested with the given data set.

Thus, the input was generated as described in Section 4.1.3 where the wave spectrum resulted from either wave radar measurements, i.e. measured spectrum, or from given sea state parameters, i.e. model spectrum.

Moreover, the heave amplitude from the given data set has a sampling frequency of 1 second, while the wave spectrum, significant wave height and wave peak period are updated every 20 minutes. Therefore, the output data consists of heave measurements for the past 20 minutes and the input data will be the wave radar measurements for the associated time period.

The system identified based on measurements from sample time j, referred to as sysARX, represents the relation between the wave spectrum and the heave energy spectrum. Thus, the k-step-ahead predicted heave motion can be defined as

$$\hat{y}_{j+k} = \text{predict}(sysARX_j, Z_{j+k}) \tag{4.11}$$

Where the data Z_{j+k} is defined as

$$Z_{j+k} = u_{j+k}, \cdots, u_0, y_j, \cdots, y_0 \tag{4.12}$$

Furthermore, the MATLAB System Identification Toolbox operates with the term *simulated* output whenever the predicted output only depends on current and past inputs

and initial conditions, and not on previous output measurements (MathWorks, 2020d). Thus, the simulated output can be defined as

$$\hat{y}_{s(j)} = \text{predict}(sysARX_j, Z_{s(j)}) \tag{4.13}$$

Where the data $Z_{s(j+k)}$ is defined as

$$Z_{s(j)} = u_j, \cdots, u_0 \tag{4.14}$$

Moreover, Chapter 6 demonstrate the performance of the parametric methodology for heave prediction.

4.1.6 Validation of the Parametric Method

After selecting the model structure and the estimation algorithm, the model has to be validated. One common validation technique presented in Ljung (1999) is to compare the measured output with the simulated or predicted output.

The parametric method was validated with the MATLAB function `compare` which compares the identified model output with the measured output (MathWorks, 2020b). The percentages in the upper right corner of the figures, like the ones from Section 4.1.4, are normalized root-mean-square error (NRMSE) fitness values which indicated how well the simulated or predicted output matches the measured data. 100% indicates perfect fit, $-\infty$ indicates bad fit and a fitness value of 0 means that the predicted output is no better at matching the measured output than a straight line.

4.2 A Non-Parametric Method for RAO Estimation and Heave Prediction

According to Molland (2008), Tupper (2013) and Aarsnes et al. (2013), the the heave energy spectrum is related to the wave spectrum by the square of the RAO, see Equation 4.15. Therefore, instead of identifying the whole system, it is possible that the RAO estimate can be determined from the relationship between the input and output spectra, see Equation 2.39.

This method does not make any assumptions regarding the structure of the system, thus the following implementations will be categorized as non-parametric. However, like the parametric metod, this approach also assumes a linear relation between the heave and the wave spectrum.

$$S_h(\omega) = RAO(\omega)^2 S_w(\omega) \tag{4.15}$$

As specified by Oppenheim and Verghese (2015), when the input signal itself is not accessible, i.e., the wave elevation, but the spectrum is, then the magnitude of the frequency response can still be determined as long as the output spectra can be estimated.

4.2.1 Input and Output Generation

The input spectrum, i.e. the wave spectrum S_w, is either given directly by the data set or modeled based on sea state parameters. The heave spectrum S_h, however, has to be estimated based on the given heave amplitudes.

Measured Wave Spectrum as Input

Like the parametric method, the non-parametric was also tested with the measured 1D wave spectrum from the given data set as input. As described in Section 3.2, this wave spectrum is a function of 37 linearly spaced frequencies ranging from 0.03 to 0.3 Hz and it is updated every 20 minutes.

Model Wave Spectrum as Input

Additionally, the non-parametric method, like the parametric method, was tested with the Torsethaugen model wave spectrum from Fossen and Perez (2009) as input. As the model wave spectrum is given as a function of angular frequencies and the measured wave spectrum and the predicted heave energy spectrum are in Hz, the model wave spectrum is multiplied by a factor of 2π according to Equation 4.9 (DNV, 2010).

Furthermore, Figure 4.2 shows the measured 1D wave spectrum compared with a JONSWAP spectrum with $\gamma = 3.3$, a JONSWAP spectrum with the DNVGL (2018) suggestion of γ, resulting in $\gamma = 2.1915$ and a Torsethaugen spectrum. None of the model spectra are able to capture the sea state at low frequencies. However, as illustrated in Table 4.1, the Torsethaugen spectrum gives the most accurate representation of the wave energy.

Heave Energy Spectrum as Output

Equation 4.15 is generally used to calculate the heave energy spectrum when the RAO and the wave spectrum are known. However, for this project, the RAO is subject to estimation based on heave energy spectrum and wave spectrum and therefore unknown.

Thus, the heave energy spectrum is estimated using a PSD estimate function. After trial and error, the MATLAB function `pwelch` was used to calculate the heave energy spectrum based on rig heave amplitude measurements.

4.2.2 Mean RAO vs Previous RAO

The non-parametric RAO estimation methodology was obtained by estimating the RAO from measurements and by estimating the RAO from the average of the previously estimated RAOs.

Specifically, for a data sample at time j, the RAO is estimated either as

$$RAO(j) = \frac{S_h(j)}{S_w(j)} \tag{4.16}$$

or, due to the discovery of non-captured nonlinearities, as the average of the n last RAO estimates

$$\widehat{RAO}_n(j) = \frac{RAO(j) + \cdots + RAO(j-n-1)}{n} \tag{4.17}$$

The results and comparison of Equation 4.16 and 4.17 are presented in Chapter 5.

4.2.3 Heave Prediction Based on Measured Data

Moreover, the estimated RAO is used to predict the heave energy spectrum S_h. Therefore, the heave energy spectrum at time j will be predicted as

$$S_h(j) = RAO(j-1) \cdot S_w(j) \tag{4.18}$$

Where $RAO(j-1)$ is defined by Equation 4.16 or 4.17.

Furthermore, the estimated RAO is also used to predict the heave energy spectrum k-step-ahead of time with k being the prediction horizon. Thus, the k-step-ahead predicted heave energy spectrum is defined as

$$S_h(j+k) = RAO(j) \cdot S_w(j+k) \tag{4.19}$$

Here, the wave spectrum is either given from measurements or weather forecasts. The prediction time unit is 20 minutes. Therefore, $j+1$ will in practice mean 20 minutes after time j. This is because the wave spectrum, and therefore the sea state parameters, are updated every 20 minutes, see Section 3.2.

Furthermore, the performance of the non-parametric methodology for heave prediction is demonstrated in Chapter 6.

4.3 RAO Estimation and Heave Prediction Based on Forecasts

Moreover, the RAO estimation and heave prediction methodology was implemented with model wave spectrum as input where the sea states were obtained from weather forecasts from the Norwegian Meteorological Institute, see Section 3.1.2.

4.3.1 Extracting Sea State Parameters

The sea state parameters of interest for this project are the significant wave height and the wave peak period. These parameters are given as three-dimensional matrices with dimensions

$$\textit{relative longitude} \times \textit{relative latitude} \times \textit{time}$$

where the unit of time is hours.

The wave model which gives the forecasts is run on a rotated grid. Therefore, to access the desired parameters for a given location in latitude and longitude, the coordinates has to be transformed to relative coordinates.

Scientist at the Norwegian Meteorlogical Institute, Ole Johan Aarnes, shared his algorithm, $find\_nearest\_gridcell$, which uses triangulation to extract the indices which

connects the relative latitude and longitude to the actual latitude and longitude, see Listing B.1 in Appendix B.1.

When the relation between relative and actual coordinates have been established, the desired forecast parameters can be extracted, see Listing B.2 in Appendix B.1. Specifically, significant wave height and wave peak period for a given location can be used to generate a model wave spectrum. This model spectrum based on forecasts can be used to predict future heave motion, see Equation 4.19.

Further, the forecast files overlap by 60 hours, which means that more than one file can contain forecasts for the desired point in time. Therefore, the newest file, i.e. the forecast file closest in time with time j is chosen.

Figure 4.7 shows the significant wave height from the measured wave spectrum compared with significant wave heights from forecasts from the Norwegian Meteorological Institute. As described in Section 3.1.2, the forecasts are updated four times daily, resulting in four NetCDF files each day. The forecasts in Figure 4.7 are from 22 hours, 16 hours, 10 hours and 4 hours ahead, respectively.

The performance of the RAO estimation and heave prediction methodology based on weather forecasts for both the parametric and the non-parametric methods are demonstrated in Chapter 7.

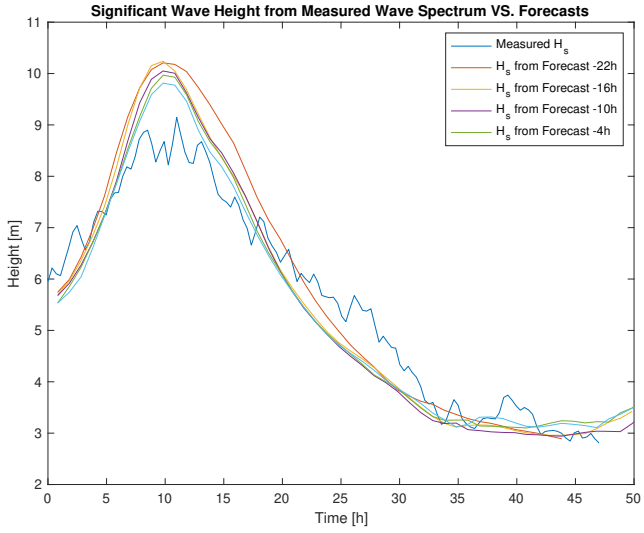

Figure 4.7: The measured significant wave height compared with the significant wave height from forecasts from the Norwegian Meteorological Institute. The forecasts are from 4, 10, 16 and 22 hours ahead.

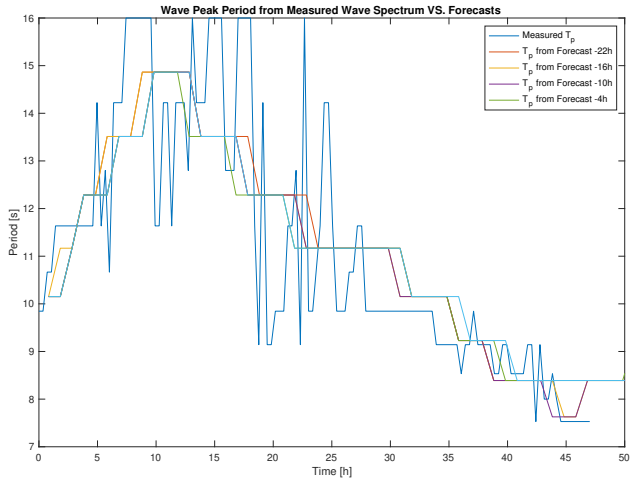

Figure 4.8: The measured wave peak period compared with the wave peak period from forecasts from the Norwegian Meteorological Institute. The forecasts are from 4, 10, 16 and 22 hours ahead.

4.4 Statistical Analysis

The performance of the proposed methods for RAO estimation and heave prediction was statistically evaluated by a heave prediction error defined in terms of a normalized root-mean-square error (NRMSE) fitness value. Here, the NRMSE function is defined as

$$\text{NRMSE} = 1 - \frac{||y - \hat{y}||}{||y - \text{mean}(y)||} \tag{4.20}$$

Where $||$ indicates the 2-norm of a vector. Specifically, the MATLAB functions `compare` (MathWorks, 2020b) and `goodnessOfFit` (MathWorks, 2020c) are utilized for the parametric and the non-parametric methods, respectively, to calculate the NRMSE fitness value.

Furthermore, these prediction errors were illustrated with box plots, using the MATLAB function `boxplot` (MathWorks, 2020a). Particularly, the box plot shows the median of the prediction error marked as a red horizontal line within the box, while the upper and lower edges represent the 75th and the 25th percentile, respectively. Outliers are marked as red plus signs.

Chapter 5

RAO Estimation Based on Measured Data

This chapter will demonstrate the performance of the non-parametric methodology for RAO estimation illustrated by its ability to predict the heave energy spectrum. The heave energy spectrum was estimated using overlapping segments of the time-domain heave amplitude signal, also known as Welch's technique. Using the relationship established in Equation 4.15, the heave energy spectrum was predicted based on the estimated RAO and the measured wave spectrum.

The heave prediction errors are expressed in terms of NRMSE fitness values as introduced in Section 4.4. Moreover, the heave energy spectrum predicted from the associated measured or modeled wave spectrum and the estimated RAO based on the average of the n last measurements will be compared to the heave energy spectrum predicted from the associated wave spectrum and the estimated RAO based on only the last wave and heave measurements. After trial and error $n = 2, 4, 5$.

Thus, the heave prediction errors will be given as

$$e_{avg} = y_j - \hat{y}_{avg} \tag{5.1a}$$

$$e_{last} = y_j - \hat{y}_{last} \tag{5.1b}$$

for heave energy spectrum, y, and wave measurements, u, at sample time $j+1$, where $\hat{y}_{avg}$ is predicted based on an RAO defined by Equation 4.17 at time j and $\hat{y}_{last}$ is predicted based on an RAO defined by Equation 4.16 at time j.

Thus, this chapter will present how the RAO estimation based on an average of the last n RAOs and RAO estimation based on only one set of input-output data affects the method's ability to predict the heave energy spectrum.

The prediction errors will be presented in box plots, see Section 4.4, resulting from ten random samples from the given data set, see Section 3.2. The intention is that these random samples can provide helpful insight into the performance of the proposed methods.

Furthermore, the significant wave height and wave peak period of the ten random samples are listed in Table 5.1, while the median, mean, maximum and minimum values of the significant wave height and wave peak period from the given data set are listed in Table 3.3.

Significant Wave Height [m]	Wave Peak Period [s]
6.5673	11.6364
7.5500	11.6364
8.8544	16.0000
8.8052	11.6364
8.6725	16.0000
6.2575	9.8462
5.0935	9.8462
3.9084	9.8462
3.4384	9.1429
3.3650	8.5333

Table 5.1: Significant wave height and the associated wave peak period of the ten random samples from the given data set. The median, mean, maximum and minimum value of the sea state parameters from the data set are presented in Table 3.3.

Additionally, the prediction horizon, k, will in this case be 20 minutes, due to the specifications of the measurements described in Section 3.2.

5.1 The Non-Parametric Method With Measured Wave Spectrum as Input

As described in Section 4.2.1, the non-parametric method was tested with measured wave spectra from the given data set as inputs.

First of all, the non-parametric method with measured wave spectrum as input was tested with $n = 2$, meaning that the RAO was estimated based on an average of the last two estimated RAOs and then used to predict the heave energy spectrum 1-step-ahead. Furthermore, this predicted heave energy spectrum was compared to the heave energy spectrum predicted 1-step-ahead based on the RAO estimated from only the previous input-output data.

Figure 5.1 shows the box plot of the heave prediction errors for the heave energy spectrum predicted from an average of the last 2 estimated RAOs and from only the last RAO estimate.

Additionally, Table 5.2 shows the median and the mean of the prediction errors illustrated in Figure 5.1, where the prediction errors are defined by Equation 5.1.

Prediction Errors	Median	Mean
e_{avg}	0.5871	0.5887
e_{last}	0.4880	0.4956

Table 5.2: The median and the mean of the prediction errors defined by 5.1 for the ten random data samples from Table 5.1. Here, e_{avg} is defined as the predicted heave based on average of the last 2 estimated RAOs, see Equation 4.17 for $n = 2$, while e_{last} is based on the RAO defined by Equation 4.16.

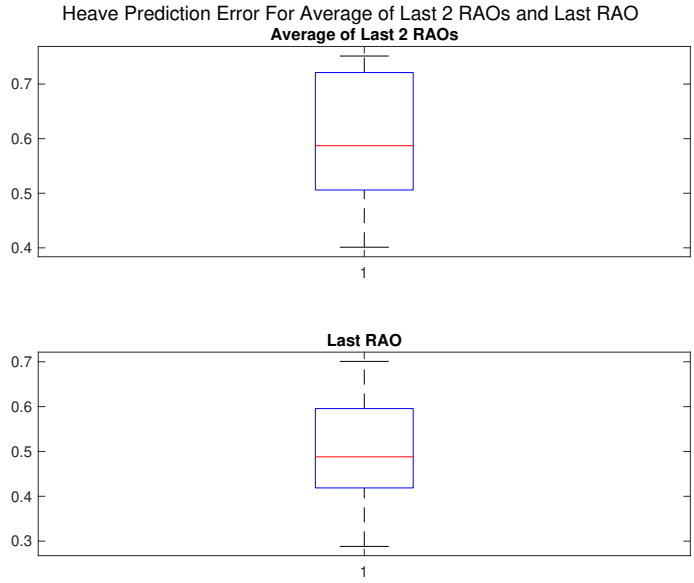

Figure 5.1: The box plots of the prediction errors defined by Equation 5.1 for the ten random samples form Table 5.1. The e_{avg} is the predicted heave based on the estimated RAO defined by Equation 4.17 for $n = 4$, while e_{last} is based on the RAO defined by Equation 4.16, with real wave spectra. The median is marked as a red line and the upper and lower edges of the box represents the 75th and the 25th percentile, respectively.

The average of the two last RAOs gives a marginally better NRMSE fitness value compared to the RAO from only the last input-output data.

Figure 5.2 shows the average of the last two RAOs compared with the previous, last RAO and the next (actual) RAO, which is the RAO estimated at time $j + 1$. For this particular example, the prediction errors, e_{avg} and e_{last} are 0.7514 and 0.5455, respectively. From Table 5.2, these prediction errors are far above average. Moreover, the sea state parameters are 6.5673m and 11.6364s, which according to Table 3.3 are above average.

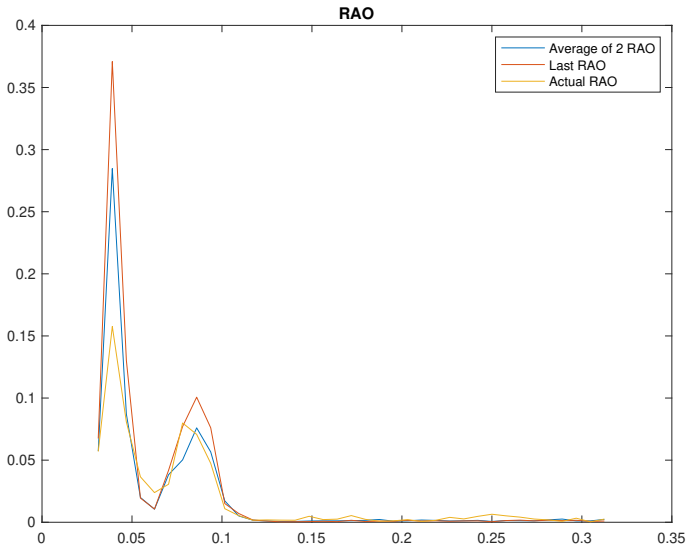

Figure 5.2: The estimated RAOs based on Equation 4.16 in red and Equation 4.17 in blue for the data sample at time j compared with the RAO for the data sample at time $j + 1$ in yellow. The significant wave height is 6.5673m and the wave peak period is 11.6364s for this particular example, which are above average according to Table 3.3. The prediction errors, e_{avg} and e_{last} are 0.7514 and 0.5455, respectively, which are above average, see Table 5.2.

Secondly, the non-parametric method with measured wave spectrum as input was tested with $n = 4$, meaning that the RAO was estimated based on an average of the last four estimated RAOs and then used to predict the heave energy spectrum 1-step-ahead. Furthermore, this predicted heave energy spectrum was compared to the heave energy spectrum predicted 1-step-ahead based on the RAO estimated from only the previous input-output data.

Figure 5.3 shows the box plot of the heave prediction errors for the heave energy spectrum predicted from an average of the last four estimated RAOs and from only the last RAO estimate.

Additionally, Table 5.3 shows the median and the mean of the heave prediction errors illustrated in Figure 5.3 and defined by Equation 5.1.

Prediction Error	**Median**	**Mean**
e_{avg}	0.6318	0.6214
e_{last}	0.4880	0.4956

Table 5.3: The median and the mean of the prediction errors defined by 5.1 for the ten random data samples from Table 5.1. Here, e_{avg} is defined as the predicted heave based average of the last 4 estimated RAOs, see Equation 4.17 for $n = 4$, while e_{last} is based on the RAO defined by Equation 4.16.

Furthermore, Figure 5.4 shows the estimated RAO based on the average of the last four measurements compared with the estimated RAO based on the last measurements from the

data sample at time j and the actual RAO, i.e. the RAO estimated at time $j + 1$. Here, the prediction errors, e_{avg} and e_{last} are 0.7527 and 0.4291, respectively. According to Table 5.3, these values are above and below average, respectively.

Moreover, the significant wave height is 5.0935m and the wave peak period is 11.6364s, which are below and above average, respectively according to Table 3.3.

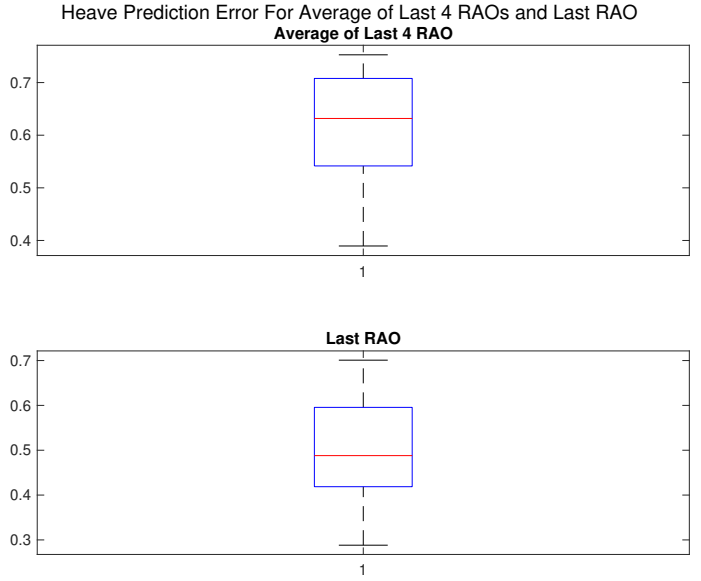

Figure 5.3: The box plots of the prediction errors defined by Equation 5.1 for the ten random samples form Table 5.1. The e_{avg} is the predicted heave based on the estimated RAO defined by Equation 4.17 for $n = 4$, while e_{last} is based on the RAO defined by Equation 4.16. The median is marked as a red line and the upper and lower edges of the box represents the 75th and the 25th percentile, respectively.

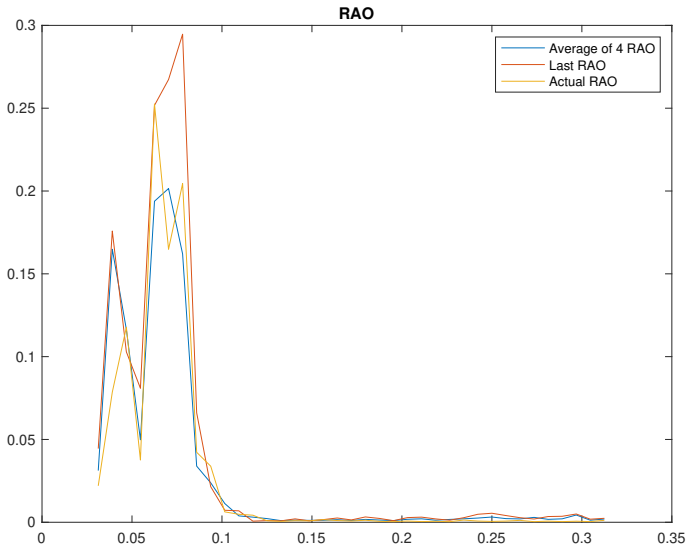

Figure 5.4: The estimated RAOs based on Equation 4.16 in red and Equation 4.17 in blue for the data sample at time j compared with the RAO for the data sample at time $j + 1$ in yellow. The significant wave height is 5.0935m and the wave peak period is 9.8462s for this particular example, which are below average according to Table 3.3. The prediction errors, e_{avg} and e_{last} are 0.7527 and 0.4921, respectively, which are above an below average, see Table 5.3.

Lastly, the non-parametric method with measured wave spectrum as input was tested with $n = 5$, meaning that the RAO was estimated based on an average of the last five estimated RAOs and then used to predict the heave energy spectrum 1-step-ahead. Furthermore, this predicted heave energy spectrum was compared to the heave energy spectrum predicted 1-step-ahead based on the RAO estimated from only the previous input-output data.

Figure 5.5 shows the box plot of the heave prediction errors for the heave energy spectrum predicted from an average of the last five estimated RAOs, compared to the predicted heave energy spectrum from only the last RAO estimate.

Likewise, Table 5.4 shows the median and the mean of the heave prediction errors illustrated in Figure 5.5 and defined by Equation 5.1.

Prediction Error	**Median**	**Mean**
e_{avg}	0.6434	0.6157
e_{last}	0.4880	0.4956

Table 5.4: The median and the mean of the prediction errors defined by 5.1 for the ten random data samples from Table 5.1. Here, e_{avg} is defined as the predicted heave based average of the last 5 estimated RAOs, see Equation 4.17 for $n = 5$, while e_{last} is based on the RAO defined by Equation 4.16.

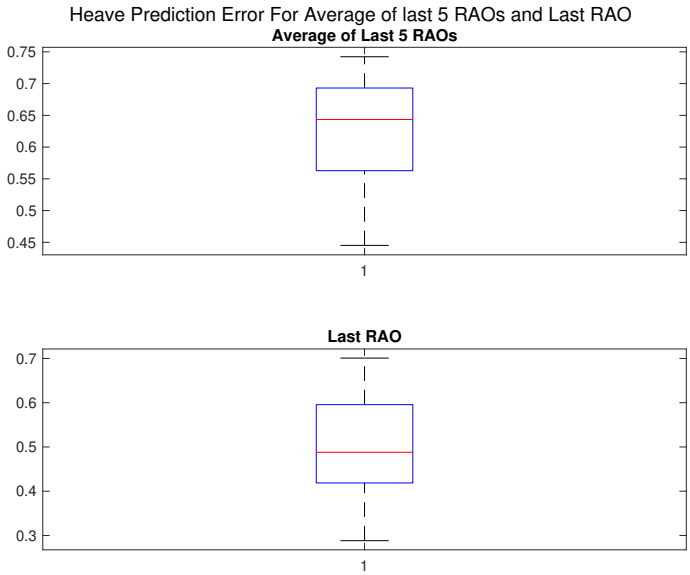

Figure 5.5: The box plots of the prediction errors defined by Equation 5.1 for the ten random samples form Table 5.1. The e_{avg} is the predicted heave based on the estimated RAO defined by Equation 4.17 for $n = 5$, while e_{last} is based on the RAO defined by Equation 4.16, with real wave spectra. The median is marked as a red line and the upper and lower edges of the box represents the 75th and the 25th percentile, respectively.

Furthermore, Figure 5.6 shows the estimated RAO based on the average of the last five estimates from time j, compared with the RAO estimated only on the previous measurements from the data sample at time j and the actual RAO estimated at time $j + 1$. For this particular example, the prediction errors, e_{avg} and e_{last} are 0.7423 and 0.4305, respectively, which are above and below the average values for the prediction errors, see Table 5.4.

Moreover, the sea state parameters are 8.8052m and 11.6364s, which are above average, see Table 3.3.

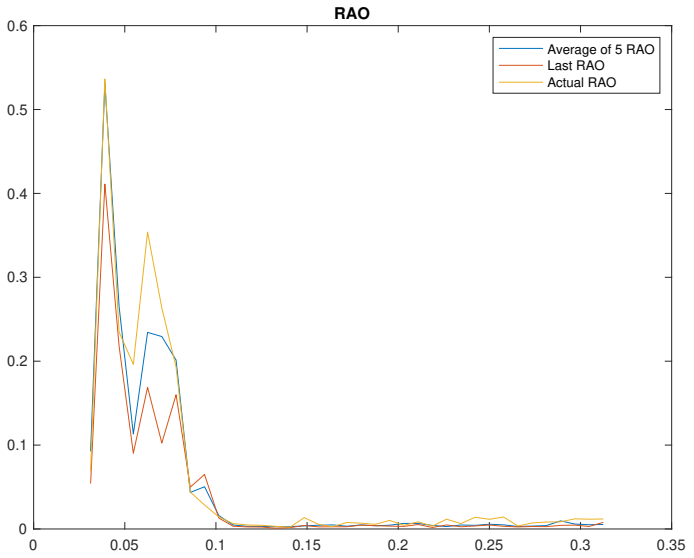

Figure 5.6: The estimated RAOs based on Equation 4.16 in red and Equation 4.17 in blue for the data sample at time j compared with the RAO for the data sample at time $j + 1$ in yellow. The significant wave height is 8.8052m and the wave peak period is 11.6364s for this particular example, which are above average according to Table 3.3. The prediction errors, e_{avg} and e_{last} are 0.7423 and 0.4305, respectively, which are above and below average, see Table 5.4.

5.2 The Non-Parametric Method With Model Wave Spectrum as Input

Moreover, the non-parametric estimation methodology was tested with a model wave spectrum as input, see Section 4.2.1.

First of all, like the previous section, the non-parametric method with a model wave spectrum as input was tested with $n = 2$, meaning that the RAO was estimated based on an average of the last two estimated RAOs and then used to predict the heave energy spectrum 1-step-ahead. Furthermore, this predicted heave energy spectrum was compared to the heave energy spectrum predicted 1-step-ahead based on the RAO estimated from only the previous input-output data.

Figure 5.7 shows the box plots of the heave prediction errors for the heave energy spectrum predicted from an average of the last two estimated RAOs and from only the last RAO estimate. There is one outlier, marked with a red plus sign, at -0.6405 for the average of the last two RAOs, and at -0.9213 for the heave energy spectrum estimated based on only the previous estimated RAO. The former is from the sample where the significant wave height is 8.6725m and the wave peak period is 16.0000s, which compared to Table 3.3 are more or less the maximum values of the sea states. Moreover, the latter outlier is from a sample where the sea states are 6.2575m and 9.8462s, respectively, which are both close to the median of the sea states.

Furthermore, Table 5.5 shows the median and the mean of the prediction errors illustrated in Figure 5.7 and defined by Equation 5.1.

Prediction Error	Median	Mean
e_{avg}	0.6622	0.4660
e_{last}	0.4691	0.3741

Table 5.5: The median and the mean of the prediction errors defined by 5.1 for the ten random data samples from Table 5.1. Here, e_{avg} is defined as the predicted heave based average of the last 2 estimated RAOs, see Equation 4.17 for $n = 2$, while e_{last} is based on the RAO defined by Equation 4.16.

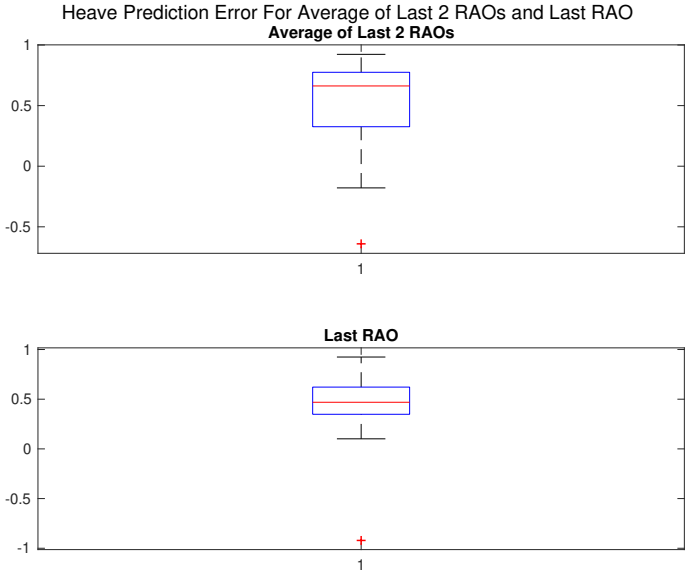

Figure 5.7: The box plots of the prediction errors defined by Equation 5.1 for the ten random samples form Table 5.1. The e_{avg} is the predicted heave based on the estimated RAO defined by Equation 4.17 for $n = 2$, while e_{last} is based on the RAO defined by Equation 4.16, with model wave spectra. The median is marked as a red line and the upper and lower edges of the box represents the 75th and the 25th percentile, respectively. Outliers are marked with red plus signs.

Figure 5.8 shows the estimated RAO based on the average of the last two estimates from time j, compared with the last RAO, at time j and the next estimated RAO, at time $j + 1$. For this example, the prediction errors, e_{avg} and e_{last} were 0.9229 and 0.9244, respectively. Compared to Table 5.5 these values are far above average.

Furthermore, the significant wave height and wave peak period was 3.3650m and 8.5333s, which are below average, see Table 3.3.

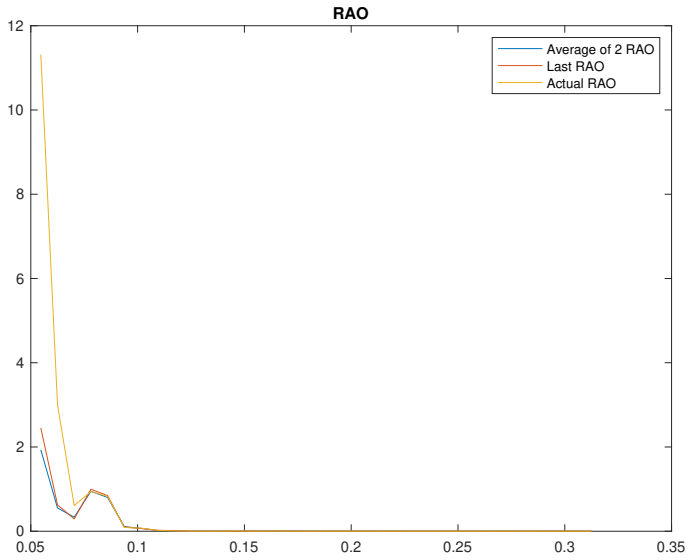

Figure 5.8: The estimated RAOs based on Equation 4.16 in red and Equation 4.17 in blue for the data sample at time j compared with the RAO for the data sample at time $j + 1$ in yellow. The significant wave height is 3.3650m and the wave peak period is 8.5333s for this particular example, which are below average according to Table 3.3. The prediction errors, e_{avg} and e_{last} are 0.9929 and 0.9244, respectively, which are above average, see Table 5.5.

Secondly, the non-parametric method with a model wave spectrum as input was tested with $n = 4$, meaning that the RAO was estimated based on an average of the last four estimated RAOs and then used to predict the heave energy spectrum 1-step-ahead. Furthermore, this predicted heave energy spectrum was compared to the heave energy spectrum predicted 1-step-ahead based on the RAO estimated from only the previous input-output data.

Figure 5.9 shows the box plots of the heave prediction errors for the heave energy spectrum predicted from an average of the last four estimated RAOs and from only the last RAO estimate.

Notice the outliers at -0.0507 for e_{avg} and at -0.9213 for e_{last}. Both outliers are from the same data sample where the sea states are 6.2575m and 9.8462s, respectively, which are both close to the median of the sea states.

Further Table 5.6 shows the median and the mean of the prediction errors illustrated in Figure 5.9 and defined by Equation 5.1.

Prediction Error	Median	Mean
e_{avg}	0.5806	0.4818
e_{last}	0.4691	0.3741

Table 5.6: The median and the mean of the prediction errors defined by 5.1 for the ten random data samples from Table 5.1. Here, e_{avg} is defined as the predicted heave based average of the last 4 estimated RAOs, see Equation 4.17 for $n = 4$, while e_{last} is based on the RAO defined by Equation 4.16.

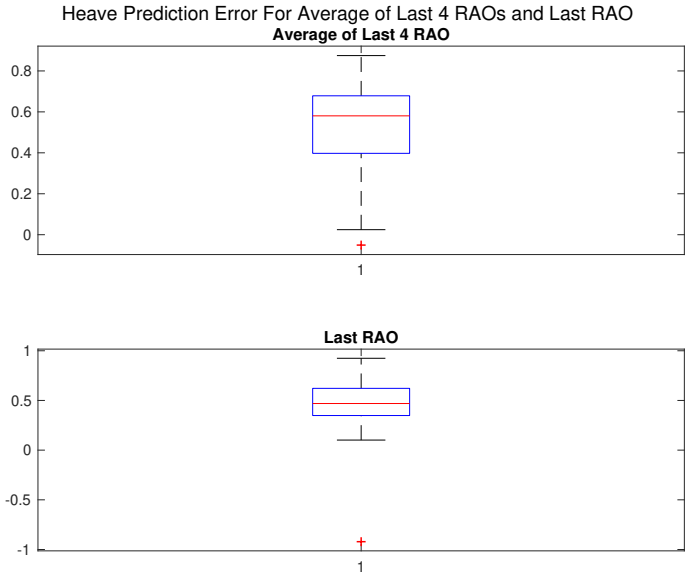

Figure 5.9: The box plots of the prediction errors defined by Equation 5.1 for the ten random samples form Table 5.1. The e_{avg} is the predicted heave based on the estimated RAO defined by Equation 4.17 for $n = 4$, while e_{last} is based on the RAO defined by Equation 4.16, with model wave spectra. The median is marked as a red line and the upper and lower edges of the box represents the 75th and the 25th percentile, respectively. Outliers are marked with red plus signs.

Figure 5.10 shows the estimated RAO based on the average of the last four estimates at time j, compared with the estimated RAO defined by Equation 4.16 at time j and the next estimated RAO, the actual RAO, estimated at time $j + 1$. For this example, the prediction errors, e_{avg} and e_{last} were 0.8749 and 0.9244, respectively. Compared to Table 5.6, these values are far above average.

Moreover, the sea state parameters were 3.3650m and 8.5333s, which are below average according to Table 3.3.

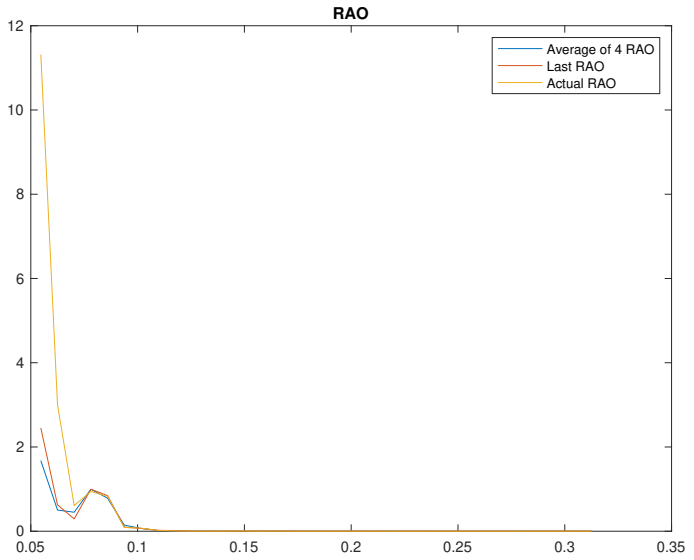

Figure 5.10: The estimated RAOs based on Equation 4.16 in red and Equation 4.17 in blue for the data sample at time j compared with the RAO for the data sample at time $j + 1$ in yellow. The significant wave height is 3.3650m and the wave peak period is 8.5333s for this particular example, which are below average according to Table 3.3. The prediction errors, e_{avg} and e_{last} are 0.8749 and 0.9244, respectively, which are above average, see Table 5.6.

Lastly, the non-parametric method with a model wave spectrum as input was tested with $n = 5$, meaning that the RAO was estimated based on an average of the last five estimated RAOs and then used to predict the heave energy spectrum 1-step-ahead. Furthermore, this predicted heave energy spectrum was compared to the heave energy spectrum predicted 1-step-ahead based on the RAO estimated from only the previous input-output data.

Figure 5.11 shows the box plots of the heave prediction errors for the heave energy spectrum predicted from an average of the last five estimated RAOs and from only the last RAO estimate. The outliers at -0.0507 for e_{avg} and at -0.9213 for e_{last} are both from the same data sample where the sea states are 6.2575m and 9.8462s, respectively, which are both below average and close to the median of the sea states.

Further Table 5.7 shows the median and the mean of the prediction errors illustrated in Figure 5.11 and defined by Equation 5.1.

Prediction Error	Median	Mean
e_{avg}	0.5642	0.4457
e_{last}	0.4691	0.3741

Table 5.7: The median and the mean of the prediction errors defined by 5.1 for the ten random data samples from Table 5.1. Here, e_{avg} is defined as the predicted heave based average of the last 5 estimated RAOs, see Equation 4.17 for $n = 5$, while e_{last} is based on the RAO defined by Equation 4.16.

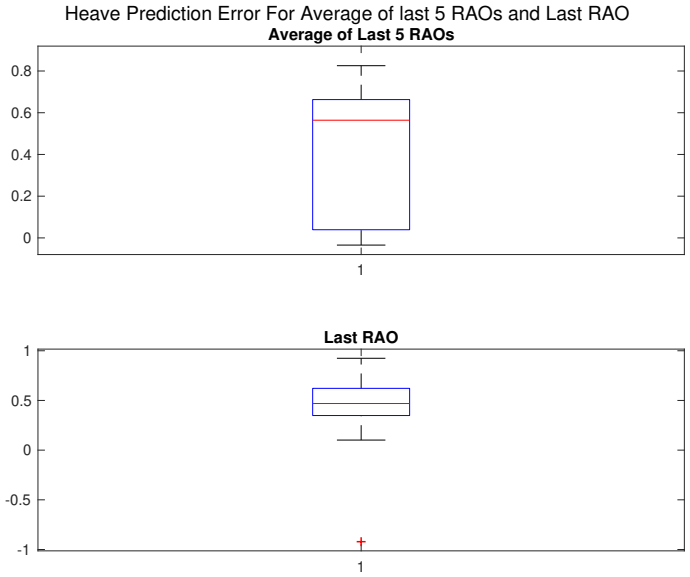

Figure 5.11: The box plots of the prediction errors defined by Equation 5.1 for the ten random samples form Table 5.1. The e_{avg} is the predicted heave based on the estimated RAO defined by Equation 4.17 for $n = 5$, while e_{last} is based on the RAO defined by Equation 4.16, with model wave spectra. The median is marked as a red line and the upper and lower edges of the box represents the 75th and the 25th percentile, respectively. Outliers are marked with red plus signs.

Figure 5.12 shows the estimated RAO based on the average of the last five estimates at time j, compared with the last RAO estimated based on Equation 4.16 at time j and the next estimated RAO, the actual RAO, at time $j + 1$. For this example, the prediction errors, e_{avg} and e_{last} were 0.8255 and 0.9244, respectively. According to Table 5.7 these values are above average.

Moreover, the significant wave height was 3.3650m and the wave peak period was 8.5333s, which both are below average according to Table 3.3.

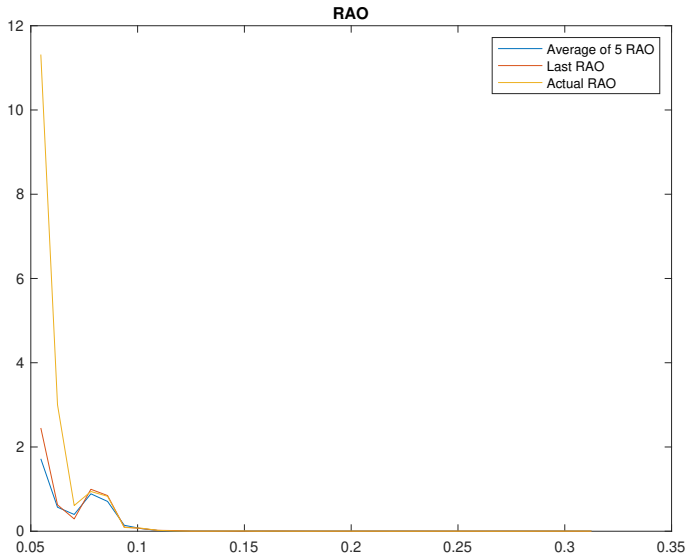

Figure 5.12: The estimated RAOs based on Equation 4.16 in red and Equation 4.17 in blue for the data sample at time j compared with the RAO for the data sample at time $j + 1$ in yellow. The significant wave height is 3.3650m and the wave peak period is 8.5333s for this particular example, which are above average according to Table 3.3. The prediction errors, e_{avg} and e_{last} are 0.8255 and 0.9244, respectively, which are above an below average, see Table 5.7.

Chapter 6

Heave Prediction Based on Measured Data

This section will present the results from the proposed RAO estimation and heave prediction methods introduced in Chapter 4. Like the experiments demonstrated in Chapter 5, the results in this chapter are based on ten random samples from the given data set. The significant wave height and wave peak period of these samples are shown in Table 5.1, while the median, mean, maximum and minimum values of the sea states from the whole data set are shown in Table 3.3.

Specifically, the parametric method for heave prediction introduced in Section 4.1 and the non-parametric method for heave prediction introduced in Section 4.2 were tested with both measured wave spectrum and model wave spectrum as inputs.

6.1 The Parametric Method

The parametric system identification method using an ARX model to describe the rig heave motion, presented in Section 4.1, was tested with both measured wave spectra and model spectra as the input spectrum.

Furthermore, the parametric method was validated as described in Section 4.1.6, using the MATLAB function `compare` to obtain magnitude and phase plots of the output responses. The simulation and prediction errors are presented in box plots as specified in Section 4.4.

Due to the specifications related to the System Identification Toolbox in MATLAB, the prediction horizon inherit the time unit of the data set. Thus, the prediction horizons, $k = 1, 2, 5, 10, 20$, will for the parametric method be in seconds.

Moreover, as introduced in Section 4.1.4, the simulated output is only based on input data and initial conditions while the predicted output at some future point in time is based on past and current values of input and output data, as well as initial conditions (MathWorks, 2020d).

The simulation and prediction errors are defined by Table 6.1

$$e_{sim} = y_j - \hat{y}_{s(j)} \tag{6.1a}$$
$$e_1 = y_{j+1} - \hat{y}_{j+1} \tag{6.1b}$$
$$e_2 = y_{j+2} - \hat{y}_{j+2} \tag{6.1c}$$
$$e_5 = y_{j+5} - \hat{y}_{j+5} \tag{6.1d}$$
$$e_{10} = y_{j+10} - \hat{y}_{j+10} \tag{6.1e}$$
$$e_{10} = y_{j+20} - \hat{y}_{j+20} \tag{6.1f}$$

Where y_j is the measured output response at sample time j, while $\hat{y}_{j+k}$ for $k = 1, 2, 5, 10, 20$ is the k-step-ahead predicted output response based on Equation 4.11 and y_{sim} is the simulated output based on Equation 4.13.

6.1.1 Measured Wave Spectrum as Input

The given data set includes a 1D wave spectrum measured from a wave radar, see Section 3.2. The linear approximation of the measured wave spectrum with added noise was then used as input spectrum to the ARX model, like the procedure presented in Section 4.1.3.

The heave simulation and prediction errors, defined by Equation 6.1, are illustrated in Figure 6.1. As the prediction horizon increases, the NRMSE cost decreases, meaning that the difference between the measured heave and the predicted heave increases as the prediction horizon increases.

Notice the outliers at -0.0753 for e_{sim}, 0.7485 for e_1 and at 0.1753 for e_{20}. The former is associated with sea state parameters of 8.8052m and 11.6364, which are above average according to Table 3.3. Moreover, the outlier for e_1 is associated with a significant wave height of 3.4384m and a wave peak period of 9.1429s, which are far below average. The latter outlier is associated with sea state parameters equal to 8.6725m and 16.0000s, which in fact are far above average and the maximum value of the wave peak period, respectively.

Table 6.1 shows the median and the mean of the heave prediction errors. As described in Section 4.4, 1 would be an indication of perfect fit and $-\infty$ would indicate bad fit. A zero value would imply that the predicted heave is no better at matching the measured heave than a straight line.

Error	Median	Mean
e_{sim}	0.0055	-0.0025
e_1	0.8106	0.8038
e_2	0.6486	0.6417
e_5	0.3565	0.3323
e_{10}	0.1592	0.1531
e_{20}	-0.0137	-0.0105

Table 6.1: The heave simulation and prediction errors defined by Equation 6.1. 1-step-ahead prediction will in this example be in the timescale of 1 second due to the specifications of the System Identification Toolbox in MATLAB (Ljung, 2014).

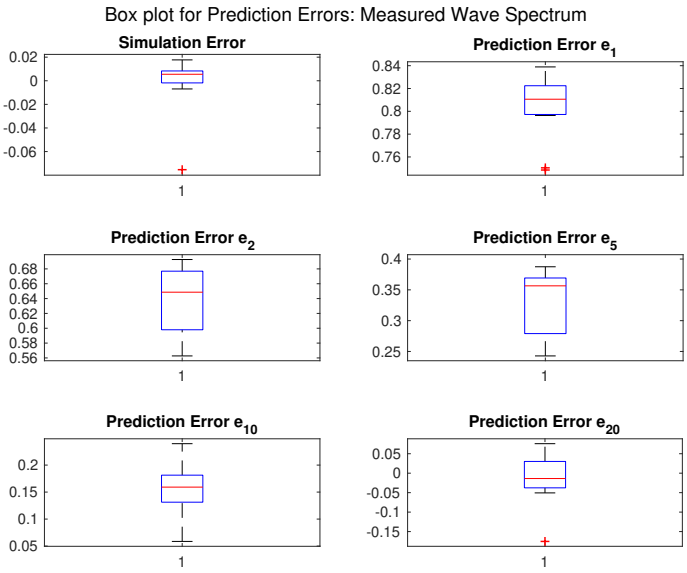

Figure 6.1: The box plots of the simulation and prediction errors defined by Equation 6.1 for the ten random samples form Table 5.1 for the parametric method with measured wave spectrum as input. The median is marked as a red line and the upper and lower edges of the box represents the 75th and the 25th percentile, respectively. Outliers are marked with red plus signs.

Furthermore, Figure 6.2 shows the magnitude and phase plots of the 1-step-ahead predicted output response, sysARX, compared with the measured output response, validation1. For this particular example, the sea state parameters are 5.0935m and 9.8462s, which are below average according to Table 3.3. The prediction error were 0.8389, 0.6924, 0.3788, 0.2107 and 0.0758, or above average as seen from Table 6.1.

Likewise, Figure 6.3 shows the associated magnitude and phase plots of the simulated output compared with the measured output response. The simulation error was 0.0055 or 0.5536%.

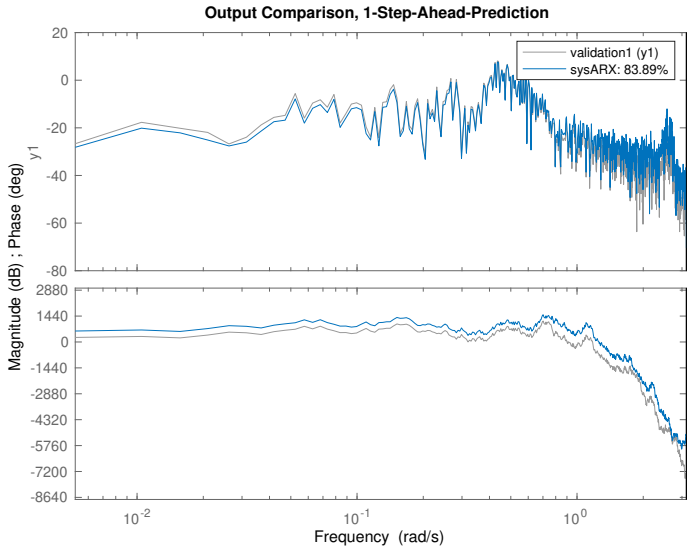

Figure 6.2: The 1-step-ahead predicted output response, sysARX, compared with the measured output response, validation for the parametric method with measured wave spectrum as input. The plot is generated with the MATLAB `compare` function and the percentage in the upper right corner is the NRMSE fitness value where 100% is perfect fit. The prediction error is defined by 6.1.

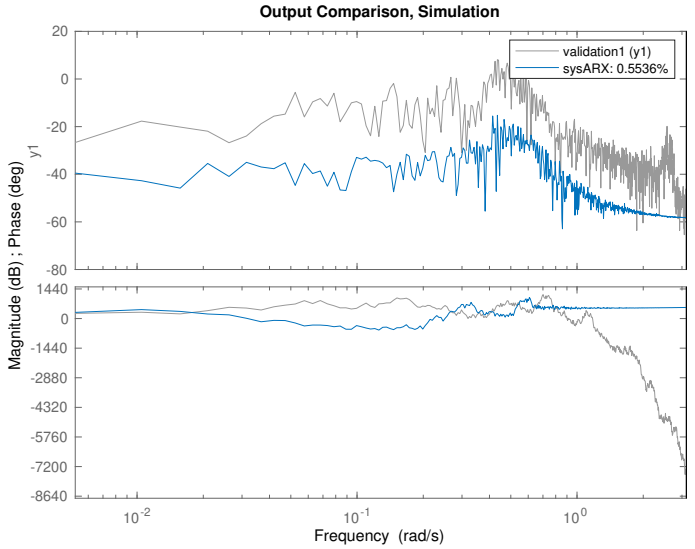

Figure 6.3: The simulated output response, sysARX, compared with the measured output response, validation for the parametric method with measured wave spectrum as input. The plot is generated with the MATLAB `compare` function and the percentage in the upper right corner is the NRMSE fitness value where 100% is perfect fit. The simulation error is defined by 6.1.

6.1.2 Model Wave Spectrum as Input

Moreover, if a measured wave spectrum is not available, sea state parameters can be used to generate a model wave spectrum as discussed in Section 4.1.4. Therefore, the parametric method was tested with a Torsethaugen model spectrum created with significant wave height and wave peak period from the given data set. The input to the ARX model was then generated based on a linear approximation of the model spectrum with added noise, see Section 4.1.3.

Figure 6.4 shows the box plots of the heave simulation and prediction errors, defined by Equation 6.1 and represented using a NRMSE cost function. Similarly to what is seen in Section 6.1.1, the NRMSE cost decreases when the prediction horizon increases, illustrating that the difference between the measured heave and the predicted heave increases as the prediction horizon increases. Again, notice the outliers at 0.0157, 0.0175 and -0.0203 for e_{sim}, 0.7585 for e_1 and at -0.1719 for e_{20}. The outliers at 0.0157 and -0.1719 are both associated with sea state parameters of 8.6725m and 16.0000s, which according to Table 3.3 are above average and the maximum value, respectively.

Moreover, the outlier at 0.0175 has a significant wave height of 8.8544m and a wave peak period of 16.0000s, which are above average and in fact the maximum value of the wave peak period. Likewise, the outlier at -0.0203 is associated with sea state parameters of 8.8052m and 11.6364s, which are both above average. Lastly, the outlier at 0.7585 is associated with sea state parameters of 3.4384m and 9.14929s, which are both below average.

Table 6.2 shows the median and the mean of the heave prediction error. Again, as explained in Section 4.4, 1 would be an indication of perfect fit and $-\infty$ would indicate bad fit. A zero value would imply that the predicted heave is no better at matching the measure heave than a straight line.

Prediction error	**Median**	**Mean**
e_{sim}	0.0037	-0.0032
e_1	0.8139	0.8043
e_2	0.6589	0.6412
e_5	0.3497	0.3294
e_{10}	0.1623	0.1534
e_{20}	-0.0022	-0.0112

Table 6.2: The heave simulation and prediction errors defined by Equation 6.1. 1-step-ahead prediction will in this example be in the timescale of 1 second due to the specifications of the System Identification Toolbox in MATLAB (Ljung, 2014).

Furthermore, like the example in the previous section, Figure 6.5 shows magnitude and phase plots of the 1-step-ahead predicted output response, sysARX, compared with the measured output response, validation1. Again, the sea state parameters are below average, see Table 3.3, with a significant wave height of 5.0935m and a wave peak period of 9.8462s. For this particular example the prediction errors were 0.8389, 0.6924, 0.3788, 0.2107 and 0.07162.

Moreover, Figure 6.6 shows the associated magnitude and phase plots of the simulated

output response compared with the measured output response. The simulation error was 0.0062 or 0.6224%.

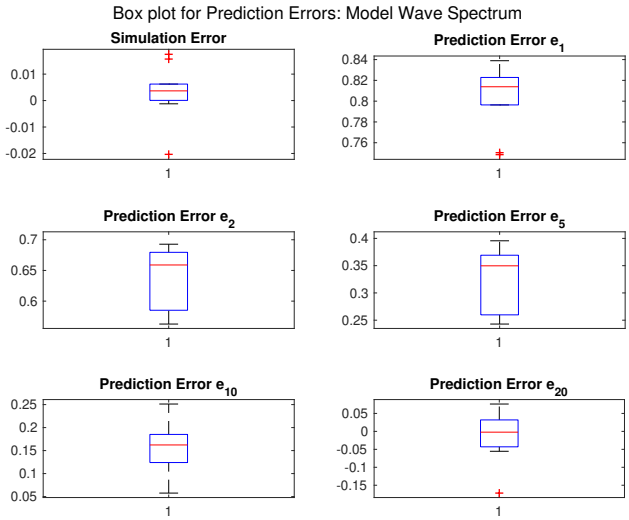

Figure 6.4: The box plots of the simulation and prediction errors defined by Equation 6.1 for the ten random samples form Table 5.1 for the parametric method with model wave spectrum as input. The median is marked as a red line and the upper and lower edges of the box represents the 75th and the 25th percentile, respectively. Outliers are marked with red plus signs.

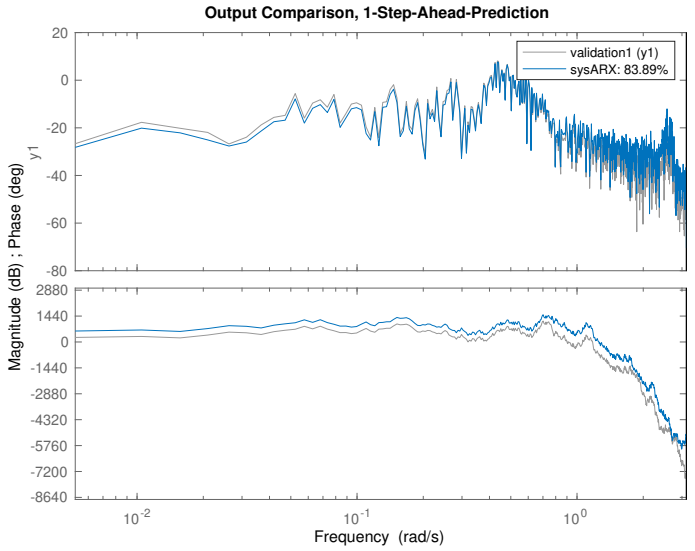

Figure 6.5: The 1-step-ahead predicted output response, sysARX, compared with the measured output response, validation for the parametric method with measured wave spectrum as input. The plot is generated with the MATLAB `compare` function and the percentage in the upper right corner is the NRMSE fitness value where 100% is perfect fit. The prediction error is defined by 6.1.

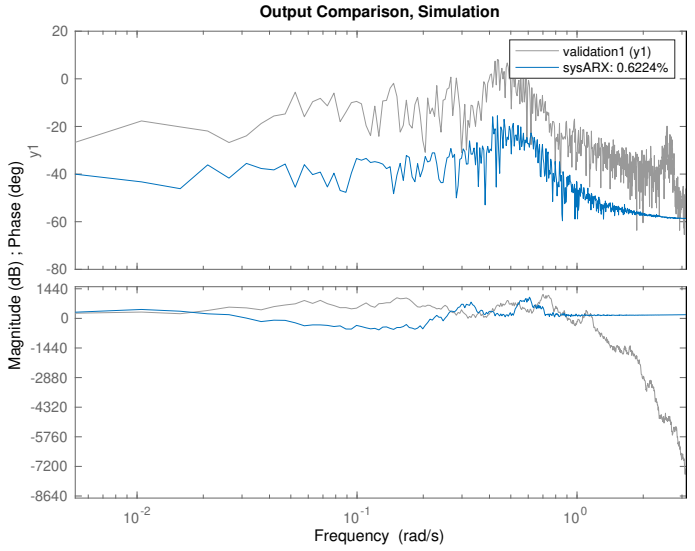

Figure 6.6: The simulated output response, sysARX, compared with the measured output response, validation for the parametric method with measured wave spectrum as input. The plot is generated with the MATLAB `compare` function and the percentage in the upper right corner is the NRMSE fitness value where 100% is perfect fit. The simulation error is defined by 6.1.

6.2 The Non-Parametric Method

The non-parametric method was implemented as described in Section 4.2, with both measured wave spectra and model wave spectra as inputs. This method does not make any a priori assumptions regarding the system which is why this method is also referred to as non-parametric, see Section 2.1.3.

Identically to Chapter 5, the heave energy spectrum was estimated using overlapping segments of the time-domain heave amplitude signal, also known as Welch's technique. Using the relationship established in Equation 4.15, the heave energy spectrum was predicted based on the estimated RAO and the measured wave spectrum.

Based on the results from Chapter 5, the non-parametric heave prediction method is based on the average of the last four estimated RAOs. Furthermore, this predicted heave spectrum is compared to the heave spectrum predicted based on only the last estimated RAO.

The heave prediction errors are defined by

$$e_1 = y_{j+1} - \hat{y}_{j+1} \tag{6.2a}$$
$$e_2 = y_{j+2} - \hat{y}_{j+2} \tag{6.2b}$$
$$e_5 = y_{j+5} - \hat{y}_{j+5} \tag{6.2c}$$
$$e_{10} = y_{j+10} - \hat{y}_{j+10} \tag{6.2d}$$
$$\tag{6.2e}$$

Where y_{j+k} is the heave energy spectrum based on measurements at sample time $j+k$ and $\hat{y}_{j+k}$ is the predicted heave energy spectrum at sample time $j+k$ for $k = 1, 2, 5, 10$, defined by Equation 4.18. Here, the time unit of the prediction horizon k is 20 minutes since the wave measurements are updated approximately every 20 minutes.

Moreover, the heave prediction errors are presented in terms of NRMSE and illustrated with box plots, as described in Section 4.4.

6.2.1 Measured Wave Spectrum as Input

The given data set includes a 1D wave spectrum, see Section 3.2 and this section will present the results from the heave prediction methodology based on Equation 4.15 with the measured wave spectrum as input.

Average of 4 RAOs

First of all, Figure 6.7 shows the box plots for the the prediction errors defined in Equation 6.2 when the RAO is based on the average of the last four estimated RAOs. As previously discovered, when the prediction horizon increases, the value of the NRMSE cost function decreases, which implies that the difference between the measured and the predicted heave increases as the prediction horizon increases.

Notice the outlier at -0.2218 for e_2. Here, the significant wave height is 3.4384 m and the wave peak period is 9.1429s, which according to Table 3.3 are below average.

Moreover, Table 6.3 shows the median and the mean of the heave prediction errors presented in Figure 6.7. As described in Section 4.4, a value of 1 would indicate a perfect fit, while a NRMSE value $\approx -\infty$ would imply bad fit. A zero value indicates that the predicted heave is no better at matching the measured heave than a straight line.

Figure 6.8 shows the 1-step-ahead predicted heave energy spectrum based on the average of the last four estimated RAOs compared with the measured heave energy spectrum. For this particular example, the prediction errors $e_1, \cdots, e_{10}$ are 0.7079, 0.7203, 0.4015 and 0.1987, respectively, which for the most part are above average, see Table 6.3. Here, the sea state parameters are 6.5673m and 11.6364s, respectively. According to Table 3.3, this sea state is slightly above average.

Further, Figure 6.9 shows the 1-step-ahead predicted heave energy spectrum based on the average of the last four estimated RAOs compared with the measured heave energy spectrum. Here, the prediction errors $e_1, \cdots, e_{10}$ are 0.3895, -0.2217, 0.1532 and 0.2279, respectively. As seen in Table 6.3, these values are far below average.

Furthermore, for this particular example the significant wave height is 3.4384 m and the wave peak period is 9.1429s, which is the outlier associated with e_2.

Prediction error	**Median**	**Mean**
e_1	0.6318	0.6214
e_2	0.4813	0.4243
e_5	0.4141	0.3902
e_{10}	0.3968	0.3756

Table 6.3: The heave prediction errors defined by Equation 6.2 when the RAO is estimated based on Equation 4.17 for $n = 4$ and with measured wave spectra. The prediction horizon is 20 minutes due to the specifications of the given data set, see Section 3.2.

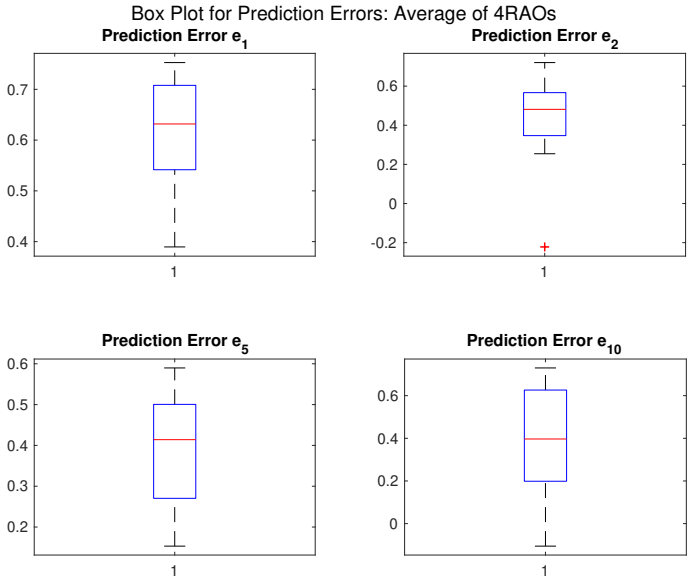

Figure 6.7: The box plots of the prediction errors defined by Equation 6.2 for the ten random samples form Table 5.1 for the non-parametric method with measured wave spectrum as input. The predicted heave is based on the estimated RAO defined by Equation 4.17 for $n = 4$. The median is marked as a red line and the upper and lower edges of the box represents the 75th and the 25th percentile, respectively. Outliers are marked with red plus signs.

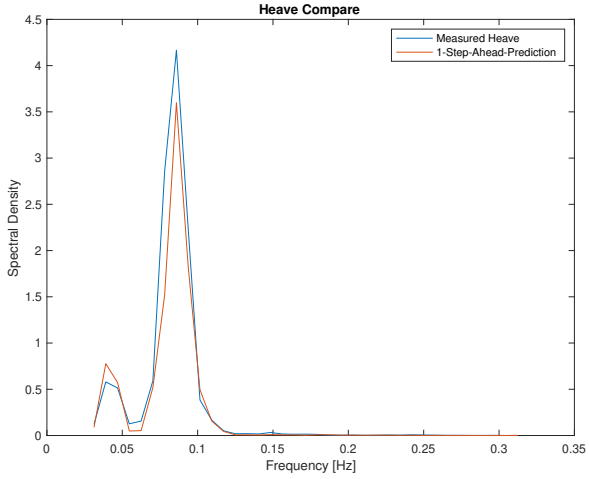

Figure 6.8: The 1-step-ahead predicted heave energy spectrum compared to the measured heave energy spectrum when the RAO is estimated based on Equation 4.17 for $n = 4$. Here, the sea state parameters were 6.5673m and 11.6364s, which are above average, see Table 3.3. The prediction error, e_1 was 0.7079, which is above average, see Table 6.3.

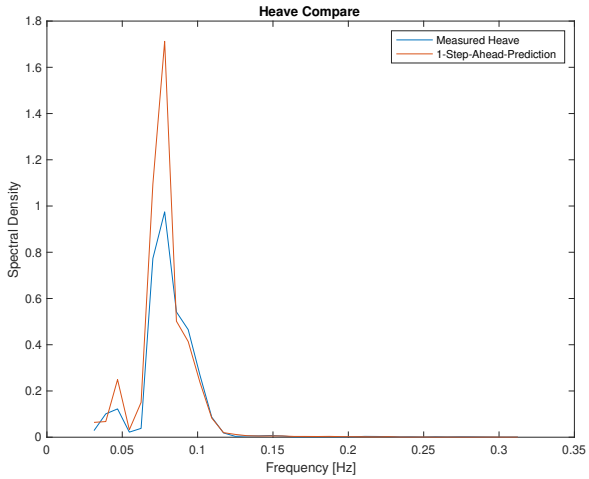

Figure 6.9: The 1-step-ahead predicted heave energy spectrum compared to the measured heave energy spectrum when the RAO is estimated based on Equation 4.17 for $n = 4$. Here, the sea state parameters were 3.4384m and 9.1429s, which are below average, see Table 3.3. The prediction error, e_1 was 0.3895, which is below average, see Table 6.3. Notice that this example is associated with the outlier for e_2, see Figure 6.7.

Last RAO

Moreover, Figure 6.10 shows the box plots for the the prediction errors defined in Equation 6.2 when the RAO is estimated only based on the previous measurements, see Equation 4.16. Similarly to what is seen in Figure 6.7, when the prediction horizon increases, the value of the NRMSE cost function decreases, which implies that the difference between the measured and the predicted heave increases as the prediction horizon increases.

Notice the outliers at -0.4135 for e_5 and at -0.8237 for e_{10}. Here, the sea states associated with the outliers are 5.0935m and 9.8462s and 6.2575m and 9.8462s, respectively. According to Table 3.3, the former significant wave height is below average while the latter is above. The wave peak period is below average.

Table 6.4 shows the median and the mean of the heave prediction errors presented in Figure 6.7. Again, a value of 1 would indicate a perfect fit, while a NRMSE value $\approx -\infty$ would imply bad fit. A zero value indicates that the predicted heave is no better at matching the measured heave than a straight line.

Figure 6.11 shows the 1-step-ahead predicted heave energy spectrum based on the previously estimated RAO compared with the measured heave energy spectrum. For this particular example, the heave prediction errors, $e_1, \cdots, e_{10}$ are 0.6899, 0.5941, 0.3683 and 0.4047, respectively. As seen in Table 6.4, these values are above average. Furthermore, the sea state parameters associated with this example are 8.8544m and 16.0000s, which according to Table 3.3 are far above average. In fact, the wave peak period is the maximum value of the wave peak period of the whole data set.

Furthermore, Figure 6.12 shows the 1-step-ahead predicted heave energy spectrum

based on the previously estimated RAO compared with the measured heave energy spectrum. For this particular example, the heave prediction errors, $e_1, \cdots, e_{10}$ are 0.2882, 0.0305, 0.1994 and -0.8236, respectively. As seen in Table 6.4, these values are below average. The sea state parameters associated with this example are 6.2575m and 9.8462s, which according to Table 3.3 are above average for the wave height and below average for the peak period.

Prediction error	Median	Mean
e_1	0.4880	0.4956
e_2	0.4533	0.4001
e_5	0.3303	0.3109
e_{10}	0.3671	0.2621

Table 6.4: The heave prediction errors defined by Equation 6.2 when the RAO is estimated based on Equation 4.16 and with measured wave spectra. The prediction horizon is 20 minutes due to the specifications of the given data set, see Section 3.2.

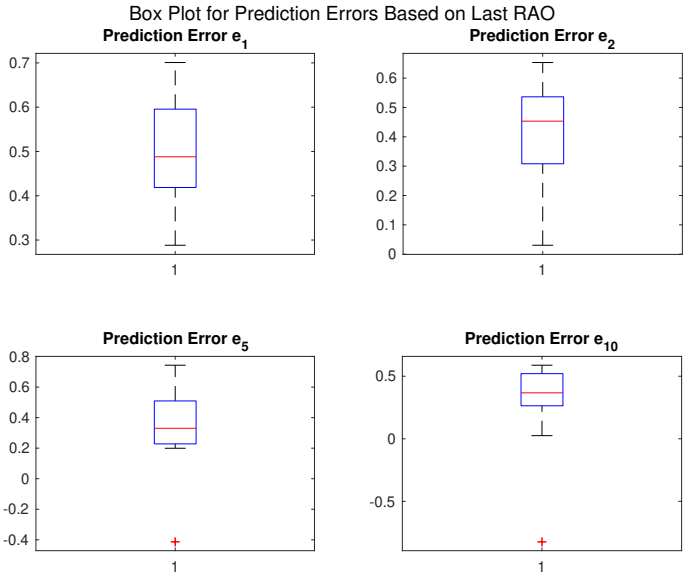

Figure 6.10: The box plots of the prediction errors defined by Equation 6.2 for the ten random samples form Table 5.1 for the non-parametric method with measured wave spectrum as input. The predicted heave is based on the estimated RAO defined by Equation 4.16. The median is marked as a red line and the upper and lower edges of the box represents the 75th and the 25th percentile, respectively. Outliers are marked with red plus signs.

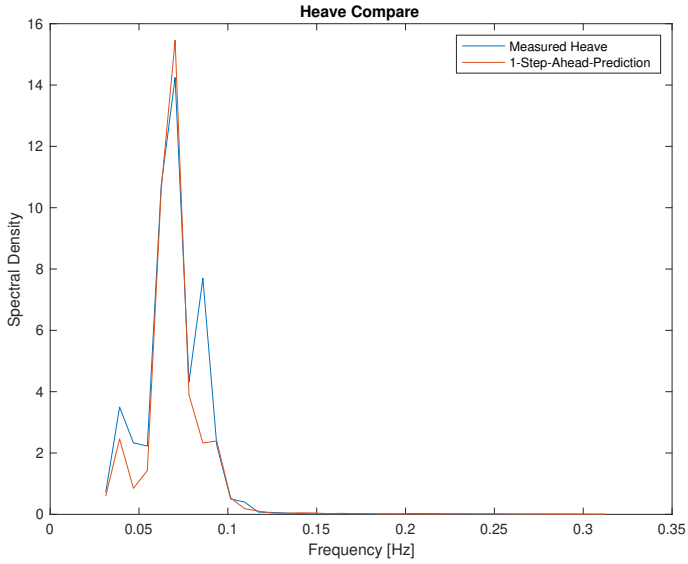

Figure 6.11: The 1-step-ahead predicted heave energy spectrum compared to the measured heave energy spectrum when the RAO is estimated based on Equation 4.16. Here, the sea state parameters were 8.8544m and 16.0000s, which are above average, see Table 3.3. The prediction error, e_1 was 0.6899, which is above average, see Table 6.4.

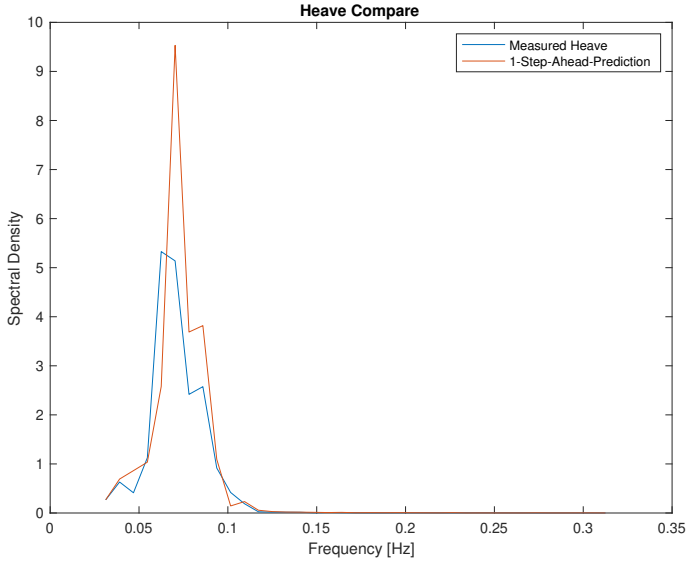

Figure 6.12: The 1-step-ahead predicted heave energy spectrum compared to the measured heave energy spectrum when the RAO is estimated based on Equation 4.16. Here, the sea state parameters were 6.2575m and 9.8462s, which are above and below average, see Table 3.3. The prediction error, e_1 was 0.2882, which is below average, see Table 6.4.

6.2.2 Model Wave Spectrum as Input

Furthermore, the non-parametric method was also tested with a Torsethaugen model wave spectrum, generated based on sea state parameters from the given data set, see Section 4.2.1, as input. Therefore, this section will present the results from the heave prediction methodology based on Equation 4.15 with the Torsethaugen wave spectrum as input.

Average of 4 RAOs

First and foremost, Figure 6.13 shows the box plots for the heave prediction errors defined by Equation 6.2 when the RAO is based on the average of the previous four estimates, see Section 5.1 and Equation 4.17. As previously discovered, when the prediction horizon increases, the value of the NRMSE cost function decreases, which implies that the difference between the measured and the predicted heave motion increases as the prediction horizon increases.

Notice the outliers at -0.0507 for e_1, -2.8023 and -5.9629 for e_5 and at -5.1009 for e_{10}. From Table 6.5, these values are mostly far below average. Moreover, the outliers at -0.0507, -5.9629 and -5.1009 are all associated with a significant wave height of 6.2575m and 9.8462s, which according to Table 3.3 are above and below average, respectively. Additionally, the outlier at -2.8023 is associated with sea state parameters equal to 8.8052m and 11.6364s, which are above average.

Table 6.5 shows the median and the mean value for the heave prediction errors illustrated in Figure 6.13 and defined by Equation 6.2. Again, as described in Section 4.4, a value of 1 would imply perfect fit, while $-\infty$ would mean bad fit. A zero value indicates that the predicted heave is no better at matching the measured heave than a straight line. There is a considerable difference between the median and the mean value of the prediction errors, particularly for e_5 and e_{10}.

Prediction error	Median	Mean
e_1	0.5806	0.4818
e_2	0.3947	0.2947
e_5	0.3583	-0.5203
e_{10}	0.2293	-0.3474

Table 6.5: The heave prediction errors defined by Equation 6.2 when the RAO is estimated based on Equation 4.17 for $n = 4$ and with model wave spectra. The prediction horizon is 20 minutes due to the specifications of the given data set, see Section 3.2.

Furthermore, Figure 6.14 shows the 1-step-ahead predicted heave energy spectrum when the RAO is estimated based on the average of the last four estimated RAOs, compared with the measured heave energy spectrum. For this particular example, the prediction errors, $e_1, \cdots, e_{10}$ are 0.6785, 0.7179, 0.3967 and 0.2001, respectively. As seen in Table 6.5, these values are above average. The sea state parameters associated with this example are 6.5673m and 11.6364s which are above average according to Table 3.3.

On the contrary, Figure 6.15 shows the 1-step-ahead predicted heave energy spectrum when the RAO is estimated based on the average of the last fours RAOs, compared with the

measured heave energy spectrum. Here, the prediction errors are -0.0507, -0.0028, -5.9629 and -5.1009. These values are far below the average prediction error values shown in Table 6.5 and the associated sea state parameters are 6.2575m and 9.8462s, which according to Table 3.3 are above and below average, respectively.

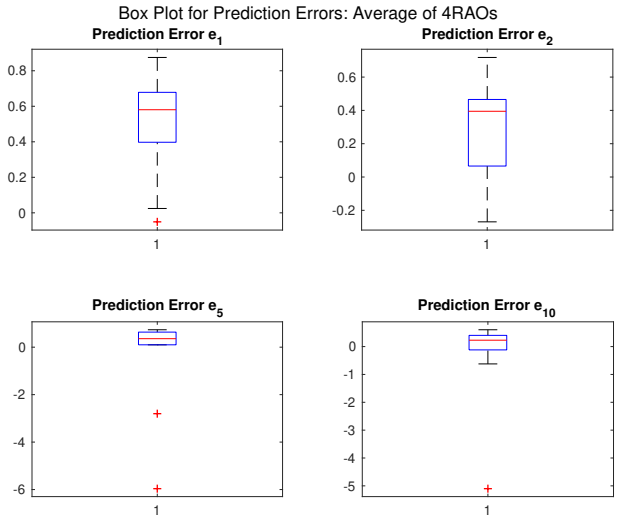

Figure 6.13: The box plots of the prediction errors defined by Equation 6.2 for the ten random samples form Table 5.1 for the non-parametric method with measured wave spectrum as input. The predicted heave is based on the estimated RAO defined by Equation 4.17 for $n = 4$. The median is marked as a red line and the upper and lower edges of the box represents the 75th and the 25th percentile, respectively. Outliers are marked with red plus signs.

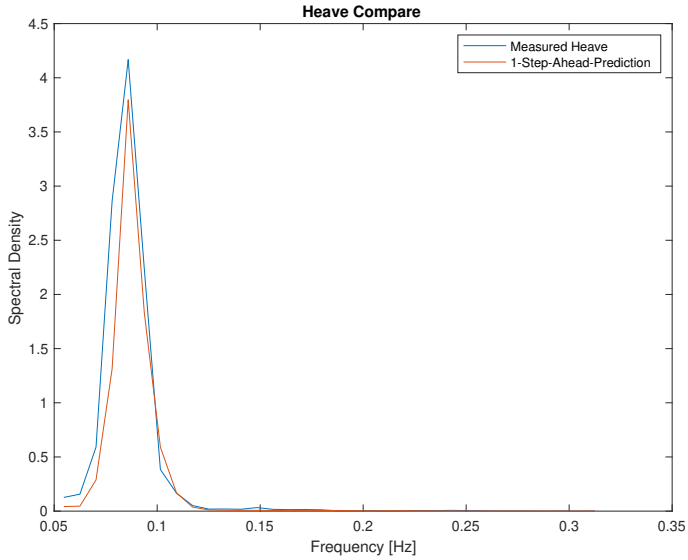

Figure 6.14: The 1-step-ahead predicted heave energy spectrum compared to the model heave energy spectrum when the RAO is estimated based on Equation 4.17 for $n = 4$. Here, the sea state parameters were 6.5673m and 11.6364s, which are above average, see Table 3.3. The prediction error, e_1 was 0.6785, which is above average, see Table 6.5.

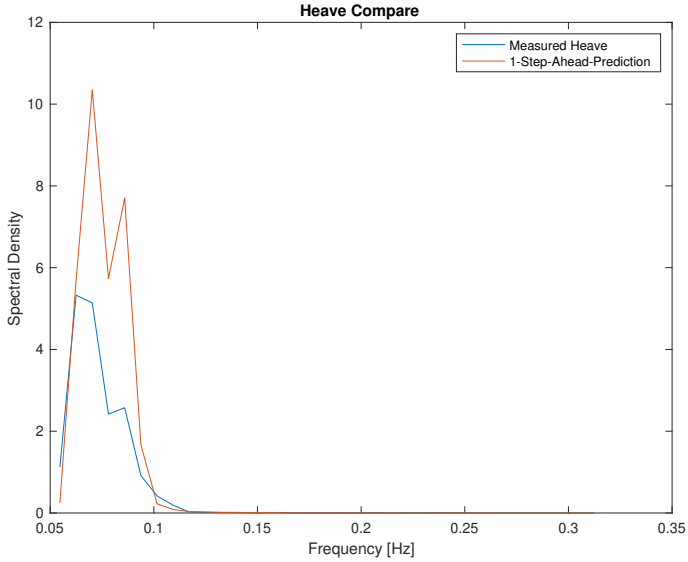

Figure 6.15: The 1-step-ahead predicted heave energy spectrum compared to the model heave energy spectrum when the RAO is estimated based on Equation 4.17 for $n = 4$. Here, the sea state parameters were 6.2575m and 9.8462s, which are above and below average, see Table 3.3. The prediction error, e_1 was 0.3895, which is below average, see Table 6.5.

Last RAO

Furthermore, Figure 6.16 shows the box plots of the heave prediction errors defined by Equation 6.2, when the RAO is estimated based on the last measurements, see Equation 4.16. Notice the outliers at -0.9213 for e_1, -2.4334 and -3.0744 for e_5 and at -9.0349 for e_{10}. Again, the outliers for e_1, e_{10} and the outlier at -3.0744 for e_5 are all associated with a significant wave height of 6.2575 m and a wave peak period of 9.8462s. The remaining outlier is associated with sea state parameters of 8.8052m and 11.6364s. According to Table 3.3, the former sea state has a significant wave height above average and a wave peak period below average, while the latter is above average for both parameters.

Table 6.6 shows the median and the mean of the heave prediction errors illustrated in Figure 6.16 defined by Equation 6.2. There is a significant difference between the median and the mean for e_5 and e_{10}, particularly.

Prediction error	Median	Mean
e_1	0.4691	0.3741
e_2	0.3228	0.2163
e_5	0.4184	-0.1892
e_{10}	0.2372	-0.7608

Table 6.6: The heave prediction errors defined by Equation 6.2 when the RAO is estimated based on Equation 4.16 and with model wave spectra. The prediction horizon is 20 minutes due to the specifications of the given data set, see Section 3.2.

Furthermore, Figure 6.17 shows the 1-step-ahead predicted heave energy spectrum when the RAO is estimated based on only the previous measurements, defined by Equation 4.16, compared with the measured heave energy spectrum. Here, the prediction errors, $e_1, \cdots, e_{10}$, are 0.6217, 0.7472, 0.4397 and 0.4716, respectively. Compared to Table 6.6, these prediction error values are far above average. Additionally, this example has sea state parameters of 5.0935m and 9.8462, which according to Table 3.3 are below average.

Similarly to Figure 6.17, Figure 6.18 shows the 1-step-ahead predicted heave energy spectrum when the RAO is estimated based on only the previous measurements, compared with the measured heave energy spectrum. Only for this particular example, the prediction errors, $e_1, \cdots, e_{10}$, are -0.9213, -0.7047, -3.0744 and -3.0349, respectively. As seen from Table 6.6, these values are far below average and again, the associated sea state parameters are 6.2575m and 9.8462s.

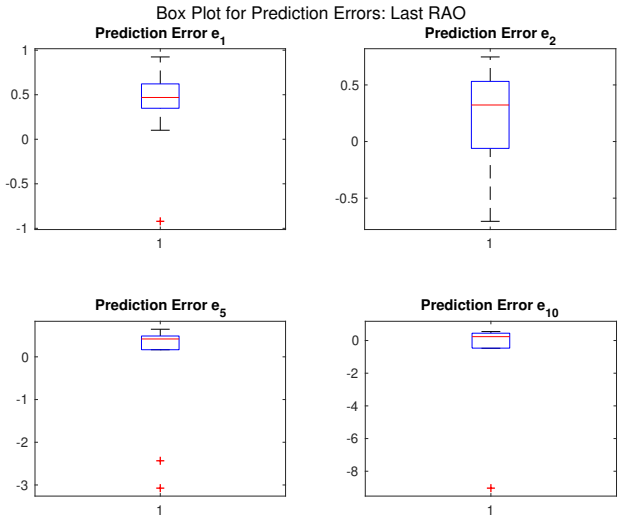

Figure 6.16: The box plots of the prediction errors defined by Equation 6.2 for the ten random samples form Table 5.1 for the non-parametric method with model wave spectrum as input. The predicted heave is based on the estimated RAO defined by Equation 4.16. The median is marked as a red line and the upper and lower edges of the box represents the 75th and the 25th percentile, respectively. Outliers are marked with red plus signs.

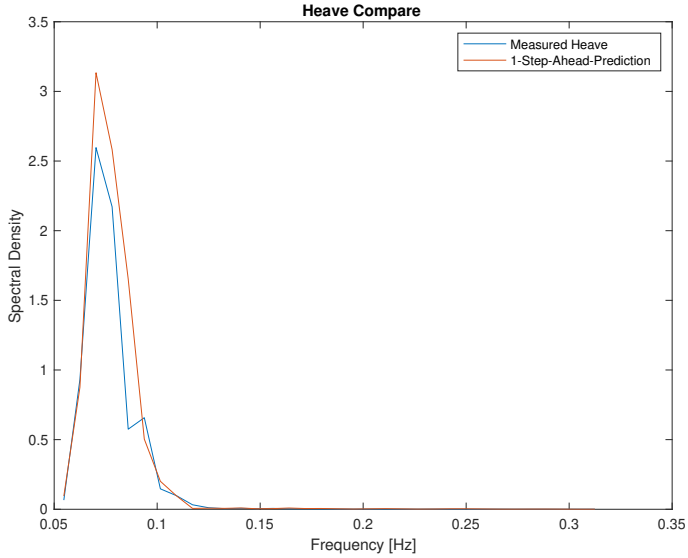

Figure 6.17: The 1-step-ahead predicted heave energy spectrum compared to the model heave energy spectrum when the RAO is estimated based on Equation 4.16. Here, the sea state parameters were 5.0935m and 9.8462s, which are below average, see Table 3.3. The prediction error, e_1 was 0.6217, which is above average, see Table 6.6.

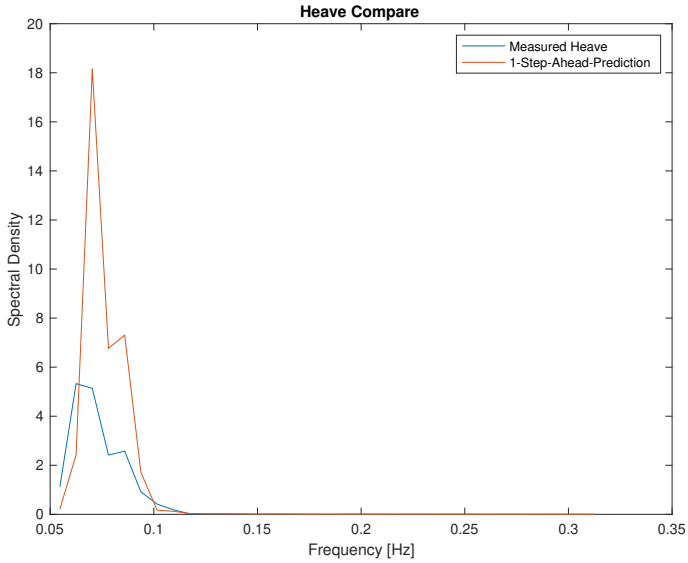

Figure 6.18: The 1-step-ahead predicted heave energy spectrum compared to the model heave energy spectrum when the RAO is estimated based on Equation 4.16. Here, the sea state parameters were 6.2575m and 9.8462s, which are below average, see Table 3.3. The prediction error, e_1 was -0.9213, which is below average, see Table 6.6.

Chapter 7

RAO Estimation and Heave Prediction Based on Weather Forecasts

As introduced in Section 3.1.2, the Norwegian Meteorological Institute operates a data server which consists of ocean wave forecasts for Europe and the Arctic, which are updated four times daily. The archive goes back to April 2015.

Hence, both the parametric and non-parametric methods are tested with a model wave spectrum based on sea state parameters from weather forecasts as input, see Section 4.3. Ten random samples from the given data set and thereby from the associated forecasts are used to predict the heave energy spectrum from estimated RAOs.

The significant wave height and the wave peak period from the ten random samples from given data are presented in Table 5.1. Moreover, the median, mean, maximum and minimum values of the sea state parameters from the given data set are shown in Table 3.3. Additionally, Table 7.1 shows the significant wave height and the wave peak period from the weather forecasts for the ten random samples.

Furthermore, Table 7.2 shows the difference between the sea state parameters from the given data set, presented in Table 5.1, and the sea state parameters from the associated weather forecasts, presented in Table 7.1. The differences, denoted as ΔH_s and ΔT_p, are defined in Equation 7.1 and given with units meter and second, respectively.

$$\Delta H_s = H_{sdata} - H_{sforecast} \tag{7.1a}$$

$$\Delta T_p = T_{pdata} - T_{pforecast} \tag{7.1b}$$

Significant Wave Height [m]	Wave Peak Period [s]
6.0428	11.1677
7.2295	12.2845
8.8306	13.5129
8.9605	14.8542
8.5041	14.8642
5.7880	12.2845
4.1356	11.1677
3.5030	10.1525
3.1590	10.1525
2.6842	8.3905

Table 7.1: Significant wave height and the associated wave peak period of the ten random samples from the weather forecasts. For comparison, the associated sea state parameters from the given data set are shown in Table 5.1, while the median, mean, maximum and minimum value of the sea state parameters from the given data set are presented in Table 3.3.

$\mathbf{\Delta H_s}$ [m]	$\mathbf{\Delta T_p}$ [s]
0.5245	0.4687
0.3205	-0.6481
0.0238	2.4871
-0.1553	-3.2178
0.1684	1.1358
0.4695	-2.4383
0.9579	-1.3215
0.4054	-0.3063
0.2794	-1.0096
0.6808	0.1428

Table 7.2: The difference between the significant wave heights from the given data set and the significant wave height from the weather forecasts, ΔH_s, and the difference between the wave peak periods from the given data set and the wave peak periods from the weather forecasts, ΔT_p, defined by Equation 7.1.

7.1 The Parametric Method With Model Wave Spectrum Based on Weather Forecasts

The parametric method was tested with model wave spectra based on weather forecasts as inputs. The sea state parameters were extracted from the forecast files as described in Section 4.3. Moreover, the input to the ARX model was generated as described in Section 4.1.3, with linear approximation of the Torsethaugen wave spectrum based on sea state parameters from weather forecasts.

The parametric method was validated as described in Section 4.1.5, with magnitude and phase plots from the MATLAB function `compare`. Additionally, the simulation and

prediction errors are presented in terms of NRMSE as described in Section 4.4.

Figure 7.1 shows the box plots of the simulation and prediction errors, defined by Equation 6.1. As described in Section 4.1.5, the simulated output only depends on the measured input and initial conditions while the predicted output depends on current and past measured input and output, in addition to initial conditions.

Furthermore, Table 7.3 shows the median and the mean of the simulation and prediction errors illustrated in Figure 7.1. Here, the time unit of the prediction is seconds due to the definition of the System Identification Toolbox in MATLAB (Ljung, 2014).

Error	Median	Mean
e_{sim}	0.0024	0.0027
e_1	0.7989	0.8119
e_2	0.6491	0.6512
e_5	0.3404	0.3377
e_{10}	0.1726	0.1754
e_{20}	0.0363	0.0325

Table 7.3: The heave simulation and prediction errors defined by Equation 6.1 for model wave spectra based on weather forecasts. Here, 1-step-ahead prediction will be in the timsecale of 1 second due to the specifications of the System Identification Toolbox in MATLAB (Ljung, 2014).

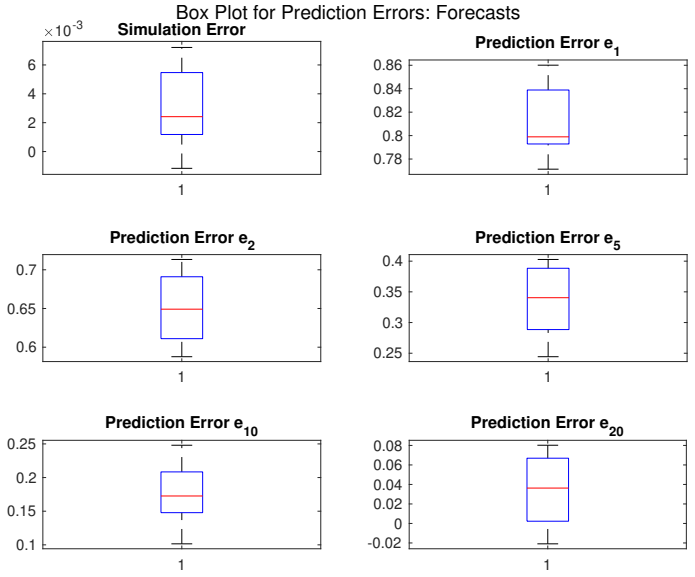

Figure 7.1: The box plots of the simulation and prediction errors defined by Equation 6.1 for the ten random samples form Table 7.1 for the parametric method with model wave spectrum based on forecasts as input. The median is marked as a red line and the upper and lower edges of the box represents the 75th and the 25th percentile, respectively. Outliers are marked with red plus signs.

Moreover, Figure 7.2 shows the magnitude and phase plots of the 1-step-ahead pre-

dicted output response and the measured output response, while Figure 7.3 shows the 10-step-ahead predicted output response and the measured output response. For this particular example, the significant wave height and wave peak period from forecasts were 8.9605m and 14.8642s, while the sea states were measured to be 8.8052m and 11.6364s. According to Table 3.3 both sea states are above average.

Furthermore, the prediction errors for this particular example were 0.8389, 0.7050, 0.4028, 0.2480 and 0.0269 and the simulation error was 0.0055. As seen in Table 7.3, these values are mostly above average.

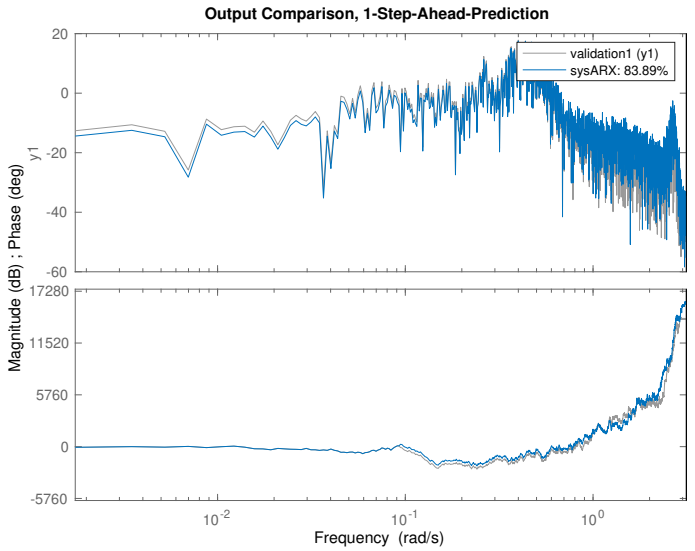

Figure 7.2: The 1-step-ahead predicted output response, sysARX, compared with the measured output response, validation for the parametric method with model wave spectrum based on weather forecasts as input. The plot is generated with the MATLAB `compare` function and the percentage in the upper right corner is the NRMSE fitness value where 100% is perfect fit. The prediction error is defined by 6.1.

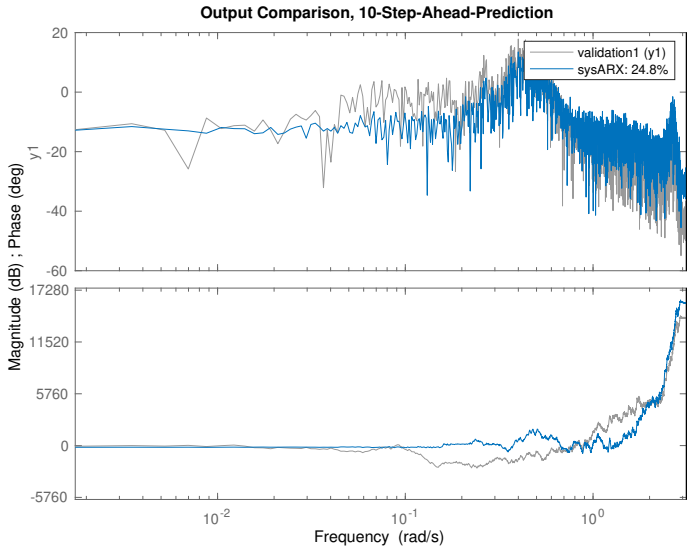

Figure 7.3: The 10-step-ahead predicted output response, sysARX, compared with the measured output response, validation for the parametric method with model wave spectrum based on weather forecasts as input. The plot is generated with the MATLAB `compare` function and the percentage in the upper right corner is the NRMSE fitness value where 100% is perfect fit. The prediction error is defined by 6.1.

7.2 The Non-Parametric Method With Model Wave Spectrum Based on Weather Forecasts

Moreover, the non-parametric method was tested with model wave spectra based on weather forecasts as inputs. Like the parametric method, the sea state parameters were extracted from weather forecast files as described in Section 4.3. These sea state parameters were then utilized to generate Torsethaugen wave spectra as described in section 4.2.1.

Thus, the heave energy spectrum was predicted based on Equation 4.15. Based on the results from Chapter 5, the RAO was estimated both as an average of the last four estimates, see Equation 4.17, and as Equation 4.16, i.e. only from the previous measurements.

Furthermore, the heave prediction errors, in terms of NRMSE as described in Section 4.4, were calculated for a prediction horizon, k, of 1, 2 and 3. The weather forecasts from the Norwegian Meteorlogical Institute are updated every hour, hence the unit of the prediction horizon is hour.

The prediction errors are now defined as

$$e_1 = y_1 - \hat{y}_1 \tag{7.2a}$$
$$e_2 = y_2 - \hat{y}_2 \tag{7.2b}$$
$$e_3 = y_3 - \hat{y}_3 \tag{7.2c}$$

Where y is the heave energy spectrum from measurements using Welch's technique as previously discussed and $\hat{y}$ is the predicted heave energy spectrum from weather forecasts and the estimated RAOs.

7.2.1 Average of 4 RAOs

As mentioned initially, the RAO was estimated based on an average of the last four estimates, defined in Equation 4.17.

Figure 7.4 shows the box plots of the heave prediction errors when the heave energy spectrum was predicted based on the average of the last 4 estimated RAOs in addition to the associated weather forecasts for the sea states.

Notice the outliers for prediction errors e_1 and e_2. Both are associated with the same data sample where the significant wave height from the weather forecasts is 2.6842m and the wave peak period is 8.3905s, while the sea states from the measured wave spectrum are 3.3650m and 8.5333s, respectively. As shown in Table 3.3, the measured sea state parameters are far below average.

Furthermore, Table 7.4 shows the median and the mean of the heave prediction errors illustrated in Figure 7.4 and defined by Equation 7.2.

Prediction Error	Median	Mean
e_1	0.4999	0.3669
e_2	0.6542	-0.5830
e_3	0.5424	0.5206

Table 7.4: The heave prediction errors defined by Equation 7.2 when the RAO is estimated based on Equation 4.17 for $n = 4$ and with model wave spectra based on forecasts. The prediction horizon is 1 hour due to the specifications of the given data set, see Section 3.1.2.

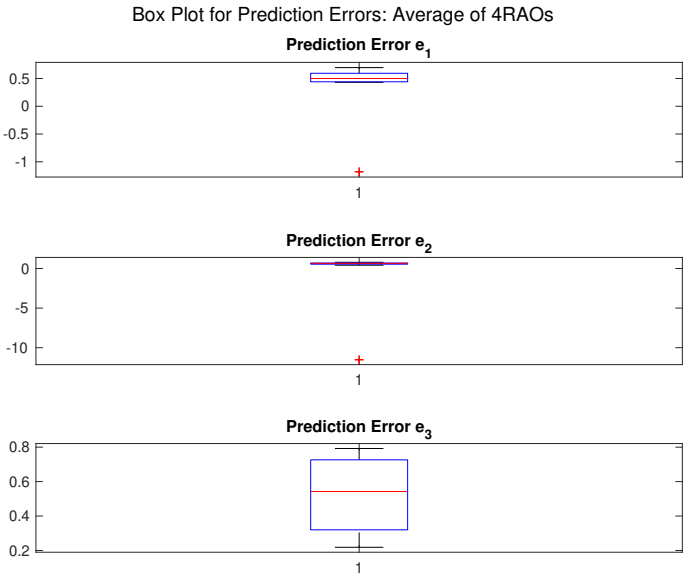

Figure 7.4: The box plots of the prediction errors defined by Equation 7.2 for the ten random samples form Table 7.1 for the non-parametric method with model wave spectrum based on forecasts as input. The predicted heave is based on the estimated RAO defined by Equation 4.17 for $n = 4$. The median is marked as a red line and the upper and lower edges of the box represents the 75th and the 25th percentile, respectively. Outliers are marked with red plus signs.

Moreover, Figure 7.5 shows the 1-, 2- and 3-step-ahead predicted heave energy spectra compared with the measured heave energy spectrum at initial sample time. In other words, the measured heave energy spectrum is from sample time j, while the 1-, 2- and 3-step-ahead predicted heave energy spectrum are from sample time $j + 1$, $j + 2$ and $j + 3$, respectively.

For this particular example, the prediction errors, e_1, e_2 and e_3 were 0.6574, 0.6732 and 0.4270, respectively. As shown in Table 7.4, these prediction error values are mostly above average.

The significant wave height and the wave peak period from the weather forecasts and the given data set for this particular example where 7.2295m, 12.2845s and 7.5500m, 11.6364s, respectively. According to Table 3.3, the measured sea state parameters are above average.

Furthermore, Figure 7.6 shows the estimated RAOs associated with the example introduced above, for 1, 2 and 3 hours ahead, resulting from an average of the last four estimated RAOs, see Equation 4.17.

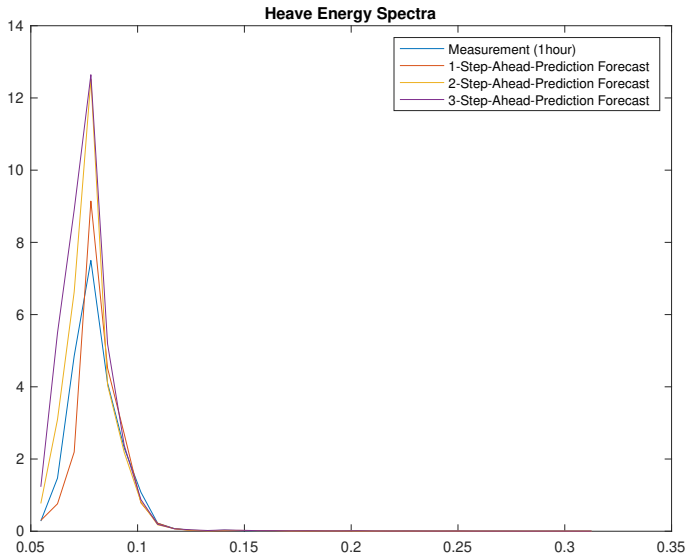

Figure 7.5: The 1-, 2- and 3-step-ahead predicted heave energy spectra from sample time $j+1$, $j+2$ and $j+3$, respectively, compared to the measured heave energy spectrum from sample time j when the RAO is estimated based on Equation 4.17 for $n=4$. The prediction errors, defined by Equation 7.2, are 0.6574, 0.6732 and 0.4270, which are mostly above average, see Table 7.4.

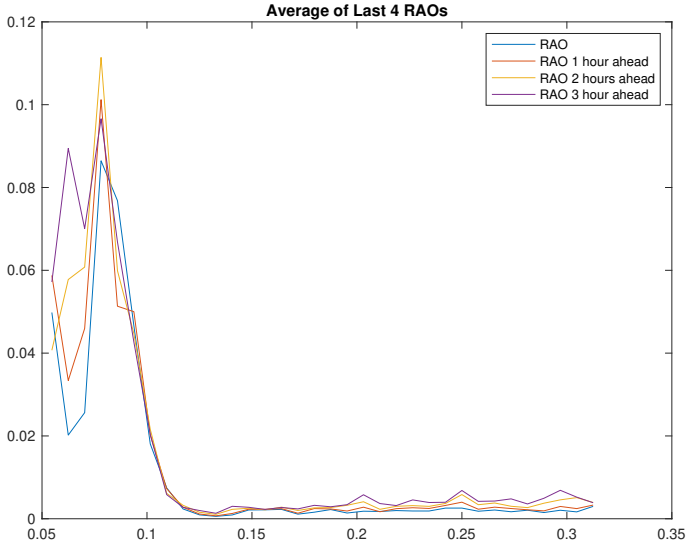

Figure 7.6: The 1-, 2- and 3-step-ahead estimated RAOs from sample time $j+1$, $j+2$ and $j+3$, respectively, compared to the estimated RAO at sample time j, based on Equation 4.17 for $n=4$. The prediction errors, defined by Equation 7.2, are 0.6574, 0.6732 and 0.4270, which are mostly above average, see Table 7.4.

Additionally, Figure 7.7 shows the 1-, 2- and 3-step-ahead predicted heave energy spectra compared with the measured heave energy spectrum at the initial time. Here, the prediction errors, e_1, e_2 and e_3 are -1.1180, -11.5253 and 0.3200, respectively, which are below average according to Table 7.4.

For this particular example, the significant wave height from the weather forecasts is 2.6842m, while the wave peak period is 8.3905s. The significant wave height from the given data set is 3.3650m and the wave peak period is 8.5333s, which is below average as seen in Table 3.3.

Moreover, Figure 7.8 shows the estimated RAOs, associated with the example introduced above, for 1, 2 and 3 hours ahead calculated from the average of the last four estimated RAOs as defined by Equation 4.17.

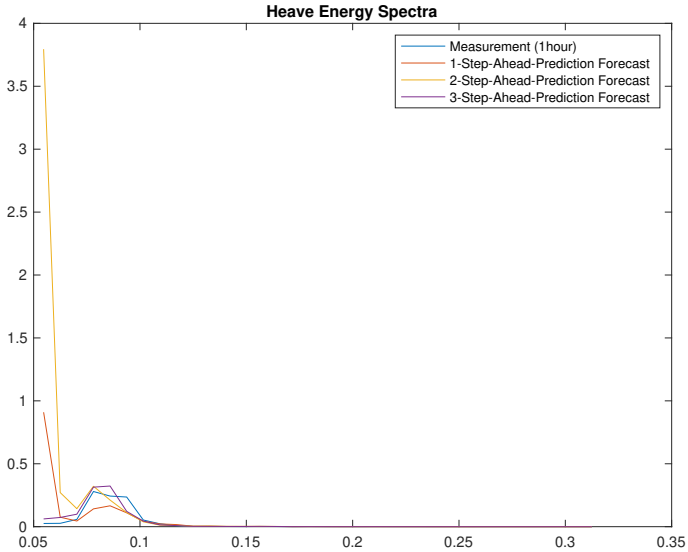

Figure 7.7: The 1-, 2- and 3-step-ahead predicted heave energy spectra from sample time $j+1$, $j+2$ and $j+3$, respectively, compared to the measured heave energy spectrum from sample time j when the RAO is estimated based on Equation 4.17 for $n = 4$. The prediction errors, defined by Equation 7.2, are -1.1180, -11.5253 and 0.3200, which are below average, see Table 7.4.

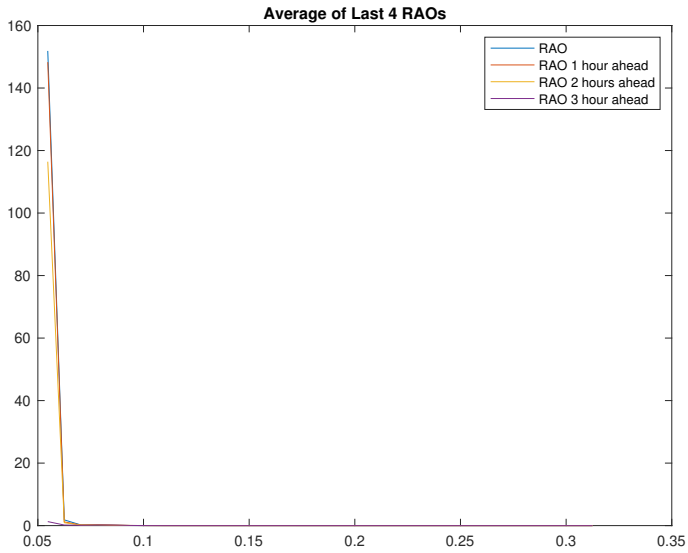

Figure 7.8: The 1-, 2- and 3-step-ahead estimated RAOs from sample time $j+1$, $j+2$ and $j+3$, respectively, compared to the estimated RAO at sample time j, based on Equation 4.17 for $n = 4$. The prediction errors, defined by Equation 7.2, are -1.1180, -11.5253 and 0.3200, which are below average, see Table 7.4.

7.2.2 Last RAO

Likewise, the RAO was estimated based on only the last measurements of heave and waves as described by Equation 4.16.

Thus, Figure 7.9 shows the box plots of the heave prediction errors, defined by Equation 7.2, when the heave energy spectrum is predicted based on the RAO calculated from the last heave measurement and the associated sea state forecasts.

Notice the outlier for the heave prediction error e_2, which results from a significant wave height at 3.5030m and a peak wave period at 10.1525s from the weather forecasts. The measured sea state parameters, from Table 5.1, give a significant wave height of 3.9084m and a wave peak period of 9.8462s. As seen from Table 3.3, the measured sea state parameters are below average.

Furthermore, Table 7.5 shows the median and the mean of the heave prediction errors illustrated in Figure 7.9.

Prediction Error	Median	Mean
e_1	0.6351	0.6060
e_2	0.4920	0.2897
e_3	0.2445	0.1538

Table 7.5: The heave prediction errors defined by Equation 7.2 when the RAO is estimated based on Equation 4.16 for and with model wave spectra based on forecasts. The prediction horizon is 1 hour due to the specifications of the given data set, see Section 3.1.2.

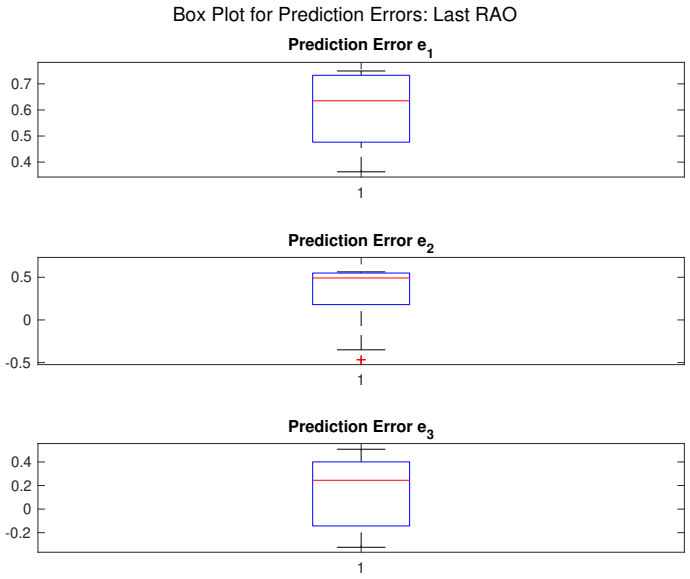

Figure 7.9: The box plots of the prediction errors defined by Equation 7.2 for the ten random samples form Table 7.1 for the non-parametric method with model wave spectrum based on forecasts as input. The predicted heave is based on the estimated RAO defined by Equation 4.16. The median is marked as a red line and the upper and lower edges of the box represents the 75th and the 25th percentile, respectively. Outliers are marked with red plus signs.

Similarly to what is seen in the previous section, Figure 7.10 shows the predicted heave energy spectra for 1-, 2- and 3-steps-ahead compared with the measured heave spectrum at the initial sample time. Thus, the measured heave energy spectrum is from sample time j, while the predicted heave energy spectra are from $j+1$, $j+2$ and $j+3$, respectively.

For this particular example, the prediction errors, e_1, e_2 and e_3 are 0.7411, 0.5496 and 0.4113, respectively, and above average according to Table 7.5. The significant wave height from the weather forecasts is 6.0428m, while the wave peak period is 11.1677s. Likewise, the significant wave height and the wave peak period from the given data set are 6.5673m and 11.6364s, respectively. As shown in Table 3.3 these measured sea state parameters are above average.

Furthermore, Figure 7.11 shows the estimated RAOs based on the last measurements of heave amplitude and sea state parameters as defined by Equation 4.16.

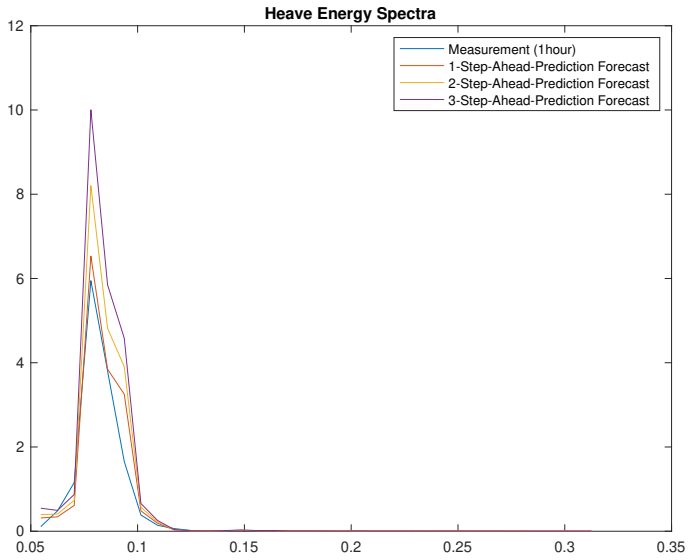

Figure 7.10: The 1-, 2- and 3-step-ahead predicted heave energy spectra from sample time $j+1$, $j+2$ and $j+3$, respectively, compared to the measured heave energy spectrum from sample time j when the RAO is estimated based on Equation 4.16. The prediction errors, defined by Equation 7.2, are 0.7411, 0.5496 and 0.4113, which are above average, see Table 7.5.

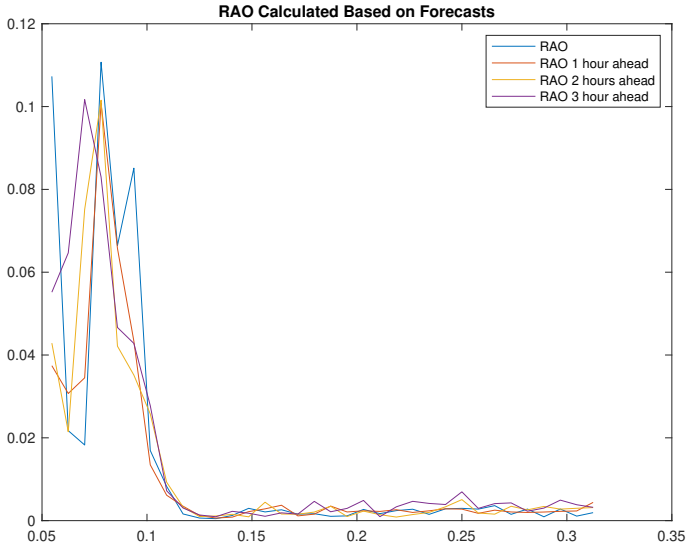

Figure 7.11: The 1-, 2- and 3-step-ahead estimated RAOs from sample time $j+1$, $j+2$ and $j+3$, respectively, compared to the estimated RAO at sample time j, based on Equation 4.16. The prediction errors, defined by Equation 7.2, are 0.7411, 0.5496 and 0.4113, which are above average, see Table 7.5.

Likewise, Figure 7.12 shows the 1-, 2- and 3-step-ahead predicted heave energy spectra compared with the measured heave energy spectrum from the initial time sample. For this particular example, the significant wave height from the weather forecasts is 2.6842m, while the wave peak period is 8.3905s. The significant wave height from the given data set is 3.3650m and the wave peak period is 8.5333s, which according to Table 3.3 are below average for the measured sea state parameters.

Furthermore, the prediction errors, e_1, e_2 and e_3 are 0.6097, -0.3504 and -0.3242, respectively. As shown in Table 7.5, these values are mostly below average.

Finally, Figure 7.13 shows the estimated RAOs associated with the example above, for 1, 2 and 3 hours ahead, calculated from the previous measurements of heave amplitude and sea state parameters as defined by Equation 4.16.

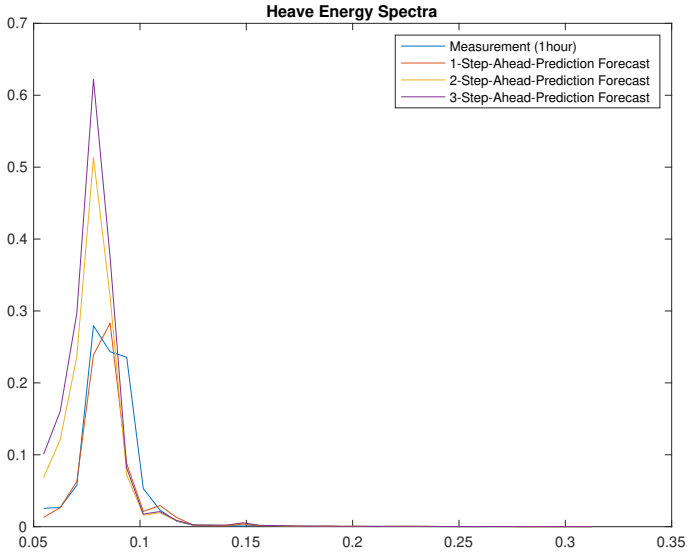

Figure 7.12: The 1-, 2- and 3-step-ahead predicted heave energy spectra from sample time $j+1$, $j+2$ and $j+3$, respectively, compared to the measured heave energy spectrum from sample time j when the RAO is estimated based on Equation 4.16. The prediction errors, defined by Equation 7.2, are 0.6097, -0.3504 and -0.3242, which are mostly below average, see Table 7.5.

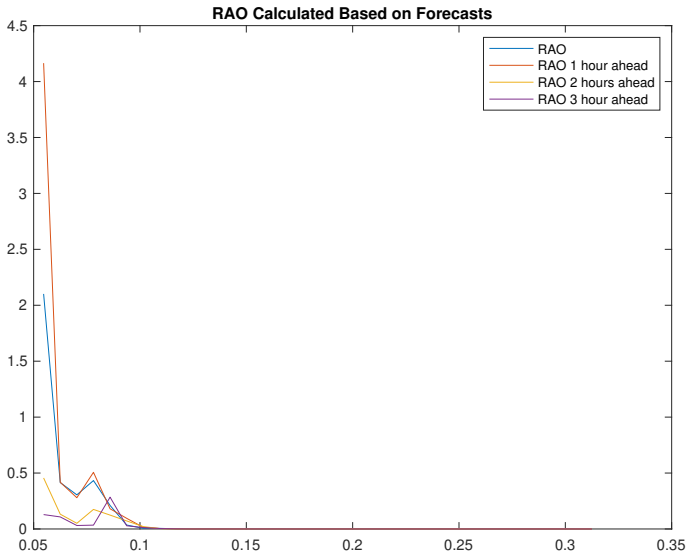

Figure 7.13: The 1-, 2- and 3-step-ahead estimated RAOs from sample time $j+1$, $j+2$ and $j+3$, respectively, compared to the estimated RAO at sample time j, based on Equation 4.16. The prediction errors, defined by Equation 7.2, are 0.6097, -0.3504 and -0.3242, which are mostly below average, see Table 7.5.

Chapter 8

Discussion and Conclusion

The objective of this MSc project is to design a methodology for RAO estimation and rig heave prediction based on available data on the rig. Moreover, the estimated RAO and predicted heave motion are indented to be a part of the downhole pressure calculations for the well-simulator developed by Heavelock AS (Kvernland et al., 2019).

Therefore, this chapter will discuss the performance of the proposed RAO estimation and rig heave prediction methods, as well as challenges related to the process of developing the methodology and finally, conclude the report.

8.1 Accessing Data

An essential part of this project was to get an overview of the available data on the rig as the format of the data limits the project. However, this task turned out to be challenging. Rig motion and wave radar measurements can be sensitive data and not necessarily uncomplicated to share with a third party. However, it would probably be possible to install an accelerometer together with the simulator on the rig and measure the heave amplitude.

Moreover, the sampling rate of the data is important. The wave peak period is typically in the range of 5-15 seconds. Thus, the heave motion has to be measured at least every second in order to capture the wave-induced motions.

Ideally, wave amplitude measurements were available such that the RAO estimation and heave prediction methodology could be implemented in the time-domain. Having access to both heave and wave amplitude measurements could possibly give more suitable information regarding the relation between ocean waves and rig heave motion and the assumption of linearity could possibly be more accurate. However, wave amplitude measurements were difficult to obtain. Therefore, this project was implemented in the frequency-domain with wave spectra instead, even though information about the phasing between waves and rig heave motion is lost.

Furthermore, wave amplitude measurements would require access to a measurement buoy placed near the rig or a type of laser measurement unit located on the rig. Moreover, the ocean waves would be measured at some point in time before they reach the rig.

Thus, the time delay between the wave measurements and the rig heave motion must be accounted for.

Nevertheless, the ocean wave measurements that eventually were obtained for this project were measured with a wave radar. Moreover, the rig heave amplitudes were measured with a MRU.

Additionally, the data server `thredds.met.no`, operated by the Norwegian Meteorological Institute, gives weather forecasts, including sea state parameters, four times daily. Thus, these sea state parameters could be used to generate model wave spectra. However, Table 7.2 indicates that the sea states from weather forecasts and the measured sea states does not always match, specifically the wave peak period.

8.2 The Results

Furthermore, the given measurements of the heave amplitude has to be transformed to the frequency-domain and presented as a energy spectrum. However, it is not trivial to obtain an energy spectrum. Thus, certain assumptions about the shape of the heave energy spectrum were made, introducing sources of error. Several energy spectrum estimation techniques were tested, such as MATLAB's `periodogram`. However, Welch's technique gave better results.

Moreover, the model wave spectra are approximately zero for low frequencies, leading to a nearly infinite RAO for low frequencies. Thus, the model wave spectra and thereby the heave energy spectra, were generated based on a linearly spaced frequency vector from 0.0547Hz to 0.3125Hz, instead of from 0.0312Hz in which the measured wave spectra are defined. This could be a reason for why the results are better for real wave spectra.

Additionally, Chapter 5 demonstrates that there are non-captured nonlinearities, i.e. the RAO is not constant, which is why an average of several estimated RAOs are mostly better at capturing the wave-heave relation than a RAO from only one set of input-output data.

However, Chapter 7 indicates that when weather forecasts are used to generate the model wave spectrum and the prediction horizon is in the time scale of hours, the RAO should be estimated based on only the last measurements, i.e. Equation 4.16.

Furthermore, the results from Chapter 6 and 7 indicate that the non-parametric methodology has a better performance than the parametric approach. The latter was tested with several models such as output error, but ARX had a better performance. Moreover, experiments with the model order did not give any better results.

Lastly, the results illustrate the importance of sufficiently rich and good data. Specifically, the data sample where the significant wave height is 6.2575m and the wave peak period is 9.8462s stands out. The measured wave spectrum related to these sea state parameters is shown in blue in Figure 8.1. The shape of the spectrum differs significantly from the shape of the wave spectrum associated with sea state parameters of 6.5673m and 11.6364s. As seen in Table 3.3, both significant wave heights are above average from the data set while the first wave peak period is below average and the later is above.

Furthermore, Figure 8.2 shows the Torsethaugen model wave spectra associated with these sea states. The blue model wave spectrum is not able to capture the form of the measured wave spectrum. However, this could arise from an odd sea state.

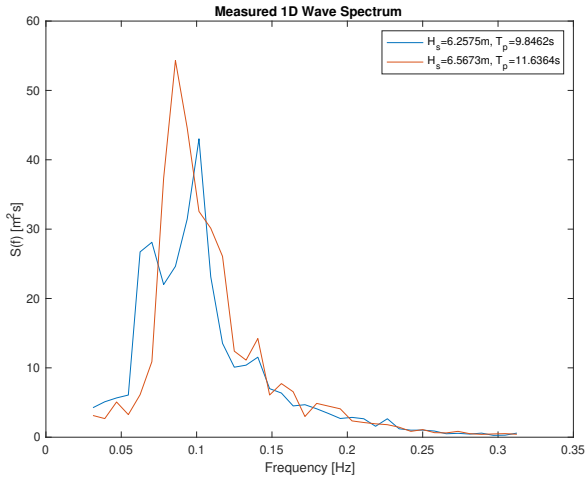

Figure 8.1: Measured 1D wave spectra with significant wave height, H_s, of 6.2575m and wave peak period, T_p, of 9.8462s, in blue and H_s of 6.5673m and T_p of 11.6364s in red.

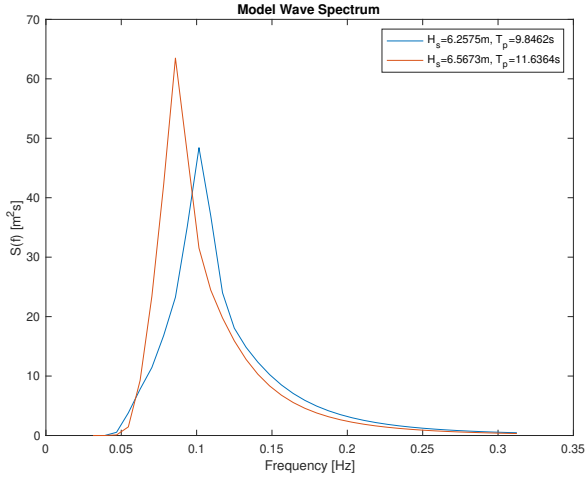

Figure 8.2: Torsethaugen model wave spectra with significant wave height, H_s, of 6.2575m and wave peak period, T_p, of 9.8462s, in blue and H_s of 6.5673m and T_p of 11.6364s in red. Compared with Figure 8.1, the former model wave spectrum is particularly bad at modeling the real wave spectrum.

8.3 Conclusion

To conclude, the data available on the rig has been investigated and it is possible to obtain measurements of rig heave amplitude with sampling frequency of 1s. Moreover, it is possible to get access to wave radar measurements, involving not only sea state parameters but 1D wave spectra as well.

Additionally, the data server `thredds.met.no`, operated by the Norwegian Meteorological Institute, includes weather forecasts of sea state parameters, among others. The forecasts are updated four times daily and contains forecasts 66 hours ahead and for the past 6 hours.

Furthermore, a parametric and a non-parametric method are developed for RAO estimation and rig heave prediction based on available data on the rig. The parametric method models rig heave as a SISO mass-spring-damper system with an ARX model. The non-parametric method is based on the relation established in Equation 2.38 where the heave energy spectrum is related to the wave spectrum by the square of the RAO.

Moreover, simulations under ideal conditions show that the parametric method recreates the simulated heave motion, which implies that the implementation is correct.

Additionally, quantified calculations of the performance of the methods indicate that the non-parametric method overall performs better with real measurements than the parametric method.

Moreover, if wave measurements are inaccessible, sea state parameters from weather forecasts services can generate wave spectra. Again, results indicate that the non-parametric method performs better than the parametric method with weather forecast data as well.

Furthermore, if the RAO is not accessible through the manufacturer or software programs such as WAMIT, the proposed non-parametric method can be valuable for the intended purpose as it introduces a procedure for heave predictions based on a given sea state.

Nevertheless, it remains to be concluded whether the proposed method has potential to improve the prediction of downhole pressure oscillations or not, as the integration with Heavelock AS's simulator remains.

Chapter 9

Further Work

The objective of this project is to estimate the RAO and utilize this data-driven estimate to predict the rig heave motion. Eventually, the intention is that the proposed methodology can improve the simulator designed by Heavelock's ability to predict of the downhole well pressure.

Thus, this chapter will discuss some further improvements of the proposed methods, as well as supplementary experiments.

9.1 Simulations

First of all, it would be interesting to generate a simulation case to test if the non-parametric method actually improves the prediction of the downhole well pressure. Ideally, pressure measurements from an actual drilling operation were available such that they would verify the simulation results.

Moreover, the results from the current simulator should be compared with the non-parametric RAO estimation and heave prediction method integrated with the simulator. Only then, if the proposed method actually improves the downhole pressure prediction, it could be concluded that the proposed methodology is good enough for its purpose.

If the integration of the non-parametric method with the simulator improves the downhole pressure predictions, then that indicates that a predefined RAO is more inaccurate under the current conditions on the rig, being waves, wind, mooring, loads and so on, than the RAO estimated with the proposed method based on real measurements from the current conditions.

9.2 Extended Heave Model

However, it could also be interesting to investigate the possibility of a more complex heave motion model. Instead of a simple SISO system, the heave motion could be described with a nonlinear model.

Moreover, the heave motion has been decoupled from the other motions in order to preserve a linear relation to wave-induced motion. Thus, the model describing the heaving motion of the rig could be extended to for instance a 3DOF model. This would of course require that measurements of these motions are available.

Bibliography

Aarnes, O.J., Reistad, M., Breivik, Ø., Magnusson, A.K., Furevik, B., 2019. Validation 2D wave spectra - ECMWF. MET report .

Aarsnes, U.J.F., Aamo, O.M., Hauge, E., Pavlov, A., 2013. Limits of controller performance in the heave disturbance attenuation problem. 2013 European Control Conference, ECC 2013 , 1071–1076doi:10.23919/ecc.2013.6669620.

Baghfalaki, M., Das, S.K., Das, S.N., 2012. Analytical model to determine response amplitude operator of a floating body for coupled roll and yaw motions and frequency-based analysis. International Journal of Applied Mechanics 4. doi:10.1142/S1758825112500445.

Behrens, A., 2013. mywave/WAM Documentation. URL: https://github.com/mywave/WAM.

Clauss, G., Lehmann, E., Östergaard, C., 1992. Offshore Structures Volume I: Conceptual Design and Hydromechanics. doi:10.1007/978-1-4471-3193-9.

DNV, 2010. RECOMMENDED PRACTICE ENVIRONMENTAL CONDITIONS AND ENVIRONMENTAL LOADS. Technical Report. DNV. URL: http://www.dnv.com.

DNVGL, 2018. DNVGL-CG-0130 Wave loads. URL: https://rules.dnvgl.com/servicedocuments/dnvgl/#!/home.

Faltinsen, O.M., 1990. Sea loads on ships and offshore structures. 1 ed., Cambridge University Press, Cambridge.

Fathi, D., . ShipX - SINTEF. URL: https://www.sintef.no/en/software/shipx/.

Fossen, T.I., 2011. Handbook of Marine Craft Hydrodynamics and Motion Control. John Wiley & Sons, Ltd, Chichester, UK. doi:10.1002/9781119994138.

Fossen, T.I., Perez, T., 2009. Marine Systems Simulator (MSS). URL: https://github.com/cybergalactic/MSS.

Godhavn, J.M., 2010. Control Requirements for Automatic Managed Pressure Drilling System. SPE Drilling & Completion 25, 336–345. doi:10.2118/119442-PA.

Hasselmann, K., Barnett, T., Bouws, E., Carlson, H., Cartwright, D., Enke, K., Ewing, J., Gienapp, H., Hasselmann, D., Kruseman, P., Meerburg, A., Müller, P., Olbers, D., Richter, K., Sell, W., Walden, H., 1973. Measurements of wind-wave growth and swell decay during the Joint North Sea Wave Project (JONSWAP). Ergänzungsheft 8-12 .

Heavelock AS, . Software. URL: https://www.heavelock.no/.

Journée, J., Adegeest, L., 2003. Theoretical Manual of Strip Theory Program "SEAWAY for Windows". Technical Report. Delft University of Technology. Delft. URL: www.amarcon.com.

Kvernland, M., Christensen, M.Ø., Borgen, H., Godhavn, J.M., Aamo, O.M., Sangesland, S., 2018. Attenuating Heave-Induced Pressure Oscillations using Automated Down-hole Choking. IADC/SPE Drilling Conference and Exhibition doi:10.2118/189657-ms.

Kvernland, M., Gorski, D., Sant'Ana, M., Godhavn, J.M., Aamo, O.M., Sangesland, S., 2019. Verification of Downhole Choke Technology in a Simulator Using Data from a North Sea Well. SPE/IADC International Drilling Conference 2019 .

Landet, I., Pavlov, A., Aamo, O.M., 2013. Modelling and Controll of Heave-Induced Pressure Fluctations in Managed Pressure Drilling. IEEE Transactions on Control Systems Technology 21, 1340 – 1351. URL: https://ieeexplore.ieee.org/stamp/stamp.jsp?tp=&arnumber=6238317, doi:10.1109/TCST.2012.2204751.

Lee, C., Newman, J., 2006. WAMIT User Manual, Versions 6.4, 6.4s. Technical Report. WAMIT, Inc.. Boston. URL: www.wamit.com.

Ljung, L., 1999. System identification : theory for the user. Second ed., Prentice Hall PTR, Upper Saddle River, New Jersey.

Ljung, L., 2014. System Identification Toolbox™ User's Guide. Technical Report. MathWorks. URL: www.mathworks.com.

MathWorks, . Estimate parameters of ARX, ARIX, AR, or ARI model - MATLAB arx. URL: https://www.mathworks.com/help/ident/ref/arx.html#mw_71d11571-be67-4c6d-8756-0bbfe5d22056.

MathWorks, 2020a. Box plot - MATLAB boxplot. URL: https://se.mathworks.com/help/stats/boxplot.html.

MathWorks, 2020b. Compare identified model output and measured output - MATLAB compare. URL: https://se.mathworks.com/help/ident/ref/compare.html.

MathWorks, 2020c. Goodness of fit between test and reference data - MATLAB goodnessOfFit. URL: https://se.mathworks.com/help/ident/ref/goodnessoffit.html.

MathWorks, 2020d. Simulate and Predict Identified Model Output. URL: https://se.mathworks.com/help/ident/ug/definition-simulation-and-prediction.html.

Miros Group, 2019. Miros Wave and Current Radar. Technical Report. MIROS Group.

Molland, A.F., 2008. The maritime Engineering Reference Book. Elsevier Ltd. doi:10.1016/B978-0-7506-8987-8.X0001-7.

Oppenheim, A.V., Verghese, G.C., 2015. Signals, systems & inference. Pearson.

Ramachandran, G.K., Robertson, A., Jonkman, J.M., Masciola, M.D., 2013. Investigation of response amplitude operators for floating offshore wind turbines. Proceedings of the International Ocean, Offshore and Polar Engineering Conference , 369–376.

Salvesen, N., Tuck, E., Faltinsen, O.M., 1971. Ship Motion and Sea Loads. DNV, Oslo. URL: https://www.scribd.com/document/360459083/Salvesen-N-ship-Motions-and-Sea-1970-TRANS.

Sørensen, A.J., 2018. Marine Cybernetics Towards Autonomous Marine Operations and Systems (Lecture Notes).

Tannuri, E.A., Sparano, J.V., Simos, A.N., Da Cruz, J.J., 2003. Estimating directional wave spectrum based on stationary ship motion measurements. Applied Ocean Research 25, 243–261. doi:10.1016/j.apor.2004.01.003.

The Norwegian Meteorological Institute, . Facts about Yr – Yr help and information. URL: https://hjelp.yr.no/hc/en-us/articles/206550539-Facts-about-Yr.

Torsethaugen, K., 1993. Two peak wave spectrum model Simplified double peak spectral model for ocean waves. Proceedings of the International Conference on Offshore Mechanics and Arctic Engineering - OMAE 2, 175–180.

Tupper, E.C., 2013. Introduction to Naval Architecture. Elsevier Ltd. doi:10.1016/C2011-0-07775-X.

Vettestad, M.O., 2019. TTK4550 - Specialization Project Design and Implementation of a User Interface for HeaveSim ™. Technical Report. Norwegian University of Science and Technology (NTNU).

Appendices

Appendix A

System Identification

This section is based on Ljung (1999).

A.1 QR Factorization

QR factorization for an $n \times d$ matrix A is defined as

$$A = QR \tag{A.1}$$

Where Q is $n \times n$ and orthonormal, that is $QQ^T = I$ and R is upper triangular with dimensions $n \times d$.

This can be applied to the least-squares parameter estimation technique by introducing the following matrices

$$\mathbf{Y}^T = \left[y^T(1) \cdots y^T(N)\right], \ \mathbf{Y} \text{ is } Np \times 1 \tag{A.2a}$$

$$\Phi^T = \left[\varphi(1) \cdots \varphi(N)\right], \ \Phi \text{ is } Np \times d \tag{A.2b}$$

Where p is the dimension of y. Then the least-squares criterion can be written as

$$V_N(\theta, Z^N) = |\mathbf{Y} - \Phi\theta|^2 = \sum_{t=1}^{N} |y(t) - \varphi^T(t)\theta|^2 \tag{A.3}$$

The norm is unaffected by any orthonormal transformation applied to the vector $\mathbf{Y} - \Phi\theta$. Therefore, with Q being orthonormal with dimensions $pN \times pN$, then

$$V_N(\theta, Z^N) = |Q(\mathbf{Y} - \Phi\theta)|^2 \tag{A.4}$$

Finally, by introducing QR factorization

$$QR = \begin{bmatrix} \Phi & \mathbf{Y} \end{bmatrix} \tag{A.5}$$

With

$$R = \begin{bmatrix} R_0 \\ \cdots \\ 0 \end{bmatrix} \tag{A.6}$$

Here, R_0 is an upper triangular $(d+1) \times (d+1)$ matrix, which can be decomposed as

$$R_0 = \begin{bmatrix} R_1 & R_2 \\ 0 & R_3 \end{bmatrix}, \; R_1 \text{ is } d \times d, \; R_2 \text{ is } d \times 1, \; R_3 \text{ is scalar} \tag{A.7}$$

Which means that

$$V_N(\theta, Z^N) = |Q^T(\mathbf{Y} - \Phi\theta)|^2 = \left| \begin{bmatrix} R_2 \\ R_3 \end{bmatrix} - \begin{bmatrix} R_1\theta \\ 0 \end{bmatrix} \right|^2 = |R_2 - R_1\theta|^2 + |R_3|^2 \tag{A.8}$$

Which is minimized for

$$R_1\hat{\theta}_N = R_2, \text{ giving } V_N(\theta, Z^N) = |R_3|^2 \tag{A.9}$$

A.2 Parseval's Relationship

Parseval's relationship states that the energy of a signal can be decomposed into energy contributions from different frequencies. In other words, Equation A.10 defines the relationship between the time- and frequency-domain of a signal.

$$\sum_{k=1}^{N} |U_N(2\pi k/N)|^2 = \sum_{t=1}^{N} u(t)^2 \tag{A.10}$$

Where U_N is the Fourier transform and $|U_N(2\pi k/N)|^2$ is the periodogram of the signal $u(t)$.

Appendix B

Listings

B.1 Weather Forecasts

Listing B.1: Translation of coordinates to relative coordinates

```
function [posx,posy] = find_nearest_gridcell(lon,lat,...
lon_in,lat_in)
%
% This function finds the right grid number (posx, posy)
% according to the given lat/lon grid (a 2D matrix)
% PARAMETERS:
% lon: relative lontitude from forecasts
% lat: relative latitude from forecasts
% lon_in: actual longitude
% lon_in: actual latitude
% posx: x position in grid relating longitude to
% relative longitude
% posy: y position in grid relating latitude to
% relative latitude
%
% Written by: Ole Johan Aarnes, Scientist at the the
% Norwegian Institute of Meteorology
%

longitude=reshape(lon,size(lon,1)*size(lon,2),1);
latitude=reshape(lat,size(lat,1)*size(lat,2),1);

dt = delaunayTriangulation(longitude,latitude);
PI = nearestNeighbor(dt,[lon_in,lat_in]);

real_lon=longitude(PI);
real_lat=latitude(PI);

[posx,posy] = find(lon==longitude(PI) & lat==latitude(PI));
end
```

Listing B.2: Extraction of the sea state parameter from weather forecast file

```
function [time,Hs,Tp] = getSignificantWaveHeight(filename,longitude,...
latitude,posix)
%
% This function extracts the sea state parameters Hs and Tp and the time
% from a NetCDF weather forecast file from thredds.met.no.
% PARAMETERS
% filename: name of the NetCDF file
% longitude: the lognitude in degrees
% latitude: the latitude in degrees
% posix: boolean variable which specifies the format of output time
% time: time which forecasts are valid for, either posix or dateTime
% Hs: vector with significant wave height values for the given lon/lat
% Tp: vector with wave peak period values for given lon/lat

% Read variables
latData  = ncread(filename,'latitude');
lonData  = ncread(filename,'longitude');
timeData  = ncread(filename,'time');

% Get data
if posix == true
    time = datetime(timeData,'ConvertFrom','posixtime');
else
    time = timeData;
end

[posx,posy] = find_nearest_gridcell(lonData,latData,longitude,latitude);

Hs = squeeze(ncread(filename,'hs',[posx posy 1],[1 1 inf]));
Tp = squeeze(ncread(filename,'tp',[posx posy 1],[1 1 inf]));
end
```

Mia Olea Vettestad

Response Amplitude Operator Estimation and Prediction of Heave Motions

NTNU
Norwegian University of
Science and Technology